

POLITECNICO DI TORINO

Department of Control and Computer Engineering

Master's Degree Thesis
in Mechatronic Engineering

**AI-Assisted Gait-Analysis:
an automatic and teleoperated approach**



Academic year 2020-2021

Supervisor

Prof. Alessandro RIZZO

Co-supervisor

Dr. Daniele CAFOLLA

Candidate

Dario SIPARI

A nonna

Ogni mio traguardo sarà anche il tuo

Index

Figure Index.....	6
Abstract.....	8
Introduction	9
1. Fundamentals.....	9
1.1. What is Artificial Intelligence (AI)	9
1.2. AI applications in healthcare	14
1.3. AI approaches in Human characterization.....	17
2. State Of Art.....	23
2.1. Gait Analysis	23
2.2. Traditional gait analysis.....	30
2.3. Automatized gait analysis.....	39
3. AI-assisted Gait analysis	41
3.1. Attached problem	41
3.2. Proposed methodology	48
3.3. Methodology implementation.....	51
4. A novel approach.....	57
4.1. Human Machine Interface	58
4.2. Real-Time Data Analysis and Acquisition Modules	68
4.3. Post-Processing Data Analysis Modules	72
5. Experimental Tests and results	79
5.1. Experimental layout.....	79
5.2. Experimental tests.....	82
5.3. Results	84
6. Conclusion.....	85
References	87

Figure Index

Figure 1. 1 - number of peer-reviewed ai publications, [26]	10
Figure 1. 2 - AI 3 main categories - capabilities perspective	11
Figure 1. 3 - AI 4 main categories - functionalities perspective.....	12
Figure 1. 4 – Deep Learning multiple layers neural network example, [29].....	13
Figure 1. 5 - AI applications in healthcare: 4 areas	14
Figure 1. 6 - PoseNet key points and skeleton, [22].....	19
Figure 1. 7 - OpenPose key points and skeletons: a) BODY-25 Model, b) COCO Model, [23]	20
Figure 1. 8 - NuiTrack key points and skeleton, [24]	21
Figure 1. 9 Skeleton Tracking SDK by Cubemos key points and skeleton, [25].....	22
Figure 2. 1 Phases division of Human Gait Cycle, [35], [40]	25
Figure 2. 2 Example of the possible movements of the joints, [23].....	26
Figure 2. 3 an example of Spatial-temporal and static parameters from BTS GAITLAB	28
Figure 2. 4 an example of the Kinematic Parameters matrix from BTS GAITLAB: The grey area stands for the normal range of values, the other colours represent the left and right limb acquisitions of the specific patient.....	29
Figure 2. 5 an extract of Kinetic Parameters plots from BTS GAITLAB	29
Figure 2. 6 an example of the Kinematic Parameters matrix from Ball State Biomechanics Laboratory: “Joint angles of the pelvis, hip, knee, and ankle normalized to the gait cycle. The first column represents sagittal plane motion, the second column represents frontal plane motion, and the third column represents transverse plane motion.”, [42].....	30
Figure 2. 7 : Illustration of a motion capture system with stereophotogrammetry, [34] [43] ..	33
Figure 2. 8 some of the BTS GAITLAB basic tools, [41].....	33
Figure 2. 9 on the left: Vicon Active Wand, [45]; in the middle: BTS passive Wands, [44]; on the right: cartesian axes associated with the BTS Wands, [44].....	34
Figure 2. 10 on the left: BTS cameras dynamic daily setup and calibration; on the right: BTS cartesian frame setup, [44].....	34
Figure 2. 11 BTS digital sensory floor setup, [44]	34
Figure 2. 12 BTS EMG sensors activation, [44]	35
Figure 2. 13 anthropometric measurements and skin demarcation, [44].....	35
Figure 2. 14 EMG sensors positioning routine and signal, [44].....	36
Figure 2. 15 on the left: Marker Davis Protocol; on the right: a section of the patient fully covered with markers and EMG sensors, [44]	37
Figure 2. 16 BTS Gait acquisition and manual heel strike detection, [44].....	38
Figure 2. 17 : PosturaLab baropodometric analysis and weight distribution, [36]	40
Figure 2. 18 UFES’s smart walker system, [37].....	40
Figure 3. 1 - WS system based on (a) inertial sensors and (b) wearable force plates, [47, 33]	46
Figure 3. 2 - Commercial WS system based on inertial sensors: Xsens MVN, [46, 33]	47
Figure 3. 3 - Instrumented insole: (a) inertial sensor, Bluetooth, microcontroller and battery module; (b) coil for inductive recharging; and (c) pressure sensors, [33, 48].....	47
Figure 3. 4 - Proposed Methodology	50
Figure 3. 5 - Intel RealSense d435i - Biomechatronics Lab, Neuromed Technology Park - a) RGB acquisition; b) Depth acquisition with both stereo cameras and IR projector.....	54

Figure 3. 6 - Intel RealSense d435i - Biomechatronics Lab, Neuromed Technology Park - a): RGB acquisition; b): Depth acquisition with stereo cameras only.....	54
Figure 3. 7 - Intel RealSense d435i, components, [58]	55
Figure 3. 8 - Intel RealSense d435i, the lenses in order from the left: the right stereo camera, the infrared projector, the left stereo camera, the RGB camera, [59].....	55
Figure 3. 9 - Intel RealSense d435i, depth and -Z axis definition, [58]	55
Figure 3. 10 - Intel RealSense d435i, stereo cameras depth recognition via triangulation, [58]	56
Figure 4. 1 - Human Machine Interface Flow Chart	57
Figure 4. 2 - SANE first prototype version	61
Figure 4. 3 - SANE second prototype version.....	62
Figure 4. 4 - SANE final version - Phase 1 and tooltip example	63
Figure 4. 5 - SANE final version - Phase 2 and tooltip example	64
Figure 4. 6 - SANE final version - Phase 3 at the very beginning of a gait cycle.....	65
Figure 4. 7 - SANE final version - Phase 6 and tooltip example	66
Figure 4. 8 - SANE final version - Phase 6, Message Box example.....	67
Figure 4. 9 - SANE' s first level of filtering for outliers - a) Ankle Distance trend; b) an example of a keypoint signal (the projection on X of the signal related to the Spine joint)	76
Figure 4. 10 - SANE' s completely filtered signal (green line) vs raw data interpolation (red line) - a) Ankle Distance trend; b) an example of a keypoint signal (the projection on X of the signal related to the Spine joint)	76
Figure 4. 11 - SANE' s completely filtered signal (green line) vs raw data point cloud (red line) - a) Ankle Distance trend; b) an example of a keypoint signal (the projection on X of the signal related to the Spine joint)	77
Figure 4. 12 - SANE' s completely filtered signal with IQR, Median and LP adaptive Butterworth (green line) vs signals filtered by IQR and Median (red line) - a) Ankle Distance trend; b) an example of a keypoint signal (the projection on X of the signal related to the Right Ankle joint).....	77
Figure 4. 13 - SANE's detection of movement's start and stop (green vertical lines) through the projection on Z of the signal related to the Spine joint and its relative maxima and minima (red dots) - a) a low-noise acquisition while walking; b) a different, slightly noisier acquisition while walking with a maximum and a minimum that are not correctly taken into account during the walk recognition	78
Figure 4. 14 - SANE's gait detection (red vertical lines) through the projection on Z of the trend related to the Ankle Distance - a) Ankle Distance trend; b) an example of a keypoint signal cut within the time span associated with the gait (the projection on X of the signal related to the Right Ankle joint)	78
Figure 5. 1 - Intel RealSense d435i and SANE' s axis.....	80
Figure 5. 2 - gait analysis laboratory before the experimental layout was set up.....	80
Figure 5. 3 - Experimental layout and demarcation of the path. Following the creation of the start and stop lines, the black reflective tape was removed while the opaque white tape remained.	81
Figure 5. 4 - Experimental layout - on the left: SANE's Interface; on the right: BTS GAITLAB Smart Clinic Interface	81

Abstract

Human gait cycle can be affected by a wide variety of factors, including neurological, orthopaedic, and pathological impairments. Therefore, Gait Analysis has a wide range of applications, including the diagnosis of neurological illnesses, the analysis of disease progression, the evaluation of the effectiveness of a therapy, postural adjustment and athletic performance evaluation and improvement.

The application of new technologies in this field has resulted in significant improvement, but these systems are still struggling to come up with solutions that strike a proper balance between cost, accuracy of analysis, speed and convenience.

The goal is providing low-cost assistance to persons with motor impairments to enhance their quality of life. The study proposes a new automatized technique for motion characterization that employs Artificial Intelligence including real-time analysis, full automation, and a non-invasive, markerless analysis. This automatized approach allows rapid diagnosis and avoids human errors.

Subjects were recruited and instructed to walk at various speeds while video footage was collected using both the traditional gait analysis method and the improved SANE System. This procedure enabled for biomechanical analysis of the movement and for the evaluation of biomechanical parameters of clinical importance. All of this allowed the gait metrics derived by the two motion tracking systems to be compared.

All in all, the proposed system and its evaluation in this work of thesis allows to state that the use of Artificial Intelligence will assist rehabilitative medicine in “taking a step forward.”

Introduction

1. Fundamentals

1.1. What is Artificial Intelligence (AI)

AI (Artificial Intelligence) is a branch of computer science that studies the theoretical foundations, methodologies, and techniques that enable the development of hardware and software systems capable of providing computers with capabilities that, to the untrained eye, appear to be the sole domain of human intelligence, [1]. The goal of this field is to recreate or imitate human intellect rather than to duplicate or simulate it. Because of this theoretical distinction, it is feasible to decrease conceptual restrictions and improve the AI's autonomy by implementing tasks that aren't necessarily done as a human would do. AI can also be defined as a branch of study that focuses on the problem of how to represent, manipulate and construct knowledge about facts, actions and laws of causality. One of AI's most important contributions is to intimately link the notion of algorithm to the problem-solving process. This new philosophy requires man to be able to provide the machine with an algorithm capable of generating an algorithm on its own, thus creating meta-algorithms or inferential algorithms.

“With automatic problem-solving, we conceive the machine as having the ability not only to be fast in executing human-made algorithms, but also to construct autonomously the algorithms needed to solve problems.”, [2].

As a result, AI researchers aim to create computer programs that execute intellectual tasks while also attempting to explain the fundamental concepts of intelligence. AI has recently taken on the role of a discipline. Its formal beginnings can be traced back to the Dartmouth Summer Seminar in 1956. However, trying to establish an official date of birth and an exhaustive categorization is fairly difficult. As can be deduced from its very definition, indeed, AI as an effort to reproduce the human intellect in its infinite nuances, is in fact a dream belonging to our species since the early days of automation. As a result, it is not uncommon to come across ontological debates about Artificial Intelligence that attribute its origins in a variety of ways: some cite Leibnitz's calculus ratiocinator, capable of reducing reasoning to a kind of algebra of thought, others Warren McCulloch and Walter Pitts with the first model of artificial neurons in 1943, others even go back to the time of the self-propelled automata of Heron of Alexandria (1st century AD).

In the end the diversity of techniques is what survives today of early AI's characterization. There is also a continuous pragmatic extension of the boundaries of the discipline whenever new results are achieved. This last concept becomes increasingly true because of the exponential increase in both the number of applications, the variety of implementations, and the apparent interest expressed by the public in this discipline in recent years, as can be noticed in Figure 1. 1.

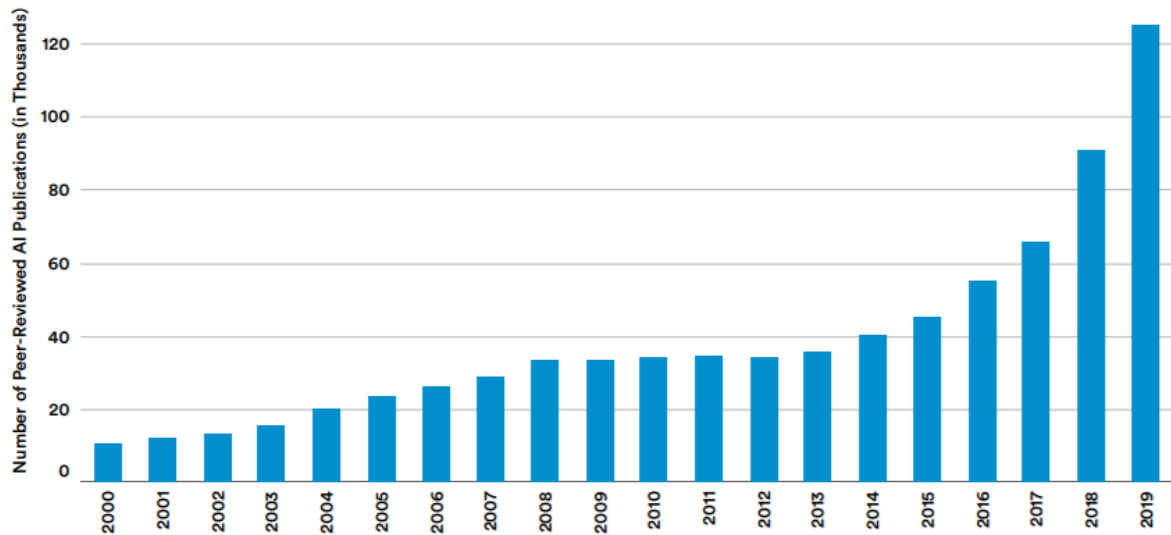


Figure 1. 1 - number of peer-reviewed ai publications, [26]

Therefore, AI turns out to be a rapidly evolving subject both as a whole and in its elements. This gives rise to more and more fluid subcategories that can only be discerned at the most basic level.

“AI is simultaneously a science and an engineering product.”, [3].

In this scenario, two sorts of AI categorizations are recognized, each approaching the subject from a different angle:

The first one looks at it from a capability perspective and contains three fields (Figure 1. 2) [21]:

- Narrow AI (ANI):

also called “Weak AI”, focuses on one narrow task and cannot perform beyond its limitations. It targets a single subset of cognitive capabilities and progresses along that spectrum.

- General AI (AGI):

also known as “strong AI”, is capable of understanding and learning any intellectual task that a human can perform. It enables a machine to apply its knowledge and skills in different situations. AGI has the ability to reason, plan, solve problems, think abstractly, comprehend complex ideas, learn quickly, and improve through experience. This branch is still under development.

- Super AI (ASI):

Super AI its meant to surpass human intelligence and perform any task better than a human. The concept of artificial superintelligence sees AI evolved to be so akin to human sentiments and experiences that it doesn't merely understand them; It also elicits its own emotions, needs, beliefs, and desires, such as scientific creativity, general wisdom, and social skills. This branch is still theoretical.

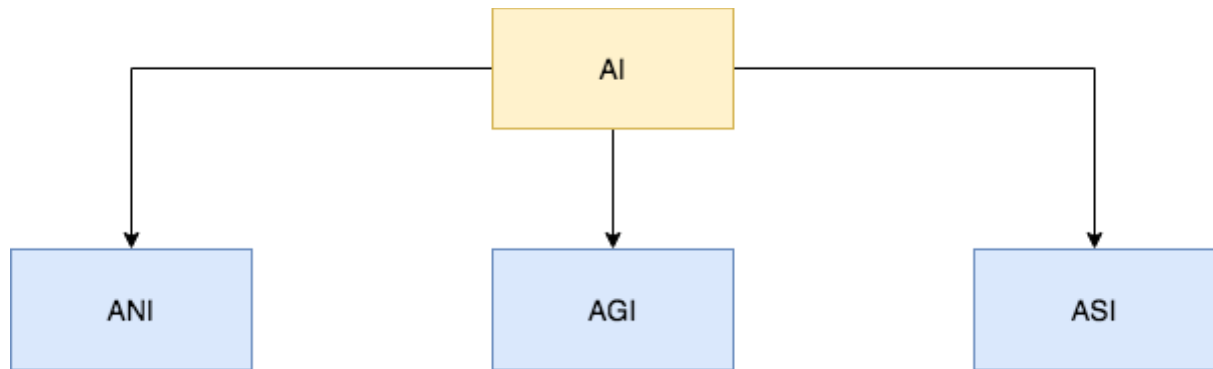


Figure 1. 2 - AI 3 main categories - capabilities perspective

The second section examines AI from a functional standpoint and contains four macro-sets (Figure 1. 3):

- **Reactive Machines:**

The most basic type of artificial intelligence that does not store memories. It acts only in the immediate present and does not make predictions.

- **Limited Memory:**

Limited Memory AI trains from past data to generate new decisions. The memory of such systems is short-lived.

- **Theory of Mind:**

Represents a high-level technology that only exists as a concept. Such an AI requires a thorough understanding of the processes of mutual influence between objects and people in a given environment. It should be able to comprehend people's feelings, sentiments, and thoughts.

- **Self-awareness:**

Self-awareness AI only exists hypothetically. Such systems are capable of not only comprehending their own internal characteristics, states, and

conditions, but also of perceiving human emotions. It is an all-round artificial consciousness

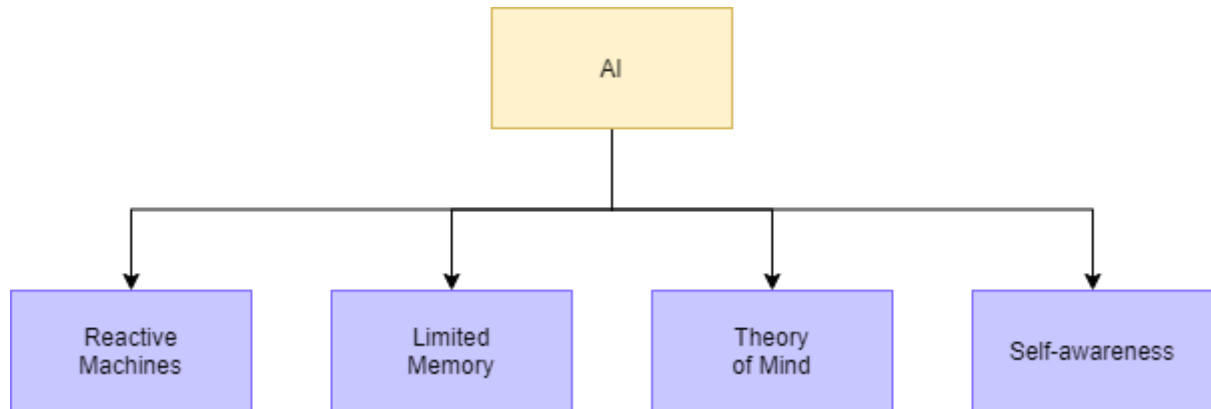


Figure 1. 3 - AI 4 main categories - functionalities perspective

Then there is another possible categorization (not strict) of AI in subdomains based on its approach to learning and its applications. We distinguish Natural Language Processing, AI in Learning (Machine Learning, Expert Learning), AI applied to probabilistic reasoning, AI with Natural/Genetic Approach, AI for problem Solving, AI in healthcare, AI in robotics and Control, AI in e-commerce, AI in human resources, AI in agriculture, AI in Social Media, AI in Marketing, AI in gaming, AI in Navigation, AI in Planning, AI in Perception, AI in Computer Vision, AI in Data Mining, AI in multiagent Systems, AI in cognitive modelling, AI for Knowledge Representation, AI in motion, AI in social Approach... The list could be much longer and each of its entries would have shared sections with the others. This aspect makes their discernment less defined.

For the purpose of our discussion, we will put the emphasis only on Machine Learning and especially in one of its subsets: Deep Learning.

We define Machine Learning (ML) as

“The field of machine learning is concerned with the question of how to construct programs that automatically improve with experience.”, [4].

It differs from the less recent Expert Systems by the fact that, although it has the purpose of learning and continuously improving performance through experience too, it does not provide a highly structured system to simulate step-by-step a decision-making process in a specific domain, but can perform solely data driven decisions with a less structured but more complex conceptual skeleton, without knowing explicitly at its base what to do and how to do it.

ML is also divided into Supervised and Unsupervised. Namely: the first requires the learning process to be based on experience with external bias and requires an initial input dataset that has already explicitly stated the correct expected output. Future assumptions about new inputs will be based on the function that the AI has created based on the already known in/out dataset. The second is conceptually more complex since it does not involve an initial dataset expressing a priori the correct outcome for each

example, but only a very large list of inputs and outputs whose relationship has never been indicated. It will be the task of the AI not only to connect the in's and out's but also to recognize and infer the most likely correct patterns that will define their nexuses. Also, in this case there are hybrid categories between the subsets of Supervised and Unsupervised ML.

To this micro-universe of Machine Learning belong:

- Reinforcement Learning (RL)

Helps a computer (agent) to learn a behaviour through repeated trial-and-error interactions with a dynamic environment. This allows the agent to implement a series of decisions that maximize a reward metric for the task, without ever being explicitly programmed for that specific task and without human intervention

- Deep Learning

It can be both Supervised and Unsupervised and hybrid. It exploits the branch of neural networks to create a network at multiple levels (Figure 1. 4). The structure that characterizes and distinguishes it is made up of a level with an array of neurons associated with the pure reception of input, a level associated with the pure representation of the output with the relative index of confidence of the answer and a variable number of intermediate levels hidden where the activity of elaboration of the nexuses takes place and that covers the apparent role of intelligent inference [29].

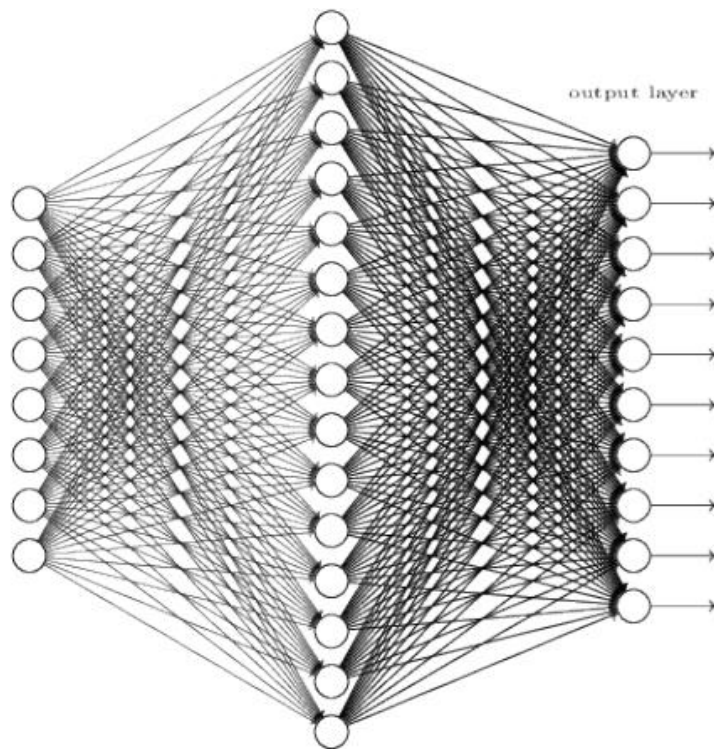


Figure 1. 4 – Deep Learning multiple layers neural network example, [29]

1.2. AI applications in healthcare

In recent years there have been numerous studies in the literature examining the potential of AI in applications to support clinical practice. Meanwhile the digital information around the world has more than doubled.

Medicine is a major player in this growth. Evidence shows that AI-based technologies have the significant potential to transfer various diagnostic procedures into the primary care setting. In addition, the digitization of health data, complemented by computer analytics, enables intelligent and effective management of the chronic patient by introducing new potential in clinical research, frontier medicine, and personalized medicine.

Through it is now feasible to give a better and more customized treatment based on the unique characteristics of each patient [5, 6]. By doing so, it is possible to pursue the goals of effectiveness, efficiency, and appropriateness that are typical of today's medicine.

Schematically, 4 areas of application of Artificial Intelligence can be strictly defined (Figure 1. 5): Patient Care; General Imaging Diagnostics; Management; Research and Development, [7].

A few examples to frame the current state of research [8]:

- AI in Neuroimaging:

The ability to recognize patterns and classify input through ML is useful in the field of Neuroimaging.

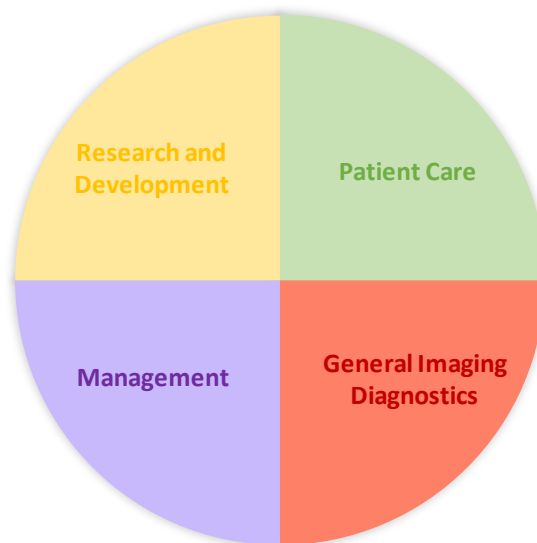


Figure 1. 5 - AI applications in healthcare: 4 areas

Currently, the initial step in a patient's diagnostic process is a qualitative assessment of brain MRI. The resulting mapping is generally analysed by radiologists and experts and finally, in case of doubts about the nature of any masses or abnormal images, it could be necessary to proceed with more invasive investigations such as biopsy. In this context, there is the potential to assist in the analysis and understanding of MRI through AI and to have a greater likelihood of averting unnecessary interventions. In the specific case of the treatment of tumour masses, for example, AI has already presented itself as a valuable tool not only for their recognition but also for the estimation of their extent and nature, providing vital information for operations.

To this has also been added the advantage of the creation of databases on the acquisitions made more interconnected and fluidly categorized, allowing to filter huge amounts of information under new and multiple aspects.

- AI in Radiology, Cardiology and Dermatology

There have been many applications in these areas.

For example, leveraging the same principles that have made AI useful in neuroimaging, radiology has developed automated triage techniques by classifying radiographs using ML. [9]

Using the same criteria in cardiology, excellent results have been obtained in terms of sensitivity and specificity in the diagnosis of acute coronary syndrome by ECG compared to cardiologists [10]. It has even been demonstrated a statistically superior diagnostic accuracy of cardiology medical staff in a case of diagnosis of arrhythmia patterns in electrocardiographic tracings [11]. DL approaches have also been recently applied in echocardiographic imaging and tested in cases such as hypertrophic cardiomyopathy, cardiac amyloidosis, and pulmonary arterial hypertension [12, 13].

The ability to recognize patterns is, even with these examples alone, increasingly useful in a boundless number of fields. Wherever there is data analysis, AI becomes a powerful tool that can no longer be ignored. It is therefore no surprise that it has also been used in dermatology, [14]. Where analysis of epithelial tissue images returned excellent results providing fully automated accurate and congruent diagnoses, [15].

- AI and Robotics in Surgery

The availability of instruments that increase the precision of surgical resection, minimizing the surgical access, and that allow to respect or increase the safety of the intervention, is immediately reflected in practice: in fact, surgical robots have now become a technological tool of choice.

An exhaustive example among many is the surgery of the pelvic district: this is one of the cases in which the dexterity of each single gesture is fundamental. The intervention, through an artificial terminal articulation

like that of the anatomical wrist, is safer and guarantees high precision and reliability. Other advantages are the reduction of invasiveness and lower risks due to distraction or fatigue of the human operator.

Artificial intelligence technologies are able, however, to take a further step forward. AIs can “reason” about data far beyond human senses, allowing them to “see” things that a human operator cannot. When it’s time to suture, the machine, for example, might determine the best locations in the tissues, design the sequence of precise micro-actions required, and then do them all by itself.

- AI in Emotion Recognition and Mental Health

AI has often been cited in applications requiring logical-mathematical inference or categorization, especially in the past. Nowadays, however, it also finds applications in other fields of intellect, increasingly expanding its limits. This is the case of AI in Emotion Recognition. The ability to recognize and connect patterns proves to be useful in partially emulating emotional intelligence and of great help also in the medical field to understand both the verbal and non-verbal language of the patient and to distinguish and monitor emotions and feelings during any therapy.

“Emotion recognition in conversation (ERC) is becoming increasingly popular as a new research frontier in natural language processing (NLP) [...]. Moreover, it has potential applications in health-care systems (as a tool for psychological analysis), education (understanding student frustration), and more. In Addition, ERC is also extremely important for generating emotion-aware dialogues that require an understanding of the user’s emotions.”, [16].

For the mentioned reasons software based on intelligent algorithms have been created to analyse and monitor the emotional state of the patient through automatic and dynamic recognition of facial expressions, breathing patterns, analysis of written text, tone of voice and monitoring of sleep-wake activity.

For example, it has been demonstrated that through the automated analysis of texts published in posts and comments on social networks such as Facebook, Instagram, YouTube, Reddit, Twitter, and others, it is possible to accurately predict (AUC 0.72) the onset of a patient’s first depressive episode up to 6 months in advance of the first clinical diagnostic detection.[17] Similar results were also obtained from the sole analysis of photographs posted on social media, [18].

Other applications for AI can be found in automated chat rooms (Chatbots) trained to perform cognitive behavioural therapy through interlocution with the patient. In one case, the tool was even used to significantly reduce symptoms of depression and anxiety by successfully acting on the based on the common scales PHQ-9 and GAD-7, [19]. AI in this field, moreover,

together with the development of digital therapies (Digital Therapeutics or DTx) is proposed as a support tool not only for depression but also for many other disorders such as the treatment for alcohol, opioid or substance abuse disorder [20].

- Ai in Motion Capture (MoCap)

Motion capture is used by doctors and therapists to help diagnose and treat their patients. This method has proven useful in improving the quality of life for patients with both physical and psychological disorders and disabilities.

Motion capture is the process of digitally recording human movements and then mapping the motion data onto a 3D digital model. There are several capture methods. One of the most promising methods leverages AI to recognize an individual's joints.

1.3. AI approaches in Human characterization

The acquisition of an individual's whole or partial body posture and the kinematic, and dynamic information plays a critical role in the treatment process of a wide spectrum of patients. Here some examples:

- Motion Capture in Orthopaedics

Using this technology, physicians and scientists are able to create a visualization of musculoskeletal dysfunction and modify their treatments to meet individual needs. It can be used to capture information about joint angles, axis symmetries, accelerations and joint stress. This data can then be compared to standard biomedical values to help identify orthopaedic dysfunction.

- Motion Capture in Injury Diagnosis and Treatment

Injury diagnosis and treatment have also benefited greatly from the use of motion capture. As in orthopaedics, motion tracking technology helps physical therapists visualize a patient's movements in order to assess their individual needs and ensure that patients are using the correct technique during treatment exercises. With this data, corrections can be made until the right posture is used to speed recovery time and avoid further injury.

- Motion Capture in Preventive Medicine

Similar to its use in physical therapy, motion capture can be used to prevent injuries before they happen. This technology is often used in athletics, as it can analyse an athlete's performance and ensure proper movements. In addition to identifying movements that could cause a sprain or fracture, MoCap can avert chronic injuries. The same procedures are also used to treat patients with concussions.

- Motion Capture and MRI Diagnostics

Motion capture along with MRI allows physicians to have a patient perform specific actions while brain activity is documented in order to analyse how these actions affect the individual's activity.

- Motion Capture in Medical Staff Training

Motion Capture data allows trainees to visualize and refine their movements as they perform a variety of procedures.

In summary, wherever there is a patient or an operator action, motion analysis emerges as a powerful and valuable tool. For these reasons, many solutions have been proposed to capture this kind of data and many innovations in this field occur frequently.

The acquisition of information on an individual's joints in their totality is also known as "Skeleton tracking". This is because, ideally, a virtual skeleton is projected onto the acquired body image and the 3D location of each joint is tracked to reconstruct the movement in space of the entire subject.

The most recent solution to perform this type of acquisition makes use of AI tools such as Cubemos, Nuitrack, OpenPose and PoseNet.

In detail:

- PoseNet

PoseNet is an open-source code. This AI was coded by making use of TensorFlow, which is a commonly used machine learning library in Python that is developed and maintained by Google. It is designed to be used in real-time with commercial and readily available acquisition systems. There are two versions of this tool: The single person pose detector, which is faster and simpler but requires only one subject present in the image and the multiple persons pose detector. The key points that PoseNet is able to recognize are 17 (Figure 1. 6): eyes, ears, nose, shoulders, knees, wrists, hips, elbows and ankles. It is therefore not able to provide information about hands and feet or some rotations. PoseNet can make use of both the CPU and the GPU. According to the statements of TensorFlow, one of the most appealing aspects of this skeleton tracking tool is its ability, in the presence of multiple individuals, not only to return false pose estimates with less probability, but also to perform almost independently of the number of subjects analysed simultaneously[22].

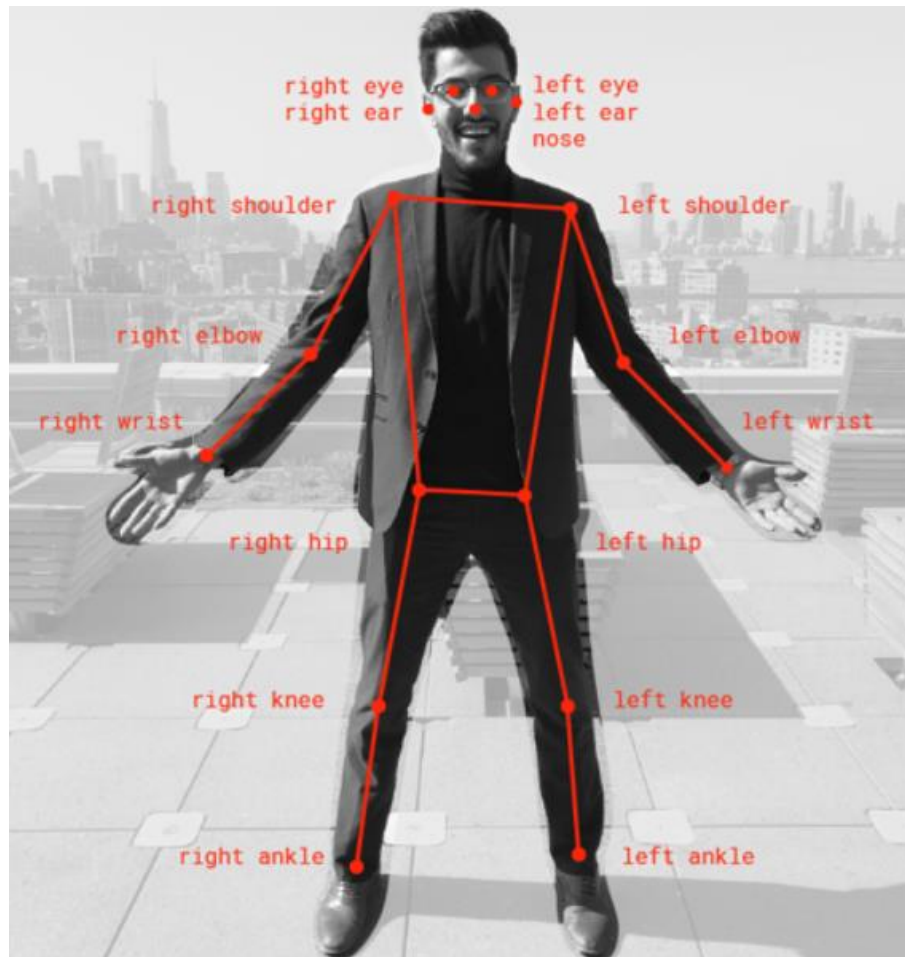


Figure 1. 6 - PoseNet key points and skeleton, [22]

- OpenPose

OpenPose is an open-source code. It is a real-time 2D multi-person estimator. It is based on the usage of a parametric representation called Part Affinity Fields (PAFs), which uses a set of two-dimensional vector fields to identify the portions of the body of all the people in the image.[27]. Currently, 2 models are available in the framework: the COCO MPI model (faster but less accurate) and the BODY 25 model. This skeleton tracking tool is one of the few that can provide a larger and more detailed number of points such as key points on the feet and their angle, Figure 1. 7. The higher the number of points, the lower the performance in terms of sampling frequency. Moreover, it can be used to discern entire body areas instead of only track key points[23].

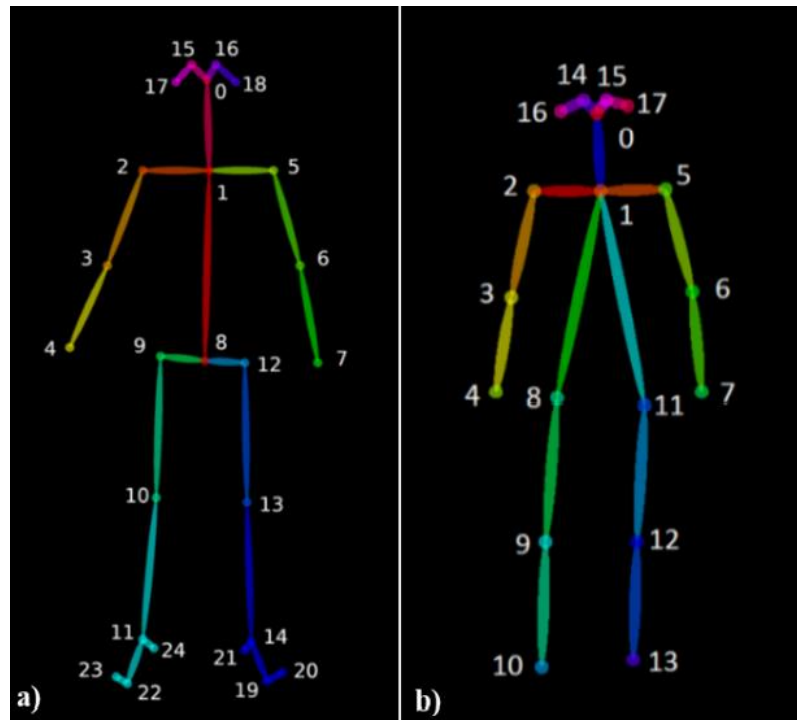


Figure 1. 7 - OpenPose key points and skeletons: a) BODY-25 Model, b) COCO Model, [23]

- NuiTrack

NuiTrack is a closed-source proprietary program. It is an AI that is built on deep learning. It's cross-platform, with 3D full-body skeleton tracking, gesture recognition, and facial tracking capabilities. NuiTrack recognizes 19 key points (Figure 1. 8): it does not track the feet, but it does track the hands.



Figure 1. 8 - NuiTrack key points and skeleton, [24]

- Skeleton Tracking SDK by Cubemos

Skeleton Tracking SDK by Cubemos is a closed-source proprietary program powered by Intel® Distribution of OpenVINO™ toolkit. It is a deep learning-based AI. It is a real-time, cross-platform, multi-person, 3D full-body pose estimator, but its use should be bounded to up to 5 people in a scene. The key points that Cubemos is able to recognize are 18 (Figure 1. 9): eyes, ears, nose, shoulders, knees, wrists, hips, elbows, ankles and spine. It is therefore not able to provide information about hands and feet or some rotations. It can make use of both the CPU and the GPU. As an Intel partner the Skeleton Tracking SDK of Cubemos is meant to be optimal in combination with Intel's products.



Figure 1. 9 - Skeleton Tracking SDK by Cubemos keypoints and skeleton, [25]

2. State Of Art

2.1. Gait Analysis

As mentioned in Chapter 1, the Gait Analysis has several applications also in the neurological field. The reason behind this is the close relationship between muscle activation, human locomotion (especially in the lower limbs), and the ability of the neural network's sensory input to allow articular movement and control of muscular contraction.

The fundamental unit of gait is the Gait Cycle (GC), which is defined as the period between a foot's initial contact with the ground and its next touch with the ground.

During each GC one lower limb propels forward while the other acts as a support and vice versa.

The gait cycle has two phases that can be defined, for a healthy person, as follows (Figure 2. 1) [23]:

- The Stance Phase

it begins with the initial contact of the foot with the ground and represents the period of adjacency to the ground where it supports all or part of the body weight. It represents approximately 62% of the entire walking cycle.

The Stance Phase is further subdivided into two sub-phases:

- a) The phase of weight acceptance, which extends from the beginning to 12% of the CG. This is subdivided even more into:
 - Initial Contact (IC): the moment when the heel of the foot makes contact with the ground (Heel Strike) and continues until the entire sole of the foot is in contact (Foot Flat). The ankle is dorsiflexed, the knee is extended, the hip is flexed, and the centre of gravity is at its lowest point.
 - Loading Response (LR): It begins with a flat foot and progresses until the opposite foot elevates. Knee flexion corresponds to the limb's cushioning response, which allows the body's weight to be transferred to the front leg. The ankle is in plantar flexion, while the hip is still flexed.
- b) The single limb support period, in which the body weight is loaded on one lower limb only. The events that characterise it are:
 - Mid-Stance (MST): The centre of gravity is at its highest position when the swinging limb passes the supporting foot. The ankle is dorsiflexed and the knee and hip begin to extend. This transition ranges from 12% to 31% of the GC.
 - Terminal Stance (TST): ranges from 31% to 50% of the GC, in other words from the lifting of the heel to the contact of the opposite foot with the ground. The calf pushes by pressing on the plantar flexion of the ankle, the knee extends again and then flexes slightly and the hip is more extended.

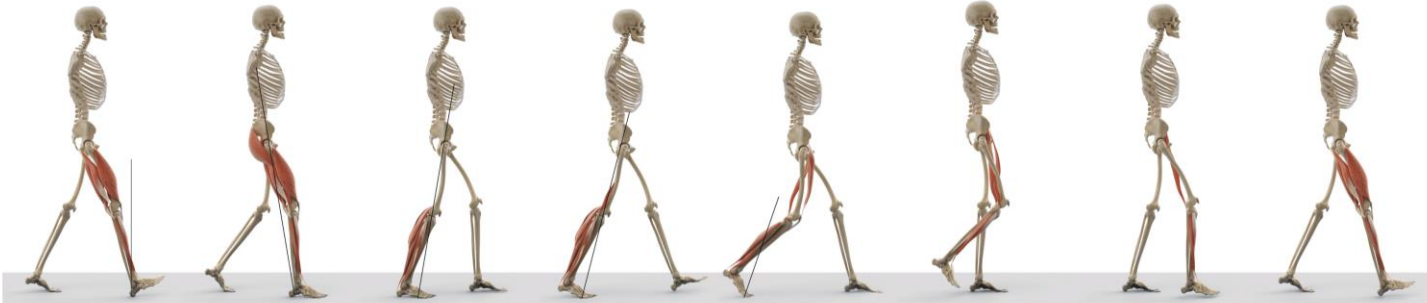
- Pre-Swing (PSW): is the final phase of the stance period, also known as the weight transfer phase, occurs when the foot leaves the ground (Toe-Off) and accounts for 50-62 % of the GC. It is characterized by increased knee flexion and ankle plantar flexion, as well as a loss of hip extension.

– The Swing Phase

The interval during which the foot does not rest on the ground but is in the air and the leg extends towards the next foot contact accounting for the remaining 38% of the stride cycle. It is therefore linked to limb advancement. It constitutes the entire period of step advancement, along with the prior pre-swing sub-phase. It is divided into:

- Initial Swing (ISW): The limb progresses by raising the foot through hip flexion and increased knee flexion, resulting in a period of acceleration (62-75 % GC). It is characterized by a slight dorsiflexion of the ankle.
- Mid-Swing (MSW): starts with both swinging and bearing limbs aligned and ends with the first limb in front of the second (75-87% GC). The hips are flexed even further, the knee is extended, and the ankle is still dorsiflexed.
- Terminal Swing (TSW): It runs from 87% to the end of the overall cycle and is the final phase of the swing but also of the deceleration. Bending the knee completes the limb progression, which finishes when the foot reaches the ground and prepares for the following stance. The hip is flexed and the ankle is dorsiflexed in a neutral position.

The eight phases of human gait cycle



Gait phases	IC Initial Contact	LR Loading Response	MST Mid Stance	TST Terminal Stance	PSW Pre Swing	ISW Initial Swing	MSW Mid Swing	TSW Terminal Swing
Gait cycle	0 %	0 – 12 %	12 – 31 %	31 – 50 %	50 – 62 %	62 – 75 %	75 – 87 %	87 – 100 %
Hip	20° flexion	20° flexion	0° flexion	-20° hyperextension	-10° hyperextension	15° flexion	25° flexion	20° flexion
Knee	0° – 5° flexion	20° flexion	0° – 5° flexion	0° – 5° flexion	40° flexion	60° – 70° flexion	25° flexion	0° – 5° flexion
Ankle joint	0°	5° – 10° plantar flexion	5° dorsal flexion	10° dorsal flexion	15° plantar flexion	5° plantar flexion	0°	0°
Muscle activity	M. quadriceps femoris M. tibialis anterior M. gluteus medius M. gluteus maximus Ischiocrurale Muskulatur	M. quadriceps femoris M. tibialis anterior M. gluteus medius M. gluteus maximus M. adductor Magnus M. tensor fascia latae M. tibialis posterior M. peroneus longus	M. gastrocnemius M. soleus	M. soleus M. gastrocnemius M. flexor digitorum longus M. flexor hallucis longus M. tibialis posterior M. peroneus longus M. peroneus brevis	M. soleus M. gastrocnemius M. rectus femoris M. adductor longus	M. extensor hallucis longus M. flexor hallucis longus M. sartorius M. iliacus M. tibialis anterior	M. semimembranosus M. semitendinosus M. biceps femoris M. tibialis anterior	M. quadriceps femoris M. semitendinosus M. semimembranosus M. biceps femoris M. tibialis anterior
Functions	• heel contact to the ground	• shock absorption in knee and ankle joint • load transmission and stability in the hip • forward motion by heel rocker	• controlled forward motion of the tibia • shifting of the gravity centre to the front by ankle rocker	• controlled dorsal extension at the ankle joint with lifting the heel from the ground	• passive knee joint flexion of 40° • plantar flexion of the ankle joint	• min. 55° knee flexion for sufficient ground clearance	• increasing hip flexion to 25° • dorsal extension of the ankle joint to neutral-zero-position	• knee joint extension to neutral-flexion • preparation for stance phase

Figure 2. 1 - Phases division of Human Gait Cycle, [35, 40]

Anatomically, the joints involved in GC, in brief, are (Figure 2. 2)[23]:

– Hip

It has 3 degrees of freedom.

- In the sagittal plane, it has the greatest range of motion (0-140° flexion and 0-15° extension) and reaches maximal flexion during the swing phase, when the foot detaches.
- In the frontal plane, abduction and adduction of approximately 0-25° and 0-30°, respectively, are allowed.
- In the transverse plane, internal and external rotation are both allowed. During the static phase, the hip is almost always internally rotated, then externally rotated at the end.

– Knee Joint

It is composed of the tibiofemoral and patellofemoral joints. The first joint allows movement in all three planes, especially in the sagittal plane which offers flexion-extension from 0° to 140°. [30].

- In the sagittal plane, Knee extension is present with a flexion-extension range of approximately 0° to 70°.
- In the frontal plane there is maximum abduction up to maximum flexion in the Mid-Swing phase
- In the transverse plane, external rotation begins during knee extension in the stance phase and peaks at the end of the swing phase. Internal rotation in the transverse plane and adduction in the frontal plane occur in tandem with flexion in the swing phase.

– Ankle joint

It is divided into the tibiotarsal joint, the proximal tibiofibular joint and the distal tibiofibular joint. They have fewer degrees of freedom. The first, for example, only allows dorsal and plantar flexion in the sagittal plane.

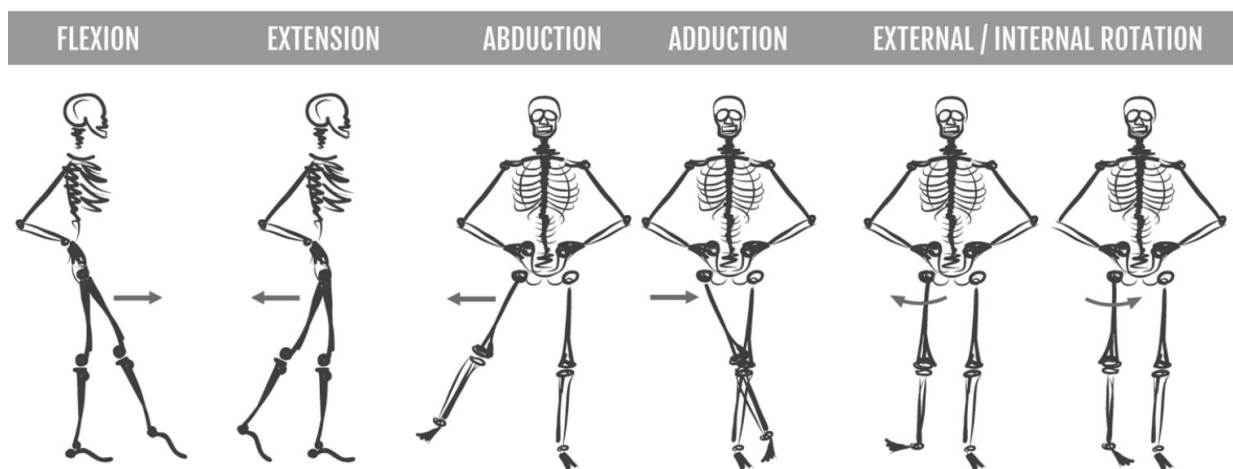


Figure 2. 2 - Example of the possible movements of the joints, [23].

In the literature, Gait Analysis provides three categories of parameters for the evaluation of the gait cycle. Although there are no well-defined official canons on the values to be provided by the analysis, there are some gold standards:

- Spatial-temporal and static parameters (Figure 2. 3)

They allow an initial evaluation of the average characteristics of the GC. They are divided into:

 - a) Temporal

They provide the average timing of the events of a GC. They include: the cadence [steps/min]; the time span, expressed as a percentage, of each GC phase mentioned above; the patient's speed, which can be expressed in several ways (either in [m/s] or as a proportion of height [%height/s]); and the total duration of the GC [s]. Sometimes emphasis is also put on the duration of the total support phase in [s] and the total swing phase in [%height/s].
 - b) Spatial

They provide the average distances covered in a cycle. They include step length and width expressed in [m] and cycle length which can be expressed in various ways (either in [m] or as a proportion of height [%height]).
 - c) Standing Angles

They represent the static measures of Gait Analysis. In the typical GC study technique, their acquisition provides clinically key info. They are rarely expressed in [deg] or [rad], although they are frequently represented in [grad]. They include, in the case of the BTS Motion Analysis Lab: pelvic obliquity; pelvic tilt; pelvic rotation; hip abduction or adduction; hip flexion-extension; hip rotation; knee flexion-extension; ankle dorsiflexion or plantarflexion; foot progression.
- Kinematic parameters (Figure 2. 4, Figure 2. 6)

They provide a clinical evaluation for Gait Cycle analysis, already to a significant extent, when combined with the previous dataset. They are frequently provided in the form of a 2D matrix. One of the two dimensions represents the planes (frontal, sagittal, transverse). The matrix is then completed by the ordered inclusion of kinematic information associated with the same angles acquired in the static phase. In addition, kinematic data related to the obliquity of the trunk (in the data sector dedicated to the frontal plane), the tilt of the trunk (in the data sector dedicated to the sagittal plane), the rotation of the trunk (in the data sector dedicated to the frontal plane), the varus-valgus of the knee (in the data sector dedicated to the frontal plane), the rotation of the knee (in the data sector dedicated to the frontal plane), the rotation of the knee (in the data sector dedicated to the transversal plane) are provided. It's also typical to see values in [grad] here.
- Kinetic parameters

They are formed by the moments associated with certain angles in the kinematic analysis in the sagittal plane. They constitute the data set that completes the entire Gait Analysis, along with the ground reaction forces (Figure 2. 5). However, they are not always provided as they require instruments for measuring the dynamic information different from those already used and sufficient to obtain the data described above. Estimates of these parameters based on kinematics and anthropometric data (including weight) are sometimes used, although they lack the same level of accuracy and precision as data obtained through direct measurement.

Finally, it is usual to represent these measurements in comparison with the range of average normal values of the patient considered healthy. Although the assessment of the GC cannot be limited to a comparison of the acquisitions with those that in the literature are associated with a patient without motor pathologies, it must provide the basis for a correct and contextualised clinical diagnosis.






<div>      </div>			
Parametri Temporal	ARTO DX	ARTO SX	NORMALITA'
Durata del ciclo (s):	1.14 ± 0	1.16 ± 0	1.1 ± .09
Durata dell'appoggio (s):	0.68 ± 0	0.71 ± .02	0.65 ± .07
Durata dell'oscillazione (s):	0.47 ± 0	0.46 ± .02	0.44 ± .05
Fase di appoggio (%):	59.39 ± .26	60.52 ± 1.55	58.98 ± 1.97
Fase di oscillazione (%):	40.61 ± .26	39.48 ± 1.55	40.03 ± 3.56
Fase singolo supporto (%):	40.17 ± 1.57	39.92 ± .25	38.87 ± 2.57
Fase doppio supporto (%):	10.91 ± .49	9.03 ± 2.18	10.27 ± 3.09
Velocità media (m/s):	1.2 ± .1		1.2 ± .2
Velocità media (%altezza/s):	64.7 ± 2.84		80 ± 5
Cadenza (passi/min):	103.8 ± .6		114 ± 4.2
Parametri Spaziali	ARTO DX	ARTO SX	NORMALITA'
Lunghezza del ciclo (m):	1.33 ± .06	1.32 ± .06	1.36 ± .11
Lunghezza del ciclo (%altezza):	74.98 ± 3.44	74.16 ± 3.38	80 ± 10
Lunghezza del passo (m):	0.67 ± .02	0.65 ± .04	0.62 ± .05
Larghezza del passo (m):	0.05 ± .02		0.08 ± .05
Angoli di Standing	ARTO DX	ARTO SX	
Obliquità pelvica (grad):	2.6 ± .5	-2.6 ± .5	
Tilt pelvico (grad):	6.6 ± .2	6.6 ± .2	
Rotazione pelvica (grad):	-6 ± .3	0.6 ± .3	
Abd-Adduzione anca (grad):	11.4 ± .5	2.4 ± .6	
Flesso-Estens anca (grad):	2.1 ± .3	0.5 ± .3	
Rotazione anca (grad):	41.7 ± .4	25.7 ± 1	
Flesso-Estens ginocchio (grad):	4.7 ± .2	-4 ± .7	
Dorsi-Plantifless caviglia (grad):	12.4 ± .1	7.7 ± .3	
Progressione del piede (grad):	-1.1 ± .1	-3.4 ± .2	
Acquisizioni Valutate:			

Figure 2. 3 - an example of Spatial-temporal and static parameters from BTS GAITLAB

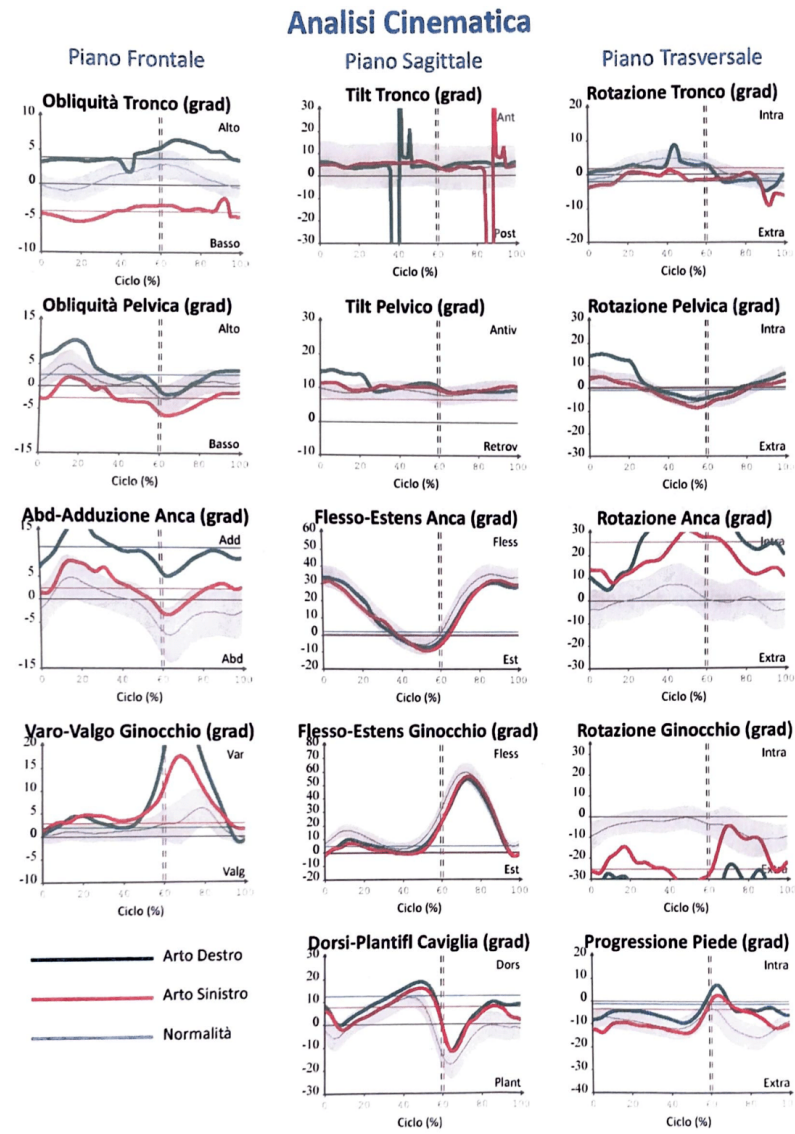


Figure 2. 4 - an example of the Kinematic Parameters matrix from BTS GAITLAB: The grey area stands for the normal range of values, the other colours represent the left and right limb acquisitions of the specific patient

Forza di Reazione al Suolo

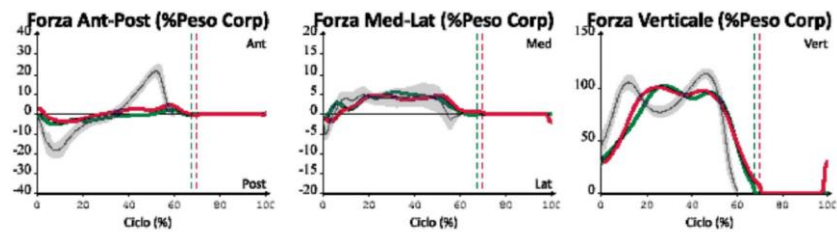


Figure 2. 5 - an extract of Kinetic Parameters plots from BTS GAITLAB

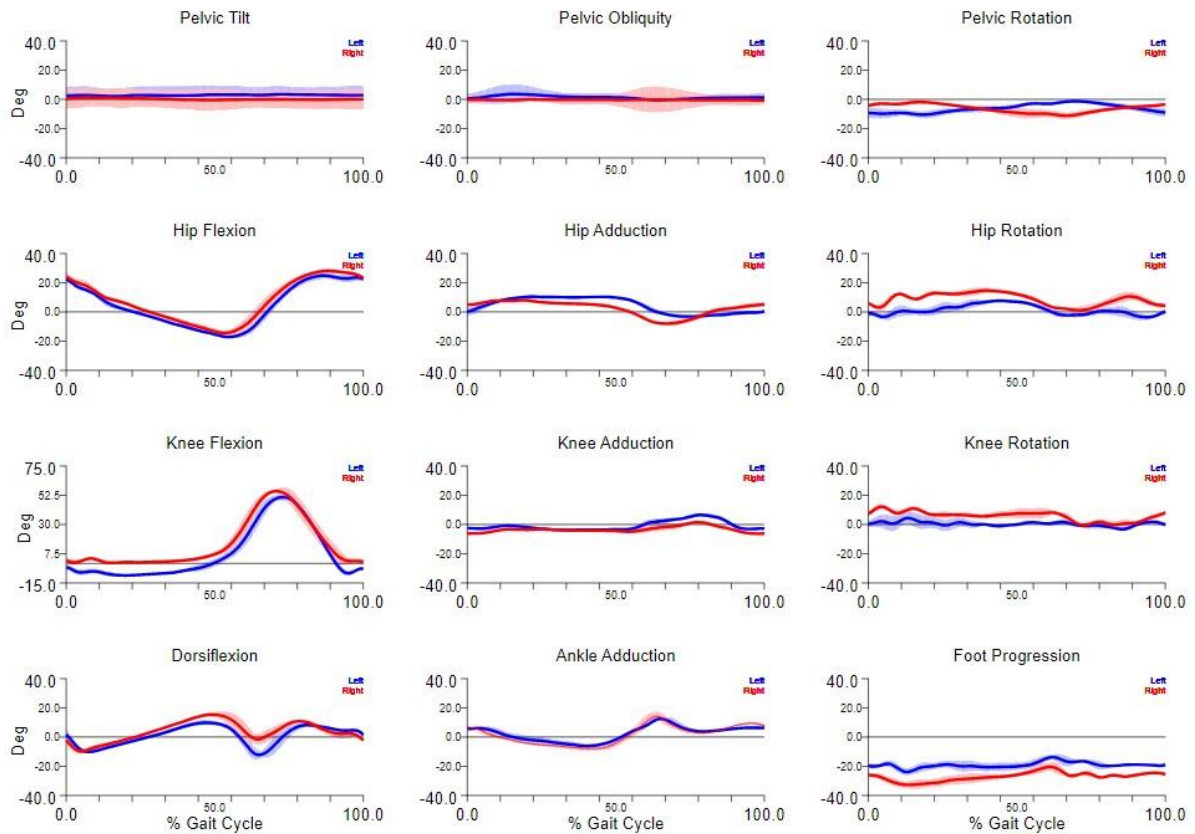


Figure 2. 6 - an example of the Kinematic Parameters matrix from Ball State Biomechanics Laboratory: “Joint angles of the pelvis, hip, knee, and ankle normalized to the gait cycle. The first column represents sagittal plane motion, the second column represents frontal plane motion, and the third column represents transverse plane motion.”, [42]

2.2. Traditional gait analysis

Human movement and its alterations can be assessed with various techniques. Depending on the needs and contexts, evaluations can be qualitative or quantitative with the application of different systems or instruments.

Although qualitative assessments are still common, there is no doubt that instrumental measurements, including cheaper ones, are more reliable and objective. Therefore, in recent years the approach for gait analysis has shifted from a qualitative to an almost entirely quantitative method. This type of evaluation avails itself of analysis tools that are divided into two macro-categories: optical and non-optical systems. [23, 39]

- Non-optical systems

- a) For kinematic analysis:

- Instruments that are magnetic, inertial, or electromechanical. These include different types of electro-goniometers that measure both 2D and 3D angular movement of joints; accelerometers that deduce angular and linear movements of joints up to six degrees of freedom from accelerations. [31, 32]

b) For dynamic analysis:

Dynamometric and pressure plates. Consisting of strain gauges or piezoelectric transducers to acquire information associated with the forces applied in the path and the movement that generated them.[33]

c) For electromyographic analysis:

Electromyographic sensors (EMG). They provide a measure of the action potentials generated by motor units and an index of the neuromuscular activity behind the movement. [33]

– Optical systems:

These are Optoelectronic Systems based on the principles of stereophotogrammetry (Figure 2. 7).

At the HW level, cameras that can acquire images at different light frequencies and markers are used for image acquisition.

In detail:

a) The number of cameras varies depending on the analysis to be carried out.

Typically, the number of cameras is around ten and can reach fifty. Mathematically speaking the number of devices must be at least 2 for a 3D reconstruction through image triangulation or through the use of information on different spectra (such as the combo depth camera + RGB). The greater the quantity of instruments in use, the greater the quality and frequency of acquisitions without the need for complex reconstructions or filtering at the software level.

By means of the motion tracking techniques mentioned above, it is possible to obtain the evolution of the position over time of each point traced by the markers and associate them with a model of the human body to trace the patient's three-dimensional movement.

b) Markers can be passive or active

- Passive markers typically have a spherical or hemispherical shape coated with a retroreflective material to reflect light or a specific frequency of light. They are often used for a system that also works in the infrared (IR) to reduce the number of possible disturbances for acquisition.
- Active markers, instead, are powered by a battery and have an LED (that usually emits in infrared light as well). Larger or more expensive than the passive solution, they halve the distance that light must travel to be captured by cameras.

At the SW level, the aforementioned motion tracking techniques with computer vision are used. In detail, some image processing techniques such as linear threshold, morphological operators and so on can be used for this task.[34]

Among the Gait Analysis systems that exploit the gold standard procedures, the best known are: Vicon, Optotrack and BTS Motion Analysis Lab.

The BTS as a representative mechanism will be discussed further down. The BTS GAITLAB is a motion-tracking-specific laboratory model. It employs at least 8 infrared cameras, 6 sensor platforms, 8 electromyographic sensors, 2 RGB cameras, at least 20 markers, and computer vision software (Figure 2. 8) [41].

For the acquisitions, the system follows clinical protocols that have been well-established in the literature. Each acquisition is preceded by two phases of preparation: One is done on a daily basis for system recalibration, and the other is done before each patient's analysis.

The recalibration phase is divided into a part dedicated to cameras, one for pressure plates and another for EMGs.

The first sub-phase is divided into a dynamic section that consists of multiple acquisitions “empty” of an operator who moves a wand consisting of markers and a static section in which a new system of Cartesian axes is manually rearranged through video recordings of an object consisting of 3 of the above-mentioned wands, identical, arranged orthogonally to each other and generally positioned in a standard point of the room to make the analyses compatible (Figure 2. 9, Figure 2. 10).

The second sub-phase consists in indicating to the processing software the precise arrangement of the pressure plate in relation to the Cartesian plane generated previously (Figure 2. 11).

The third and last sub-step is optional, and it is determined by whether the use of EMG sensors is needed. It consists in their activation and in a quick check of the correct functioning of each emitter and receiver (Figure 2. 12).

The preparatory phase for each session consists in creating the specific setup for the analysis of the patient. It requires the acquisition of anthropometric measurements and the simultaneous selection and demarcation on the skin of the areas of the patient's body that will be covered by EMG sensors (Figure 2. 13). It is sometimes associated with a simultaneous depilation of the areas involved for an optimal acquisition of muscle signals (Figure 2. 14).

This is followed by the marker positioning phase which must be consistent with the clinical protocol chosen for the analysis of the patient's images. This is the most critical phase of the setup. The protocol is then indicated in the analysis software (the most used is the Davis or a variant of it but recently new protocols specialized in the joint measurement of back movements have also appeared) (Figure 2. 15).

After a further optional check of the EMG signals, the acquisition of the actual step is carried out with a section dedicated only to the static standing phase.

The walk is then recorded and the foot contact event with the ground and the associated optimal gait cycle are manually selected off-line. For each recording, the information of a single step cycle is used (the most correct according to the operator). Finally, it is checked that each foot has rested

correctly, completely on the area inside the frame of the platforms and the software indicates by hand which foot has come into contact with the platform (Figure 2. 16).

The analysis session ends with the creation of a file that summarizes the average behaviour of the patient's gait cycle.

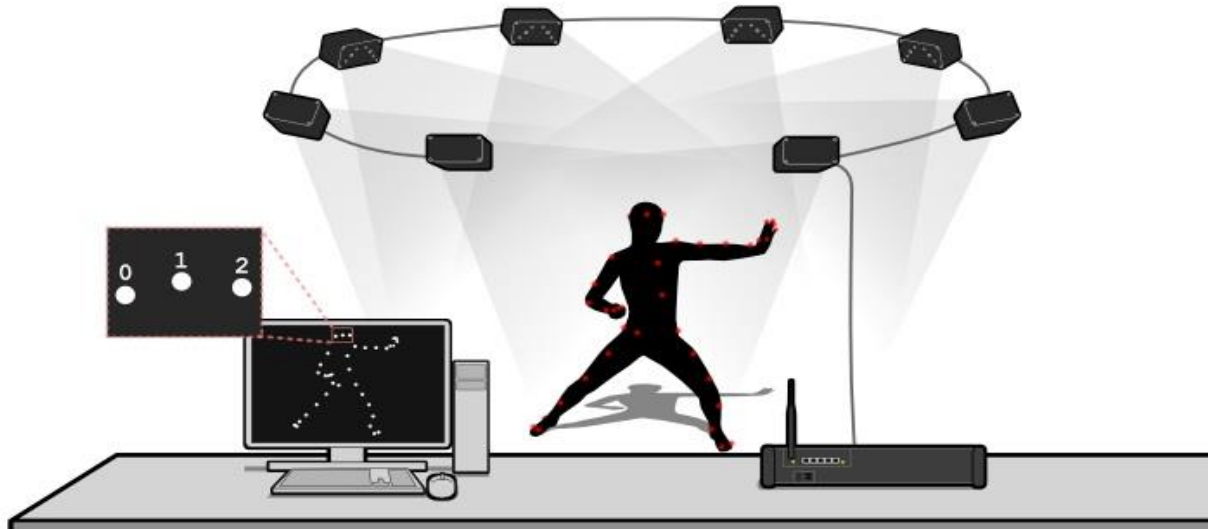


Figure 2. 7 - Illustration of a motion capture system with stereophotogrammetry, [34, 43]



Figure 2. 8 - some of the BTS GAITLAB basic tools, [41]

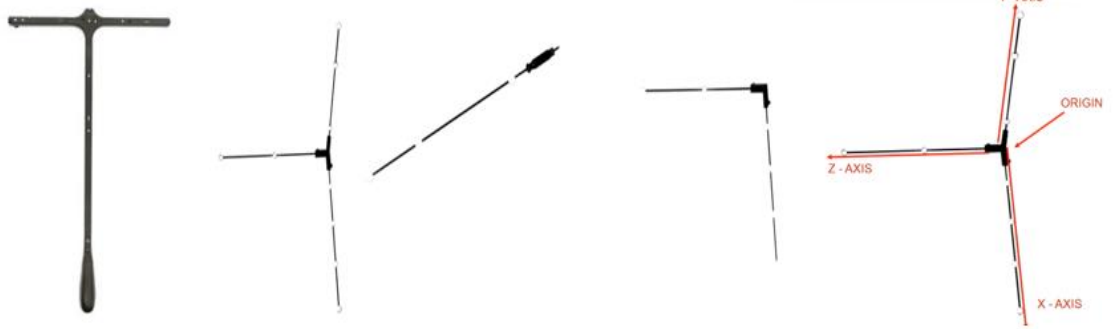


Figure 2. 9 - on the left: Vicon Active Wand, [45]; in the middle: BTS passive Wands, [44]; on the right: cartesian axes associated with the BTS Wands, [44]



Figure 2. 10 - on the left: BTS cameras dynamic daily setup and calibration; on the right: BTS cartesian frame setup, [44]



Figure 2. 11 - BTS digital sensory floor setup, [44]



Figure 2. 12 - BTS EMG sensors activation, [44]

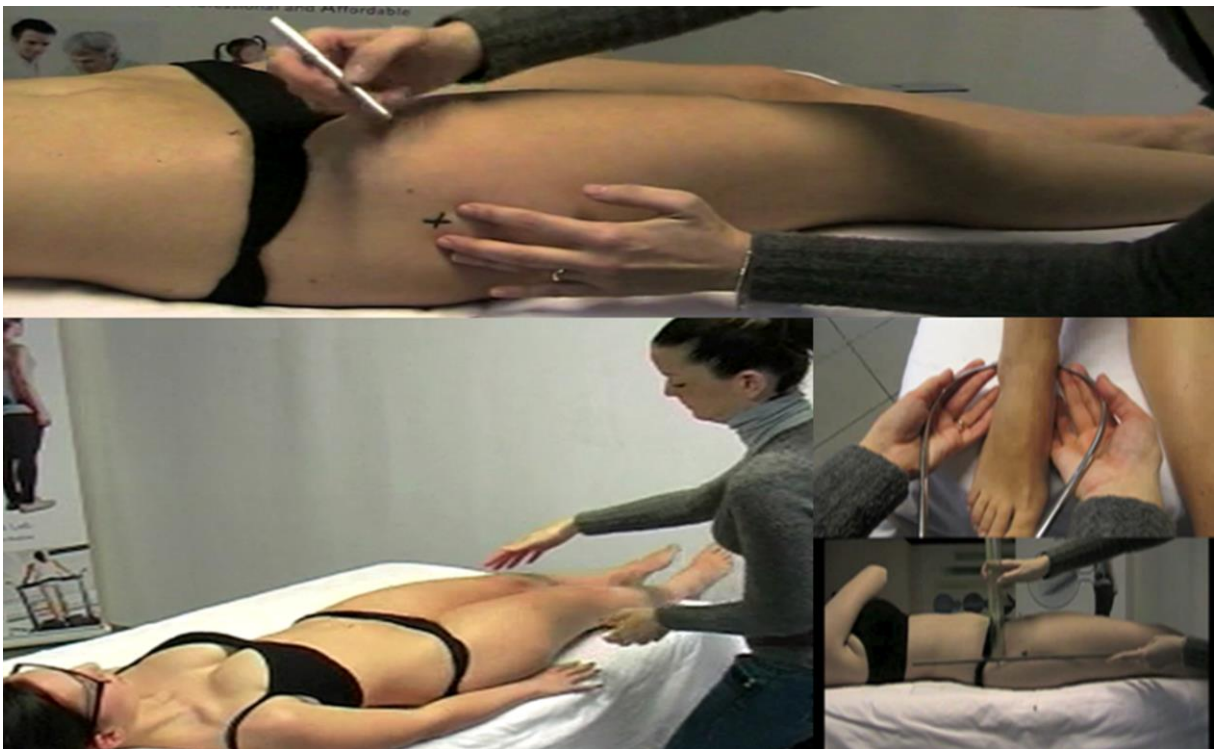


Figure 2. 13 - anthropometric measurements and skin demarcation, [44]

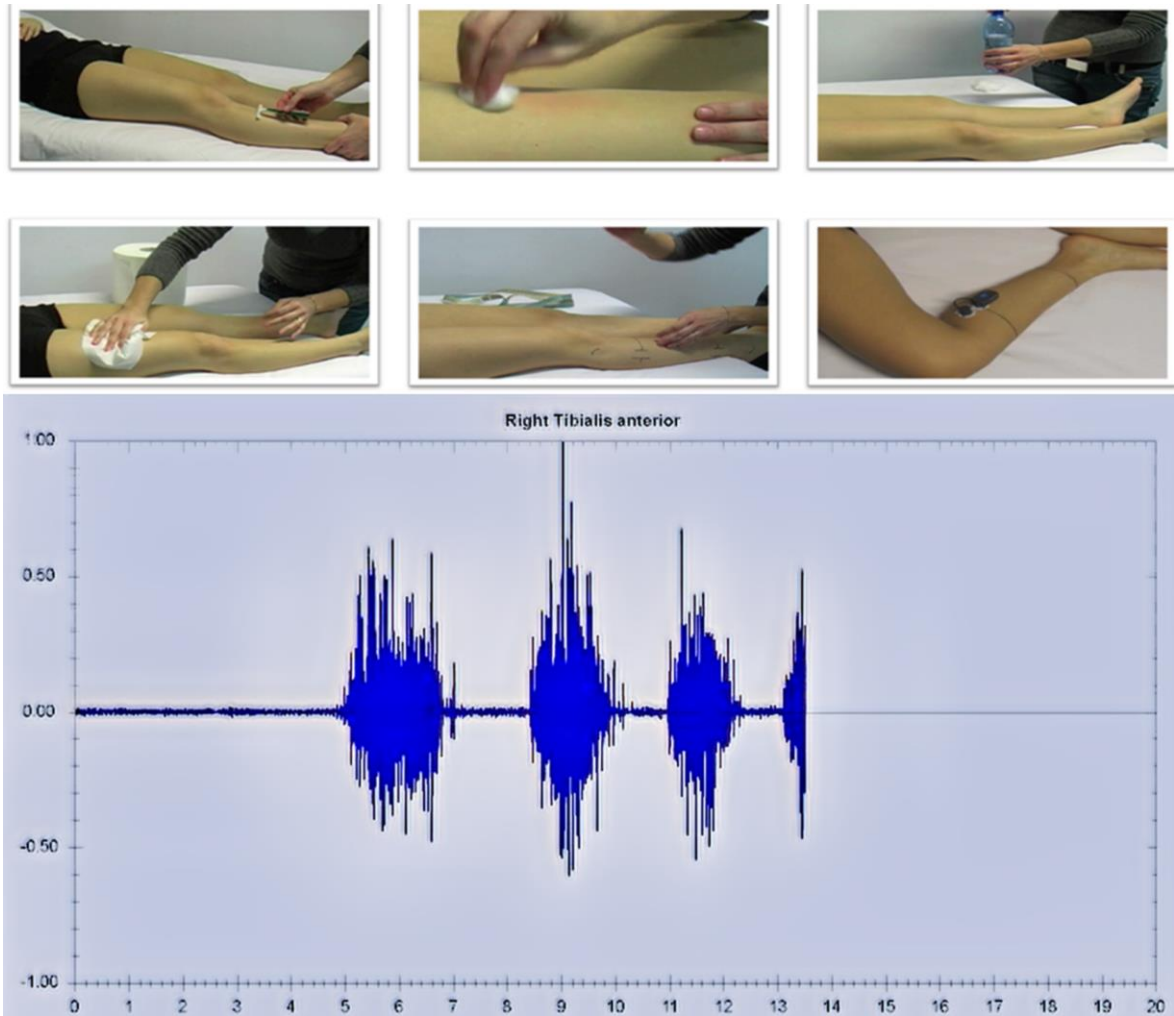


Figure 2. 14 - EMG sensors positioning routine and signal, [44]

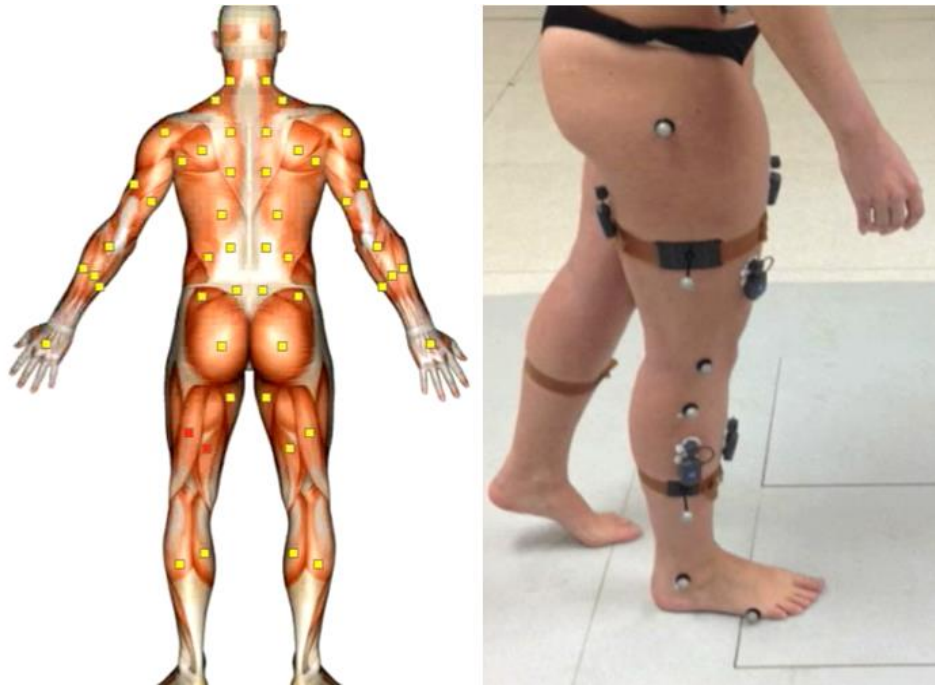


Figure 2. 15 - on the left: Marker Davis Protocol; on the right: a section of the patient fully covered with markers and EMG sensors, [44]

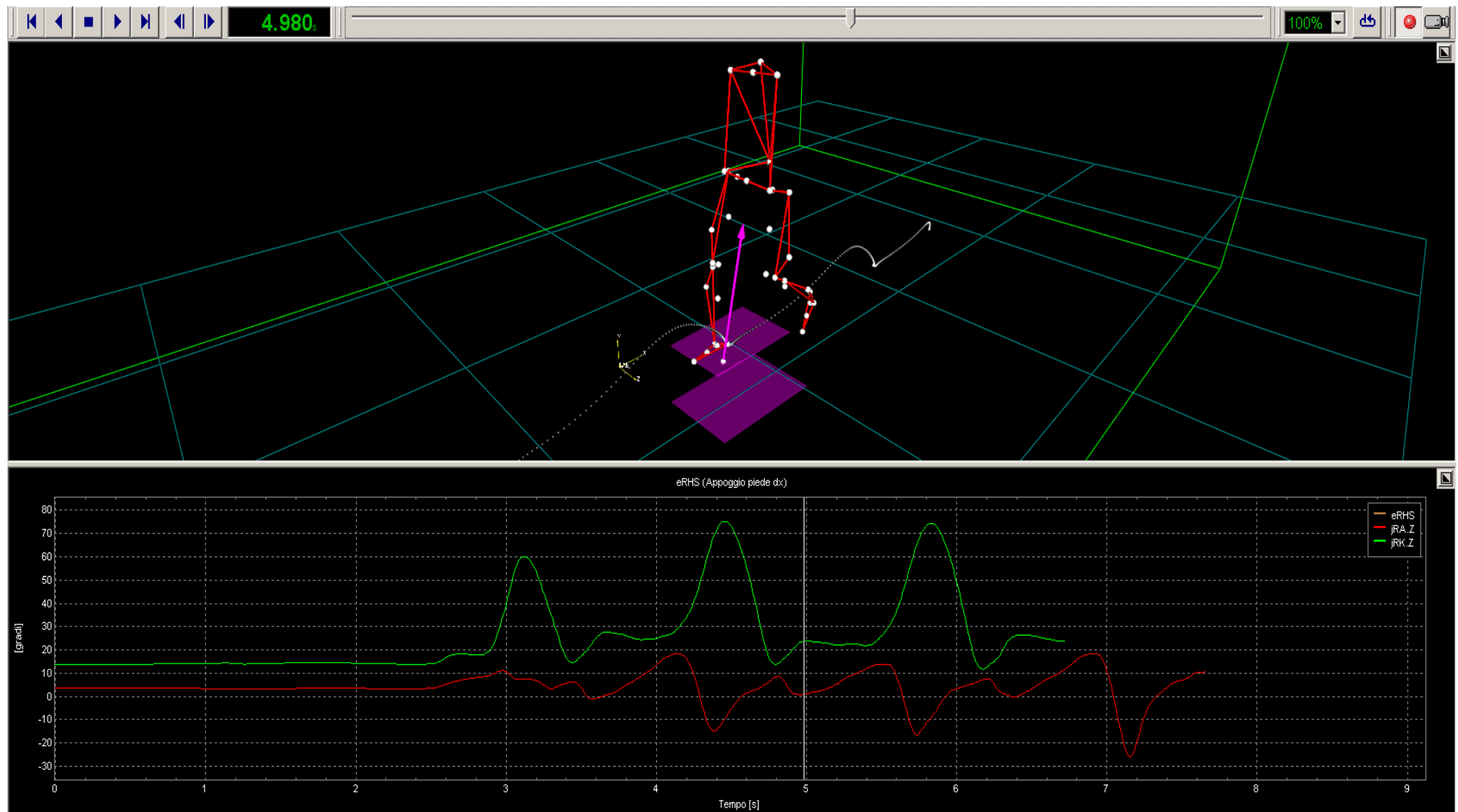


Figure 2. 16 - BTS Gait acquisition and manual heel strike detection, [44]

2.3. Automatized gait analysis

In response to the standard solutions described so far, many, increasingly high-tech, alternatives have emerged in recent years. In the field of automation, attempts have been made to provide various yardsticks for the evaluation of the gait while avoiding human error as much as possible.

Attempts have been made at the research level to provide data other than the gold standard [33], in order to recognise attitudes typical of certain diseases without a complete gait analysis. One simple example is an academic study aimed at recognising Parkinsonian attitudes and related neurodegenerative diseases. In this case, a study of acquisitions using offline Image Processing and the opensource AI TensorFlow was proposed. The finished product provides in a completely automatic way 3 values in percentage: "Upper body inclination rate", "Arms inclination rate", "Knees inclination rate". These behaviours cannot be associated with a standard Gait Analysis but are qualitatively useful indicators and above all a form of automation. [35]

Going from academic citation to commercial applications, among the products taken into consideration there is PosturaLab 3D. The analyses provided by the projects of this laboratory achieve a high level of automation while maintaining a clinically acknowledged output. In this case, the laboratory itself provides several alternatives for automated gait analysis: a solution implementing AI in combo with multiple Kinect cameras is still under development; a portable solution using a computer vision system with marker and portable platform; a stationary solution, the company's flagship, with a treadmill equipped with sensors and a 12-camera setup, also based on computer vision (Figure 2. 17). Each acquisition, even in this case, involves a preparatory phase that includes anthropometric measurements and the positioning of the markers on the patient, as well as the setting of the clinical protocol associated with the chosen arrangement of the markers. Moreover, in the case of the portable system, a standing position acquisition is used to reconstruct the relative 3D position of all the markers on the patient to avoid an excessive reduction of the information loss in the walking blind spots. The output is in this case completely automatic and does not require the selection of the gait cycle by the operator, the dynamic information provides not only the total vector of the standing position, but a whole vector field of the weight distribution on the ground. The instrumentation used is deliberately redundant and with a high sampling frequency to provide, especially in the case of the non-portable system, a high level of accuracy and reliability of the data. [36]

Finally, there are forms of automation that do not involve the use of computer vision but wearable sensors.

The study by the Intelligent Automation Laboratory of the Department of Electrical Engineering at the Federal University of Espirito Santo in [37] (Figure 2. 18).

The system involves the use of a UEFS smart-walker in combination with MARG sensors from a previous study [38] and Laser Range Finder sensors. The project is able to provide a real-time analysis of walking at a low sampling rate, fully automated through the support of MATLAB real-time, Python and PyQt for graphical interface.

The use of the walker and low-cost wearable technology can provide access to analysis not only in an ambulatory setting, but also at home. These types of analysis are not exempt from problems which will be introduced in the next chapter along with possible alternatives.

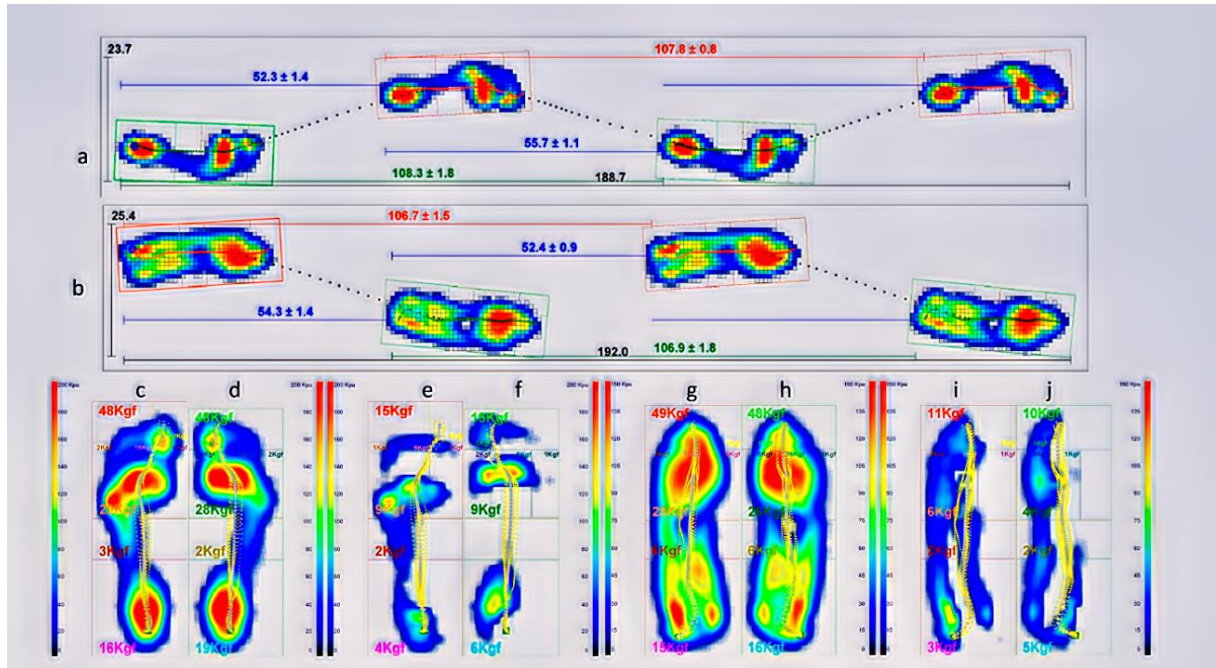


Figure 2.17 - PosturaLab baropodometric analysis and weight distribution, [36]

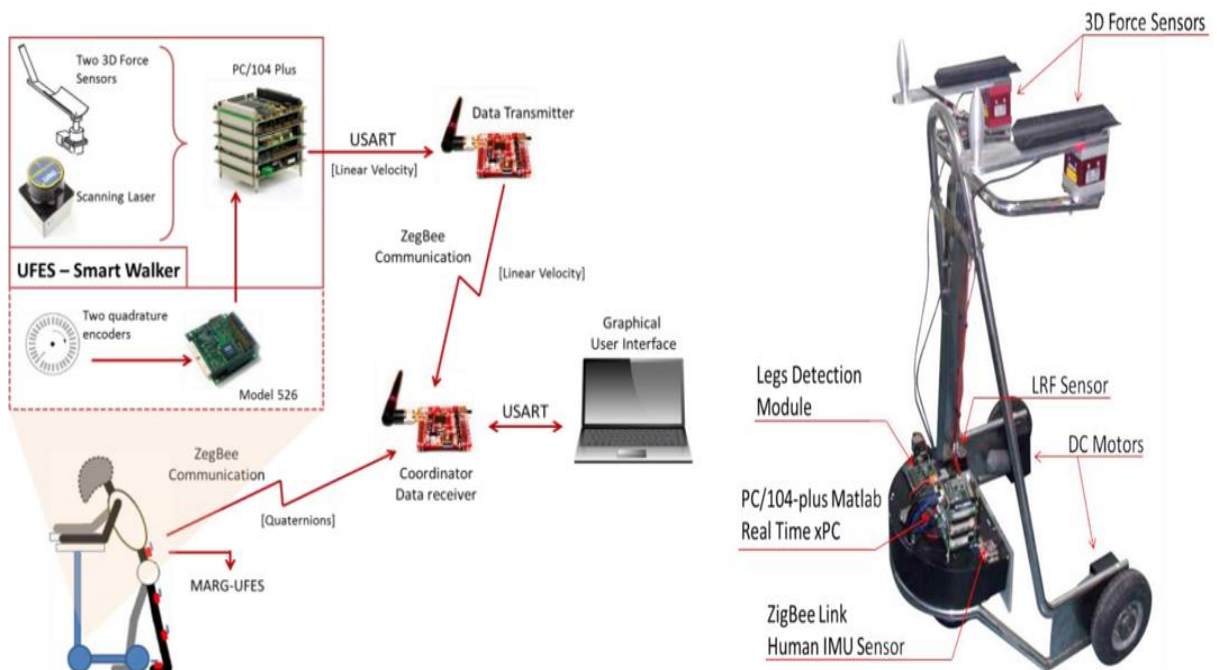


Figure 2.18 - UFES's smart walker system, [37]

3. AI-assisted Gait analysis

3.1. Attached problem

As mentioned in the previous chapter, each device used for gait analysis has its own strengths and weaknesses. Among the basic non-optical instruments there are often difficulties deriving from their own nature: since they must be applied directly to the human body, non-optical devices are prone to placement errors by the operator, who has to be well trained. Furthermore, any type of friction might compromise the wearable arrangement, and tissue movement makes sampling unstable. All instruments, whether magnetic, inertial or electromechanical, are not a priori compatible with every kind of patient or area to be examined.

Many of them, and in particular electrogoniometers, often present crosstalk problems. Regarding dynamometric platforms, although they do not suffer from the problems associated with wearability, they are constrained, on the other hand, by the sampling perimeter: here, it is no longer possible to enjoy an unlimited space for analysis and the heel strike is conditioned by the patient's need to fully centre the acquisition plates with his foot. They do, however, provide low-cost, low-computing-complexity measurements that do not require acquisition in a limited area.

Normally Surface electromyography (sEMG) sensors are used in parallel with other sensors to understand muscle activation while walking. sEMG sensors known for their highly disturbed signal, sometimes invasive and sometimes requiring special treatment following skin demarcation during anthropometric measurements.

SEMGs provide support data for analyses that would otherwise be unobtainable, and dynamometric platforms, in particular the most advanced ones, greatly facilitate the recognition of gait stages by producing dynamic data and vector fields in the stance phase, often with high precision.

For these reasons, research is still pushing in recent years to find more and more ergonomic, comfortable, miniaturised, biocompatible and less perceivable solutions in order not to alter the measurements and to combine the analysis with the actions of daily life to minimise the stress of the patient and enrich the data set on movements performed in the most varied contexts.

Many non-optical data may still be estimated using the accelerometers and gyroscopes built into mobile phones, allowing for a first level of evaluation of movement performance that is not clinically sufficient but beneficial for an initial analysis.

As accuracy and complexity increase, fully portable and wearable technologies that can be incorporated into daily apparel become possible. These non-optical systems belong to a separate category; they are more complex, recent, and advanced, and are often integrated with software at various levels: from lowest level for real-time hardware management, to the highest level for data analysis and reconstruction, which however rarely takes advantage of machine learning techniques for this purpose.

Some examples among all are Xsens MVN [46] based on inertial sensors (Figure 3.2) or the wireless M3D gait analysis system developed by Tec Gihan Co [47] (Figure

3. 1), flexible platforms equipped with sensors to overcome the limitation of dynamometer plate frames or soles equipped with sensors such as piezoresistive pressure sensors by FlexiForce [33] or the Veristride insoles (Figure 3. 3) developed by Bamberg *et al.* [48] to overcome both criticalities of fixed dynamometer plates.

However, per capita costs and consumption for a gait analysis are raised, the motion estimation algorithms become more complex, the signals are always susceptible to external disturbances and the motion itself, and the power supply, size and battery life remain limiting factors. Furthermore, as with the UEFS smart-walker in combination with MARG sensors, real-time data is provided with a lower sample rate due to the hardware restrictions of a compact wearable system.

The category of systems with quantitative, semi-subjective or fully qualitative techniques forms a universe of its own with its advantages and disadvantages that are heavily dependent on specific cases. In general as in the case of the research of Pirlo, G., & Luigi [35], the T25-Fw method, the MSWS-12 method, the POMA test, etc. [49-52], whatever the means used for the analysis, if on one hand they have the advantage of providing results that are less purely mathematical and closer to the act of diagnosis; on the other hand, for the same reasons, they cannot be considered sufficient for a rigorous evaluation, as they are hardly comparable and repeatable. Furthermore, the last of the mentioned ones have varying levels of reliability and accuracy and are susceptible to changes in the types of population under examination.

There are many different types of optical systems such as those mentioned in Chapter 2, but the vast majority share the same pros and cons. In general, stereophotogrammetry and basic optoelectronic systems, which rely only on computer vision software, are extremely susceptible to instrumental, human and systematic errors in setup. In addition, these systems have many of the same shortcomings as wearable systems due to markers, both passive and active, although in this case they can be fixed by supporting software and the variety of visual feedback. They are typically extremely expensive, require specialized infrastructure and personnel, have long analysis times, and do not allow for observations in non-clinical contexts.

However, these systems excel in accuracy in the acquisition phase and often have a high sampling rate. Moreover, they often do not need any signal reconstruction due to systems that synchronise the data of a high amount of cameras. A more detailed description will be provided in the section dedicated to BTS GAITLAB.

For a comparison on the vast world of Gait Analysis using optical systems, the study by Alvaro Muro-de-la-Herran *et al.* [33] gives an example table of the advantages and disadvantages of the systems that can be categorized in this field (Table 1).

Table 1 - Optical Systems comparison based on depth measurement performance, [33]

Method	Advantages	Disadvantages	Each Sensor Price (€)	Ref.	Accuracy
Camera Triangulation	<ul style="list-style-type: none"> - High image resolution - No special conditions in terms of scene illumination 	<ul style="list-style-type: none"> - At least two cameras needed - High computational cost 	400 to 1,900	[53,54]	70% [54]
Time of Flight	<ul style="list-style-type: none"> - Only one camera is needed - It is not necessary to calculate depth manually - Real-time 3D acquisition - Reduced dependence on scene illumination 	<ul style="list-style-type: none"> - Low resolutions - Aliasing effect - Problems with reflective surfaces 	239 to 3,700	[33]	2.66% to 9.25% (EER) [33]
Structured Light	<ul style="list-style-type: none"> - Provide great detail - Allows robust and precise acquisition of objects with arbitrary geometry and a wide range of materials - Geometry and texture can be obtained with the same camera 	<ul style="list-style-type: none"> - Irregular functioning with motion scenes - Problems with transparent and reflective surfaces - Superposition of the light pattern with reflections 	160 to 200	[55,56]	<1% (Mean diff) [56]
Infrared Thermography	<ul style="list-style-type: none"> - Fast, reliable & accurate output - A large surface area can be scanned in no time - Requires very little skill for monitoring 	<ul style="list-style-type: none"> - Cost of instrument is relatively high - Unable to detect the inside temperature if the medium is separated by glass/polythene - Emissivity problems 	1.000 to 18.440	[57]	78%–91%

In the case of more advanced optical systems such as those proposed by PosturaLab 3D, the benefit of simpler, automated, relatively faster and slightly lower cost analyses is beginning to emerge. The decision to continue using marker and computer vision systems preserves the high levels of quality and accuracy of output, but also the critical issues associated with the patient preparation phases and those intrinsic to the nature of markers. Automation in the analysis phase significantly reduces subjective operator errors, increases test repeatability, optimises acquisitions, and exploits the maximum number of gait cycles available.

In order to investigate the difficulties associated with the gold standard analysis methods, the BTS will again be used as a representative system below describing all the procedure in detail.

Let us start with the calibration phase. The negative aspects of this phase are among the least impactful. Both the reset phase of the Cartesian system and the check of the correct functioning of the cameras can require variable time spending to make sure that the whole acquisition volume perceives all markers correctly with the right conventions, as similar as possible to those used for the previous tests. This step may not, for convenience, be executed as often as planned on a daily basis, but at the cost of a loss in rigor and an increased risk of incorrect acquisition in the actual analysis phases.

Follows the patient preparation phase. Here there is not only additional time spent on taking anthropometric measurements and body demarcation and, if used, checking used sEMG signals. In this particular context, the most critical problems are encountered in the definition of these measurements, which are often made spannometrically with inadequate equipment such as simple rulers. This introduces into the system several orders of measurement error that are far from negligible, such as the sensitivity of the instruments, parallax, procedural and human errors. This is compounded by increasing stress on the patient subjected to this meticulous process, which extends to the lengthy palpation phase, often in a standing position for marker placement. In the patient preparation phase, several movements and flexions are required of the patient for the correct identification of the keypoints and joints provided in the chosen protocol. Validation of the correct alignment of the markers is equally inaccurate, rarely performed with laser beams projected onto the patient's skin and much more often with simple rulers.

The analysis phase is not as well exempt from complications. After an initial acquisition of the patient's standing pose, which can be used for yet another calibration, the dynamic and kinematic gait analysis is conducted.

In the dynamic component, the acquisition plates introduce a further obstacle: either the patient is forced to walk in an unnatural way, striving to centre the frames of the load cells with his foot, introducing a cause of falsification of the measurement, or sometimes the heel strike occurs spontaneously and randomly in non-sensitive points on the floor, forcing the operator to discard a step or an entire acquisition and to ask for a measurement repetition.

In the kinematic component the problems are similar because of the markers. The analysis can be unnatural because of the artificial movements that many patients are forced to make to avoid excessive displacement of the markers. The most critical are those in the quadriceps and calf area, which are bound with bands that are at times tight, at times too loose, and which often become misaligned due to friction with the inner thigh. Even in this case, changing the pattern on the patient requires a new acquisition. In addition, real-time feedback is not complete and is also not recommended by the BTS itself after the first measurements in order to avoid putting more stress on the test subject. Finally, one and only one step is chosen from each acquisition (the best according to the subjective choice of the operator) and the recognition of the gait cycle events is recursive and completely manual. The times are further lengthened, and yet the criticalities do not stop at the numerical, economic and procedural ones. Nor do they imply mere convenience, but a far more serious problem emerges from this picture: many patients, especially the most fragile ones and those who need gait analysis the most, are physically unable to undergo the examination and return fatigued and without

any results. Furthermore, there is very limited guarantee that, despite taking several measurements, all values for the patient are finally complete and available.

In conclusion, with the standard stereophotogrammetry method, users deal with a system designed for extremely precise, reliable and highly sampled measurement, which paradoxically, however, requires for its use inaccurate methods, tools and preliminary information.

For a concise picture of the pros and cons of the aforementioned categories of systems, reference is again made to the study by Alvaro Muro-de-la-Herran et al. [33] with the following table (Table 2):

Table 2 - Comparison between Not Wearable and Wearable systems, [33]

System	Advantages	Disadvantages
NWS	<ul style="list-style-type: none"> - Allows simultaneous analysis of multiple gait parameters captured from different approaches - Non restricted by power consumption - Some systems are totally non-intrusive in terms of attaching sensors to the body - Complex analysis systems allow more precision and have more measurement capacity - Better repeatability, reproducibility and less external factor interference due to controlled environment. - Measurement process controlled in real-time by the specialist. 	<ul style="list-style-type: none"> - Normal subject gait can be altered due to walking space restrictions required by the measurement system - Expensive equipment and tests - Impossible to monitor real life gait outside the instrumented environment
WS	<ul style="list-style-type: none"> - Transparent analysis and monitoring of gait during daily activities and on the long term - Cheaper systems - Allows the possibility of deployment in any place, not needing controlled environments - Increasing availability of varied miniaturized sensors - Wireless systems enhance usability - In clinical gait analysis, promotes autonomy and active role of patients 	<ul style="list-style-type: none"> - Power consumption restrictions due to limited battery duration - Complex algorithms needed to estimate parameters from inertial sensors - Allows analysis of limited number of gait parameters - Susceptible to noise and interference of external factors not controlled by specialist



Figure 3. 1 - WS system based on (a) inertial sensors and (b) wearable forceplates, [47, 33]



Figure 3. 2 - Commercial WS system based on inertial sensors: Xsens MVN, [46, 33]

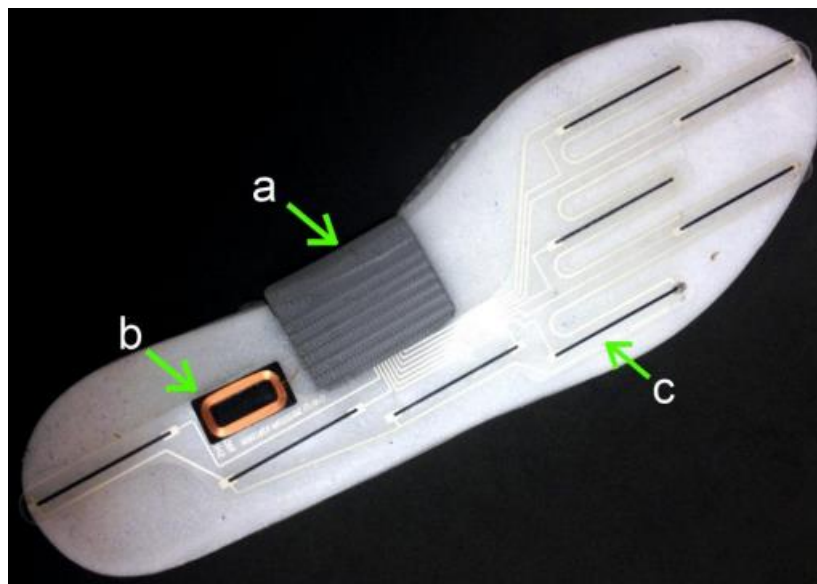


Figure 3. 3 - Instrumented insole: (a) inertial sensor, Bluetooth, microcontroller and battery module; (b) coil for inductive recharging; and (c) pressure sensors, [33, 48]

3.2. Proposed methodology

The purpose of this project is to provide low-cost tool for the gait analysis. This research presents a novel AI-based automated motion characterisation approach that includes real-time analysis, full automation, and a non-invasive analysis. This automated method enables for quick diagnosis while avoiding human mistakes, with the aim of providing an alternative, markerless, portable, testing tool adapted to the needs of the frailest patients.

As an intuitive system, SANE system allows the acquisition of scalar and kinematic data with a few simple clicks. Before the actual acquisition, a blank recording is recommended for the simple purpose of orienting the camera (4) towards the designated analysis area. With reference to Figure 3. 4 SANE through the support of artificial intelligence modules (5) detects and analyses the movements of each patient.

Specifically, the operator in charge of the analysis (3) activates the system through its interface (2) which creates the patient record (9) and activates a stream of signals from the RGBD camera (4). The RGB information is calculated in real-time by the AI (5) provided by Cubemos, each frame is then reconstructed with a two-dimensional projection of the patient's virtual skeleton keypoints. The data obtained with the Depth Camera (4) are combined with the information in (5) to deduce the third dimension of each point. This whole process appears as a video to the operator who, in real-time, can evaluate the quality of the acquisition, with the use of a real-time plotter (10), evaluating whether the acquisition is noisy or normal. The process is supported by a Logging module (6), a module for managing communication between the operator (3) and internal events (7). In detail, any error committed by the operator (3) or by the system itself, whether expected or unexpected, is notified in real-time through an abstract User-Friendly description (7) and recorded in a SANE private folder (9) with more specific details regarding the code location where the exception occurred (6). Moreover, at the end of each acquisition, always in real-time, a partial computation of the data is made (10) which provides the operator (3) with both the representation of the signals automatically filtered by the disturbances and the estimate of the number of steps, which can be considered valid by the system for each signal. If the number of data is not significant for the most relevant signals, the acquisition is automatically discarded notifying the operator (7) of the reasons for the choice so that he can make the necessary modifications. Thus, the operator is completely consciousness of what is happening and is guided in his actions so that he can always record complete and consistent data in real-time for subsequent offline analysis (12). The so far described process (1) can be repeated for several patients and by several operators at different times (11) increasing the volume of data stored in the SANE program directory. In the operational block (12) the operator (14) can access the data of a specific patient in a specific session (19) in deferred mode, via a new page of his GUI (16). All actions in (16) are monitored and strictly guided by the Logging module (17), Message Box (18) modules and GUI Widgets (16). After the acquisition phase (1) an offline computational phase (15) follows. Each signal in each section is averaged through a normalized scale of times and within a few seconds the operator is provided with a complete consciousness of the patient and its gait mean behaviour, both scalar and kinematic. The computational offline phase (15) allows a simple, fast, repeatable and unaffected by human error monitoring of patient's performance. Using this data, the operator,

or a medical doctor on his behalf, can independently assess the clinical picture associated with the gait analysis.

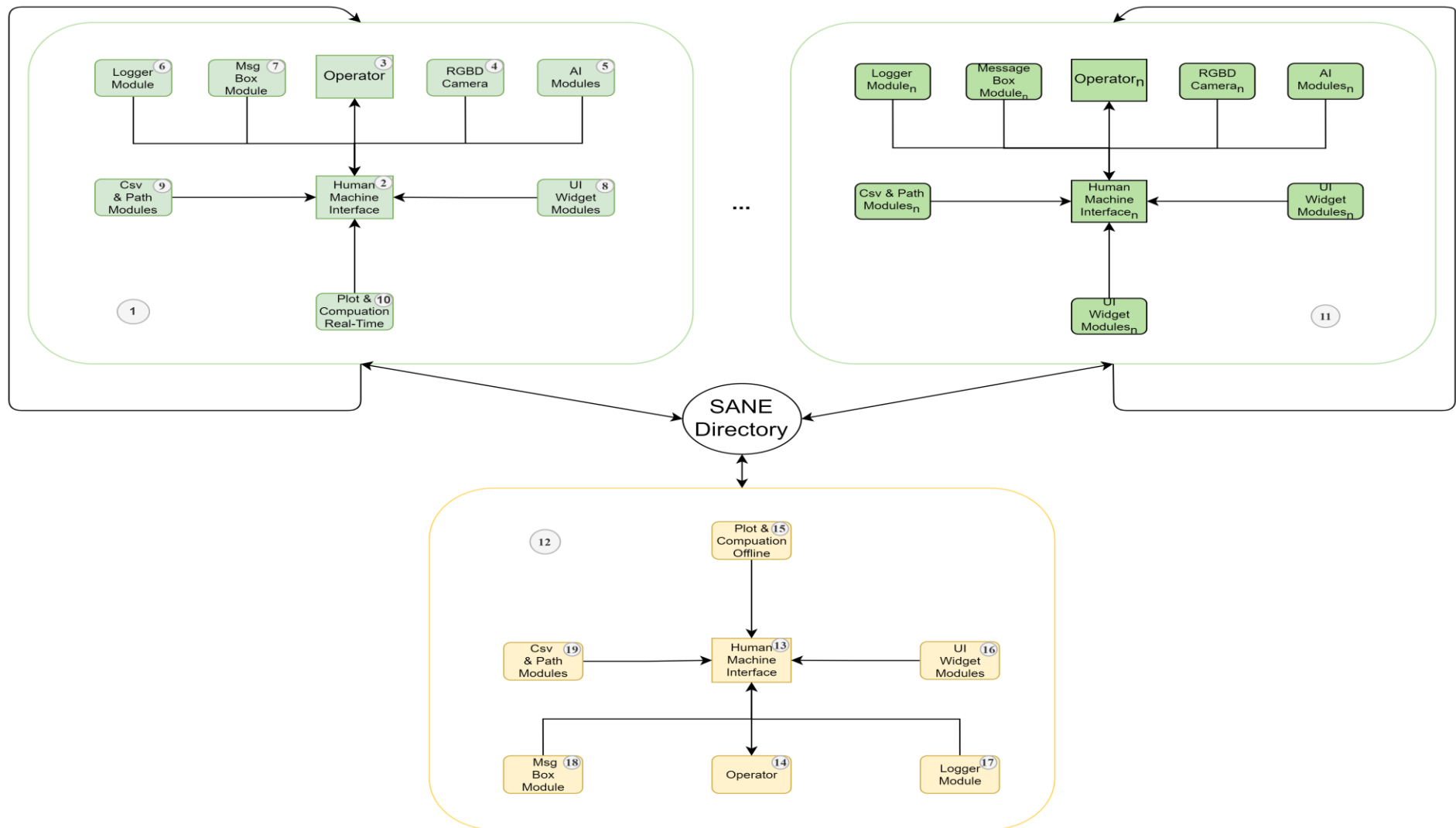


Figure 3.4 - Proposed Methodology

3.3. Methodology implementation

Several tools were used to create the system described here. Below is an overview of the components that played a crucial role in the realisation of SANE. With regard to hardware choices, the Intel RealSense d435i RGBD camera has been chosen for its compatibility in terms of cost and performance within the project requirements. The camera d435i is a kind of all-in-one depth sensor with RGB information associated. A stream of information is provided in four channels, the first three related to the three standard channels of a normal RGB camera (red, yellow, blue) and a fourth channel representing a matrix of values that can be associated with depth (D), [58]. First, depth information is reconstructed using traditional triangulation methods combining the two stereocamera lenses data (Figure 3. 10). Already known to the sensor are the relative position data of the stereocameras as a result of a fine calibration during assembly. This data is combined with that of an integrated IMU inertial sensor, which makes it possible to deduce the arrangement of the entire camera body in 3D space. This information is automatically captured and processed by the d435i's internal PCB (Figure 3. 7) to create an array of depth information that is consistent with itself and also well aligned with the RGB images. This first level of processing is supplemented by additional information associated with an independent infrared (IR) projector. The purpose of this data stream is to make the depth information even more precise. In the case, in fact, of an acquisition by the stereocameras of an image with a pattern that is not very distinguishable, because it is very homogeneous in its parts, the channel associated with the depth could have difficulty in identifying features common to the stereocameras and therefore resolve the data of the depth associated with the framed subject. The projector irradiates a pseudo-random infrared cloud of points in the acquisition zone and, from the pattern of the image returned to the sensor, deduces the differences between the predefined and the irradiated cloud, adding detail even to poorly defined subjects (Figure 3. 5). The IR cloud is, however, a support data and not essential to the generation of the RGBD data stream. This choice makes the camera self-sufficient and robust in output, even in case of intense sunlight, which can disturb the point cloud with its infrared component (Figure 3. 6, Figure 3. 8, Figure 3. 9). Furthermore, the Intel RealSense d435i is fully compatible with any deep learning software that is designed for image reconstruction. If the stream already provides well-aligned data, it can be further processed by neural network software to recognise more complex features common to the four RGBD channels and make the information even more consistent. Finally, it is possible to decide to provide a video stream either of the processed RGB data only, or of the processed RGBD data, or of the depth image data only, or of the same information aligned directly by the sensor without a neural network inside the PC.

In addition, in Figure 3. 6 it can be noticed that the depth acquisition is still feasible although it suffers from the lack of the infrared projector data. To be precise, clearly distinguishable silhouettes such as the human figure continue to be well distinguished while more homogeneous areas such as the ceiling now have regions where the depth matrix has unresolved data. For these reasons, on the software side, the suggested AI has been chosen. The AI has been developed by a partner of Intel itself: Cubemos. The latter, already described in the previous chapters, has the advantage of presenting a very basic Python package already prepared to convolve the RGB and D data with the skeleton tracking program and generate an image with the skeleton of the framed subject with a map of the three dimensions of each keypoint of the human skeleton model of Cubemos.

All in all, the Intel RealSense d435i sensor has been chosen for:

- The size (Table 3)
The compactness of the apparatus makes it extremely compatible with the desire to create a portable and simple to set up system
- Sampling frequencies (Table 4)
They are very well compatible with the requirements of gait analysis in both clinical and sporting contexts, as will be seen in Chapter 4 dedicated to the description of the signal, the frequencies of the filtering of the signal and the design choices
- Costs [59]
Two orders of magnitude lower than those of a laboratory used for Gait Analysis and one order of magnitude lower than the most advanced, portable and recent solutions with multi-chamber and Lidar.
This characteristic makes the sensor perfectly compatible with the design criterion of a low-cost system, less and less restricted to the clinical environment and with a low economic risk of usage.
- The ideal sampling distance range (Table 5)
This characteristic makes the sensor sufficient for the analysis of few gait cycles of a person of average height. However, the system was subjected to the tests presented in Chapter 0 to demonstrate in detail the compatibility of the sensor assisted by a deep learning analysis to demonstrate its conformity with the accuracy requirements of the context.

On the software side, the tools chosen to develop the system are:

- PyQt
for a simple but modern graphical interface, an ample, complete and performance-reliable package. Initially created in C++, in recent years the Qt library has also made a name for itself in Python, although the documentation in the new language is still largely to be enriched. The Qt libraries are constantly being updated, with a very active community and a very large number of efficient modules suitable for cross platform, almost as if it represented a whole new standard library. This choice was made in order to preserve design and performance and to provide a fully intuitive and guided experience for the operator without affecting Real-Time acquisition performance.
For this purpose, we will also use the built-in Multithreading module in PyQt for compatibility and efficiency.
- Pyqtgraph
for real-time plots with very low computational impact
- Pandas
for convenient manipulation of large data structures in offline
- SciPy
to benefit offline of an open-source library well known in the literature for algorithms and mathematical tools for the Python programming language
Also with very good performance.

- **Simpy**
for offline equation solving
- **Matplotlib** with the **PyQt** interface
for offline plots and plot animations that are more complex and therefore less suitable for real-time use, although attractive, flexible and with a wide range of useful associated functions.
- **MATLAB**
for tests and preliminary simulations in the early stages of the project and which is not in any way integrated into the current complete SANE system since any function exploited is completely written in Python and free of external licenses (except for the license required for the SDK associated with Intel, Cubemos).

Table 3 - Intel RealSense d435i, Mechanical Dimensions, [58]

Dimension	Min	Nominal	Max	Unit
Width	-	90	-	mm
Height	-	25	-	mm
Depth	-	25	-	mm
Weight	-	72	-	gr

Table 4 - Intel RealSense d435i, image format and stream rate with USB 3.1 Gen1, with fps column highlighted, [58]

Format	Resolution	Frame Rate (FPS)	Comment
Z [16 bits]	1280x720	6,15,30	Depth
	848x480	6,15,30,60,90	
	640x480	6,15,30,60,90	
	640x360	6,15,30,60,90	
	480x270	6,15,30,60,90	
	424x240	6,15,30,60,90	
	1920x1080	6,15,30	
YUY2 [16 bits]	1280x720	6,15,30	Color Stream from RGB camera (Camera D415 & D435/D435i)
	960x540	6,15,30,60	
	848x480	6,15,30,60	
	640x480	6,15,30,60	
	640x360	6,15,30,60	
	424x240	6,15,30,60	
	320x240	6,30,60	
	320x180	6,30,60	

Table 5 - Intel RealSense d435i features, with the ideal range highlighted, [58]

Intel® RealSense™ Depth Camera D435/D435i Features

- Intel® RealSense™ Vision Processor D4
- Up to 1280x720 active stereo depth resolution
- Up to 1920x1080 RGB resolution
- Depth Diagonal Field of View over 90°
- Dual global shutter sensors for up to 90 FPS depth streaming
- **Range** 0.2m to over 10m (Varies with lighting conditions)
- Intel® RealSense™ Depth Camera D435i includes Inertial Measurement Unit (IMU) for 6 degrees of freedom (6DoF) data

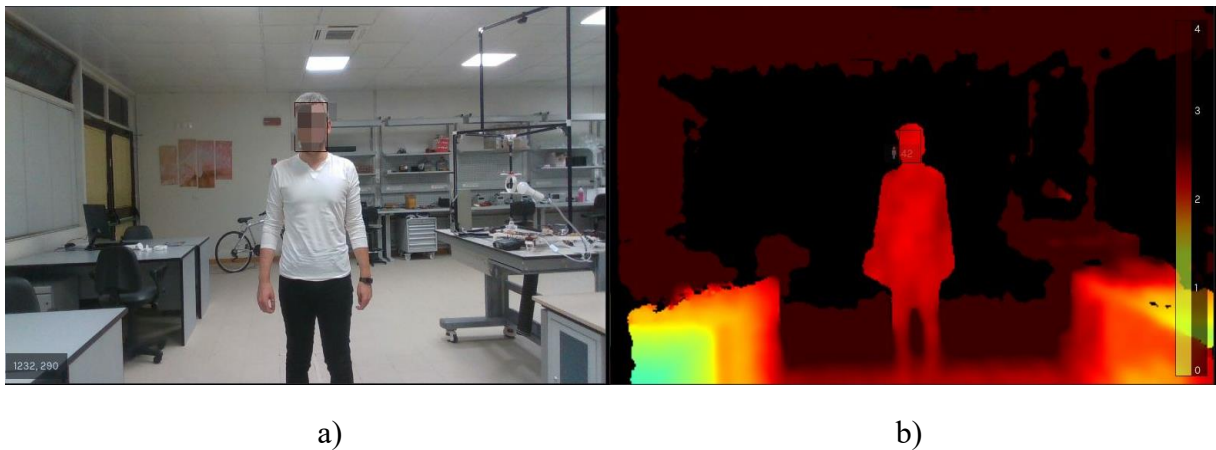


Figure 3. 5 - Intel RealSense d435i - Biomechanics Lab, Neuromed Technology Park - a) RGB acquisition; b) Depth acquisition with both stereo cameras and IR projector.

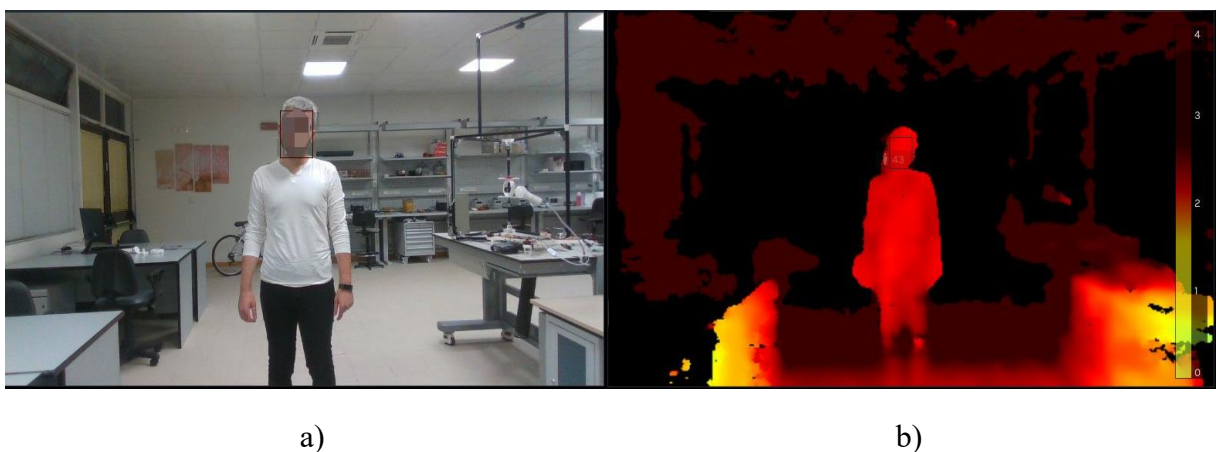


Figure 3. 6 - Intel RealSense d435i - Biomechanics Lab, Neuromed Technology Park - a): RGB acquisition; b): Depth acquisition with stereo cameras only.

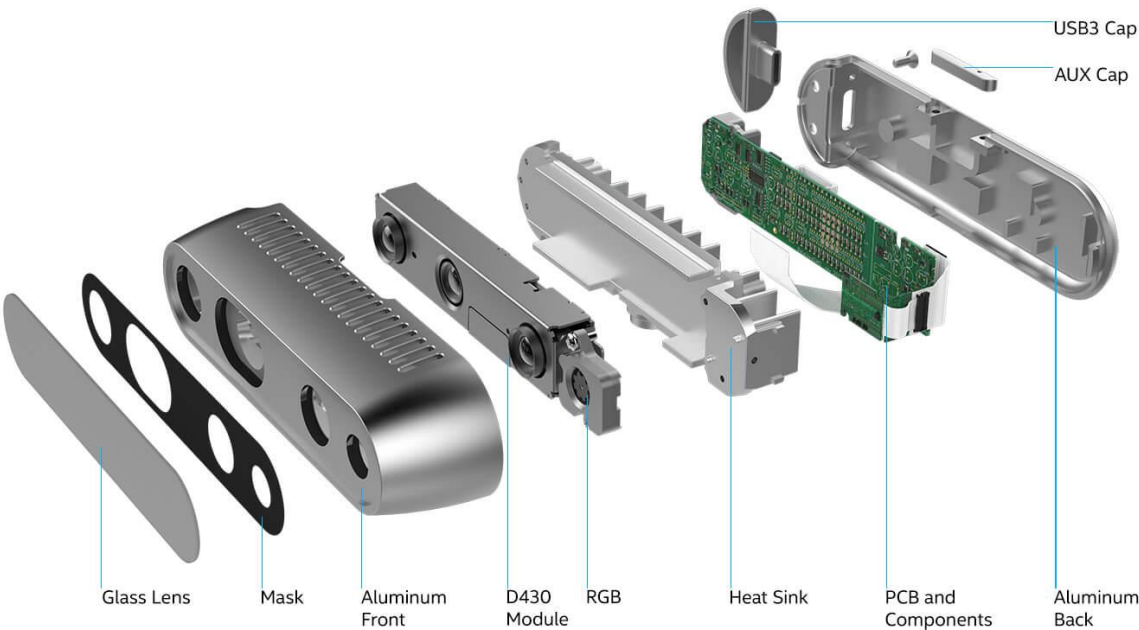


Figure 3. 7 - Intel RealSense d435i, components, [58]



Figure 3. 8 - Intel RealSense d435i, the lenses in order from the left: the right stereo camera, the infrared projector, the left stereo camera, the RGB camera, [59]

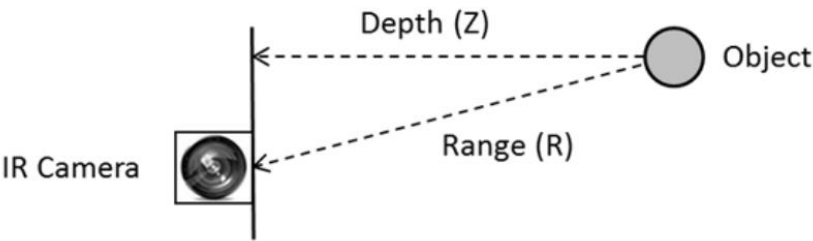


Figure 3. 9 - Intel RealSense d435i, depth and -Z axis definition, [58]

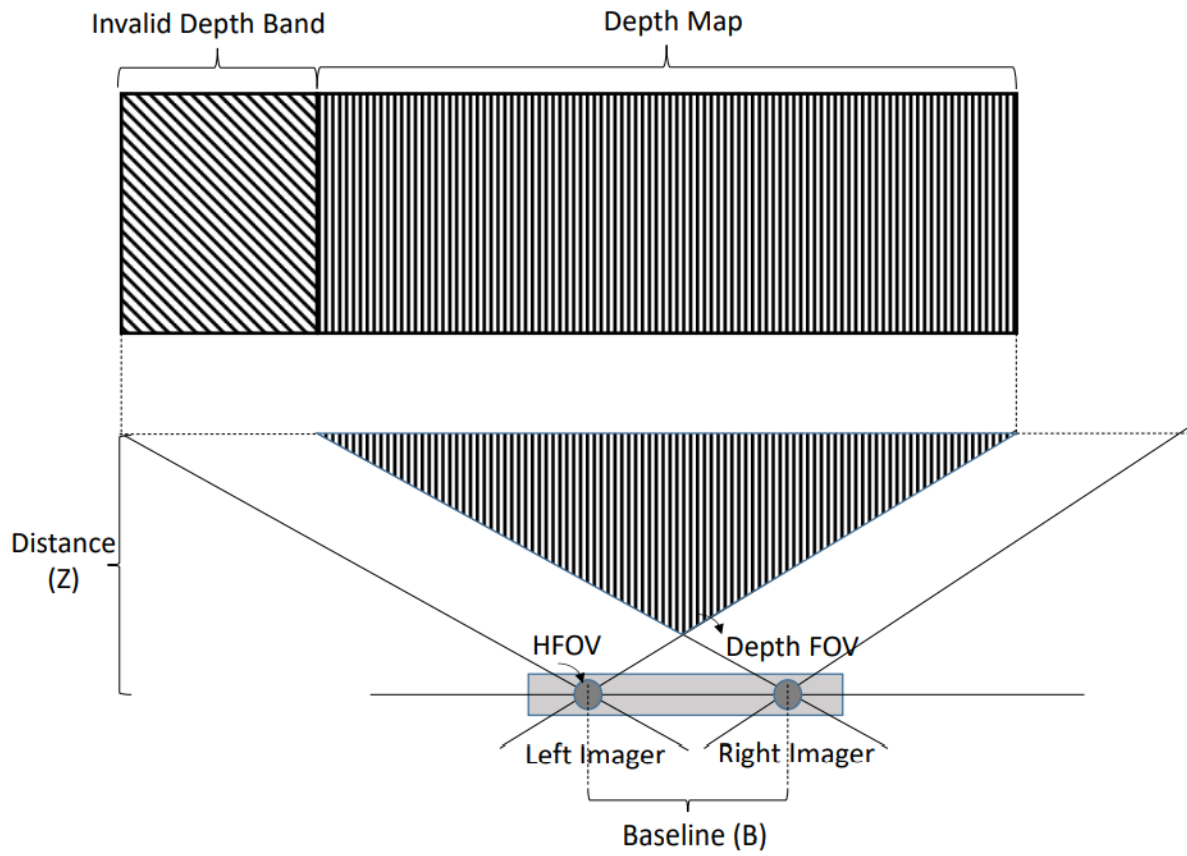


Figure 3. 10 - Intel RealSense d435i, stereo cameras depth recognition via triangulation, [58]

4. A novel approach

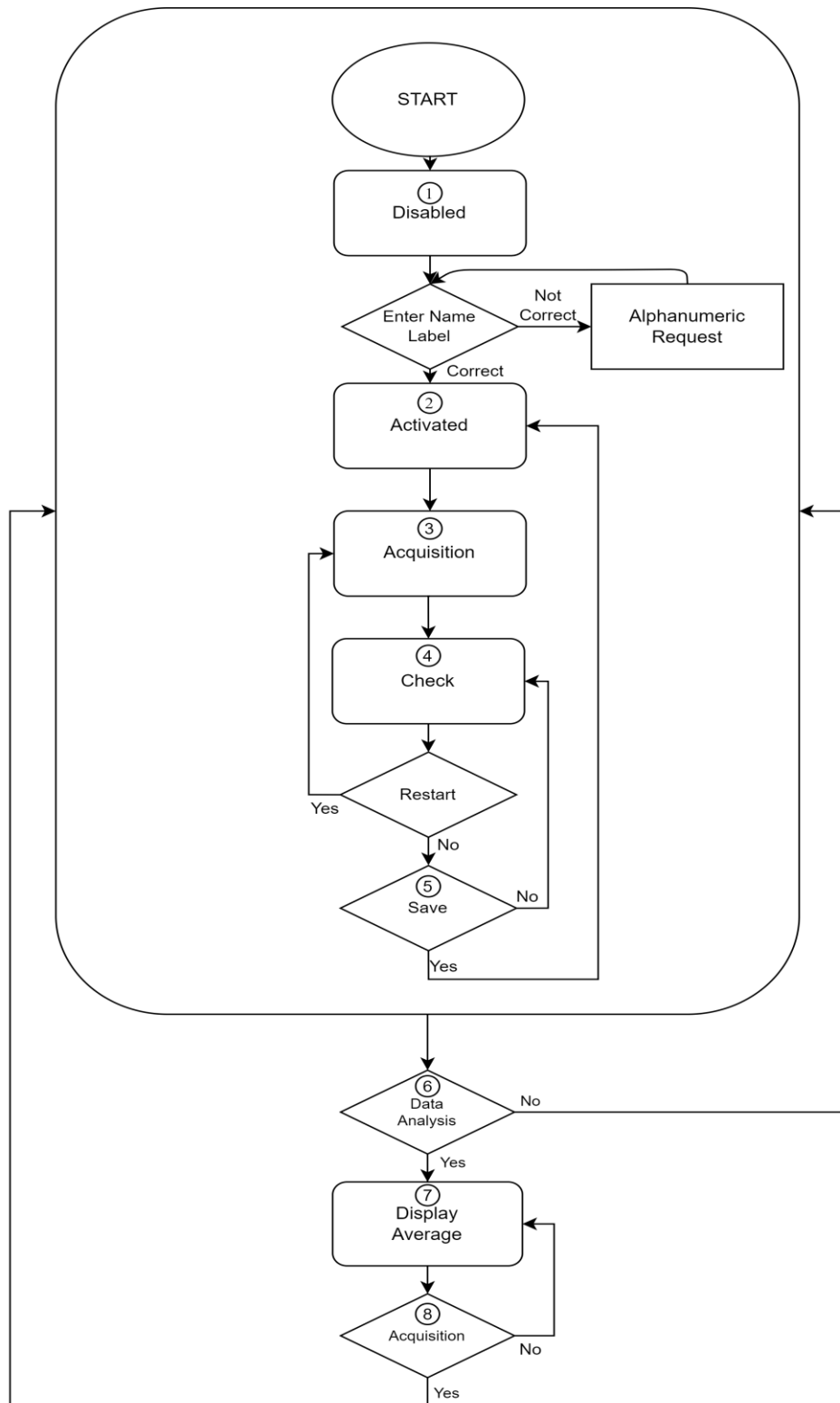


Figure 4. 1 - Human Machine Interface Flow Chart

4.1. Human Machine Interface

The graphic interface has developed significantly over the course of the project, becoming increasingly minimal as the logging and computation automation component has evolved.

For example, if the operator was required to force the patient to place one foot ahead of the other and to specify it in the interface or to indicate the characteristics of the patient's session in the beginning, as the work progressed, all of these decisions were automated, allowing the patient to be analysed by walking in an arbitrary and natural manner (Figure 4. 2, Figure 4. 3).

The graphic base and the Stylesheet have been pre-set in a neat configuration by means of the QtDesigner tool and introduced into the project storing the user interface configuration for a program; saved in an XML format and contains definitions of Qt widgets in the form of a .ui file with its resources and private icons, in order to make the most significant modules and those with the most logical contribution easy to read at code level. Each .ui file is imported by modules responsible for controlling the signals connected with each object present in the pre-set Widget, providing a second, more abstract level of graphic management and allowing modular and organized code coordination. At this level the input controls that the Gait Analysis program requires are performed. For example, the possibility to execute an acquisition via the start and stop button is blocked, as the ability to save if the patient's name does not match the folder's naming requirements. In addition, in this phase dynamic tooltip messages are generated upon the mouse hovering signal and modified each time the program enters a different execution state, in order to let the operator, know what SANE expects or why a signal has been disabled. Finally, each icon is dynamically updated in this stage in order to make the interface even more intuitive. The start and stop button, for example, has four icons: active, active, deactivated, and start without "previous saving" (i.e.: delete and restart).

The link between the signals of the interface and the functions of all the other control, calculation, and logic packages of the code is handled by a third level of the modules designated to control the GUI, which inherits from the modules indicated above. For this reason, the project main is one of the modules that belong to this level.

This level also includes customised modules in the GUI package, namely either the ones that have inherited from the standard PyQt classes and perform similar but not identical functions (such as the QDialog modules that dynamically define the style and icons of all Message Boxes or the Widgets that simulate the Matplotlib windows in the Qt environment and assign a default Navigation Toolbar for a complete, dynamic, customisable, exportable plot analysis) or the ones that override some standard Qt methods.

The flow chart in Figure 4. 1 describes the various GUI stages from the user's point of view:

- Phase 1 (Figure 4. 4)

The program opens on the first page of the QStackedWidget associated with the Main Window and does not allow navigation to other pages. All the buttons are disabled and show the same Tooltip "Disabled. Please, provide a Folder Name" and will remain disabled until an alphanumeric string corresponding to the patient's name is entered in the "Enter Name" text box. If the name entered does not match the required format, a new tooltip is generated, explicitly stating that the input must be alphanumeric.
- Phase 2 (Figure 4. 5)

The start and stop button is activated both graphically and with a new tooltip. When clicked a new threaded window associated with the Intel RealSense video is opened.

- Phase 3 (Figure 4. 6)
The start and stop button are updated both graphically and with a new tooltip so that the acquisition can be concluded when the registered stream is considered sufficient and satisfying. Meanwhile, the Skeleton Tracking is performed and the Widgets associated with the Real-Time Plotter are updated at the same frequency of the video stream with a maximum accumulation of data of up to five seconds of acquisition, guaranteeing a lag-free stream throughout the whole acquisition time, regardless of its length. Here the module inheriting from Pyqtgraph is employed.
- Phase 4
The save button is activated both graphically and with a new tooltip. The tooltip associated with the graphs is now updated to allow guided navigation once the acquisition has been completed. The operator is therefore able to evaluate the quality of the walk on the basis of the “Ankle Distance” signal and the evolution of the three dimensions of the “Spine” (of which the projection in Z can be identified as the approximate distance covered by the patient's centre of gravity towards the camera). Another window is finally opened to visualize on Matplotlib with QtAgg and Navigation Toolbar all the filtered signals and the estimation of the number of valid steps for each signal.
- Phase 5
The operator is then free to repeat the acquisition by means of the start and stop button, which is updated again, both graphically and with the tooltip, to the status of delete and restart or save the acquisition.
In the case of saving, different message boxes are called depending on whether the folder already exists, whether there are cases of homonymy, or whether the patient's name has been changed to an unsuitable format.
- Phase 6 (Figure 4. 7, Figure 4. 8)
After multiple acquisitions, the Data Analysis button can be used to access the second page of the Stacked Widget in the Main Window.
- Phase 7
The page will display a Label to insert the name of the patient whose average values are meant to be measured in a specific session and benefiting from the same textual controls as the Label used in real-time, multiple plots Matplotlib with QtAgg and Navigation Toolbar, ready to show the associated data, and a button that will open a custom QFileDialog such that only one and only one session can be selected for that specific patient indicated. Other Message Boxes are here responsible for verifying the existence of that folder, checking that the files in the folder in question are not corrupted, analysing foreign files, and guiding the user in the process.
- Phase 8
The Data Acquisition button can be used at any time to return to Phase 1.

Finally, the Main Window has all the buttons and functions of a standard window, such as split screen, window minimisation, full screen expansion and, naturally, the close button.

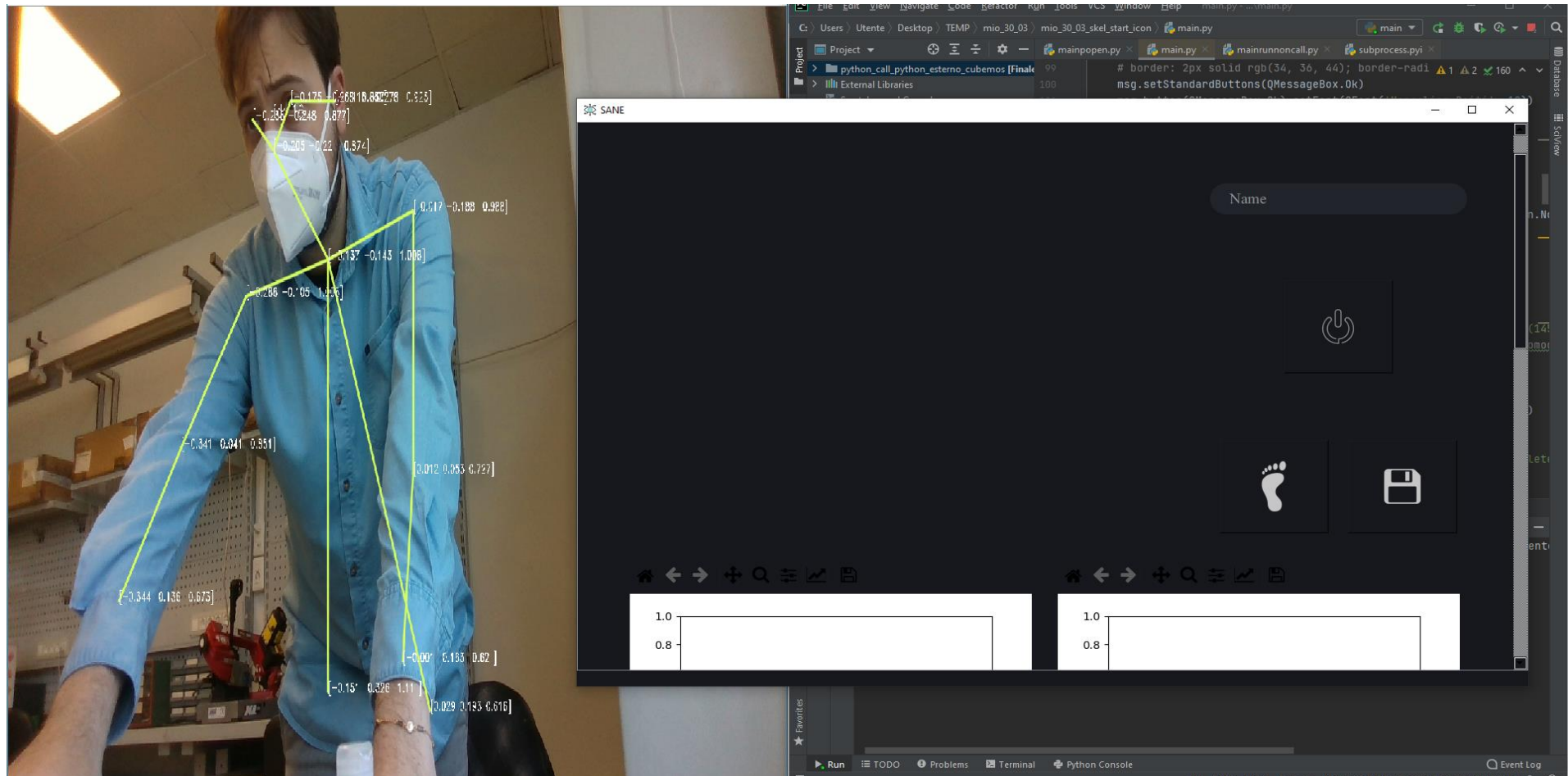


Figure 4.2 - SANE first prototype version

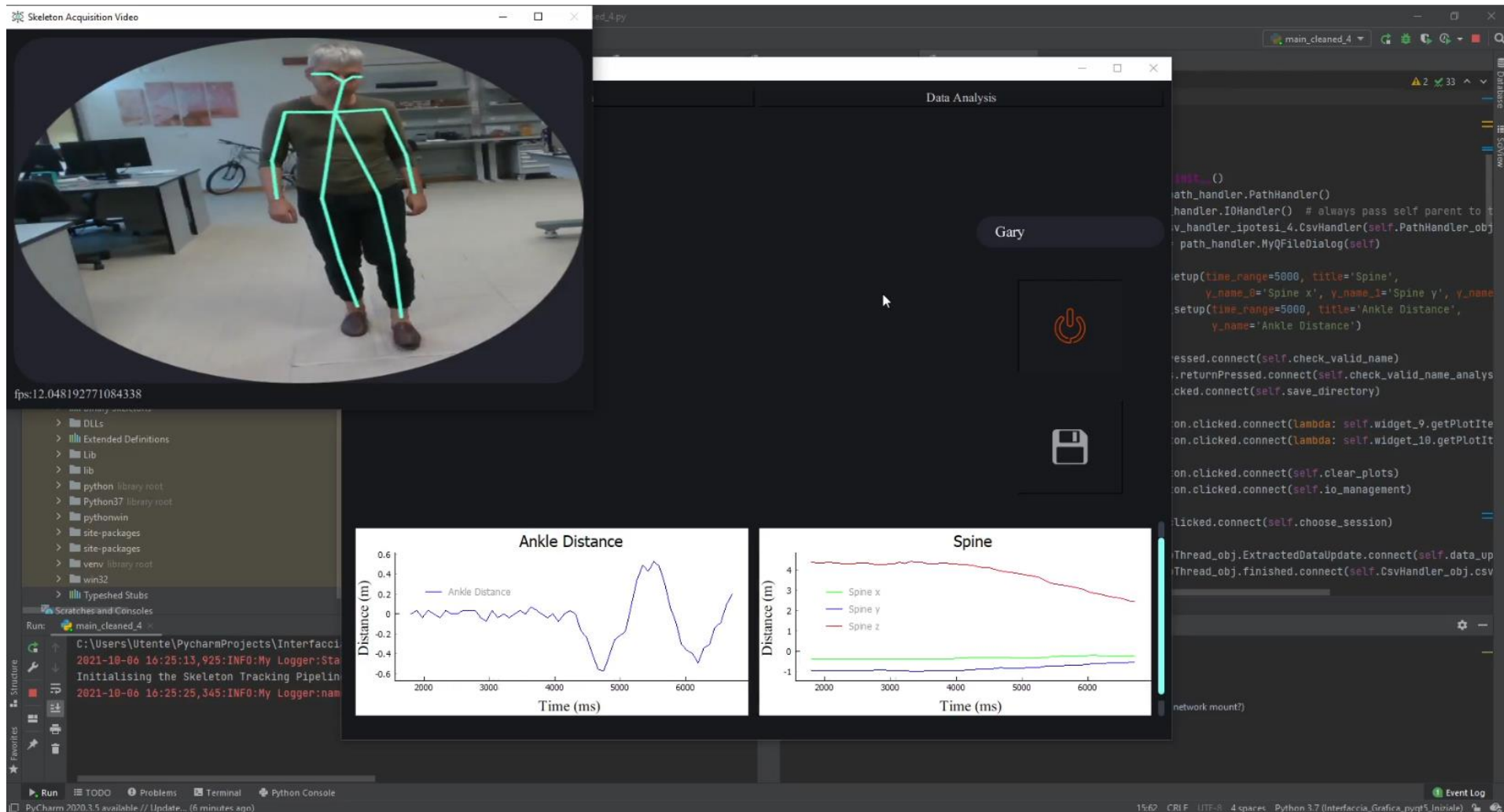


Figure 4.3 - SANE second prototype version

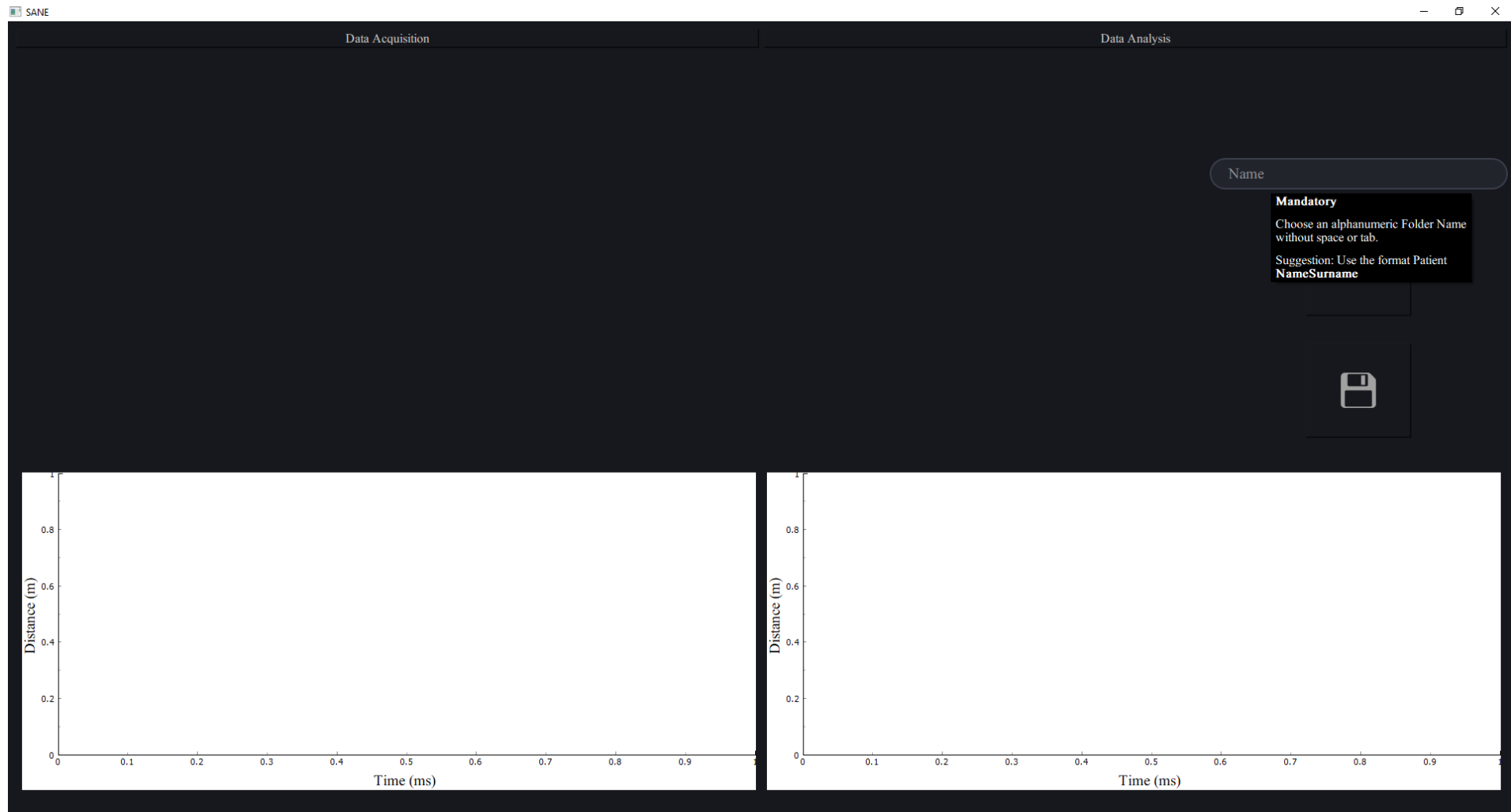


Figure 4. 4 - SANE final version - Phase 1 and tooltip example

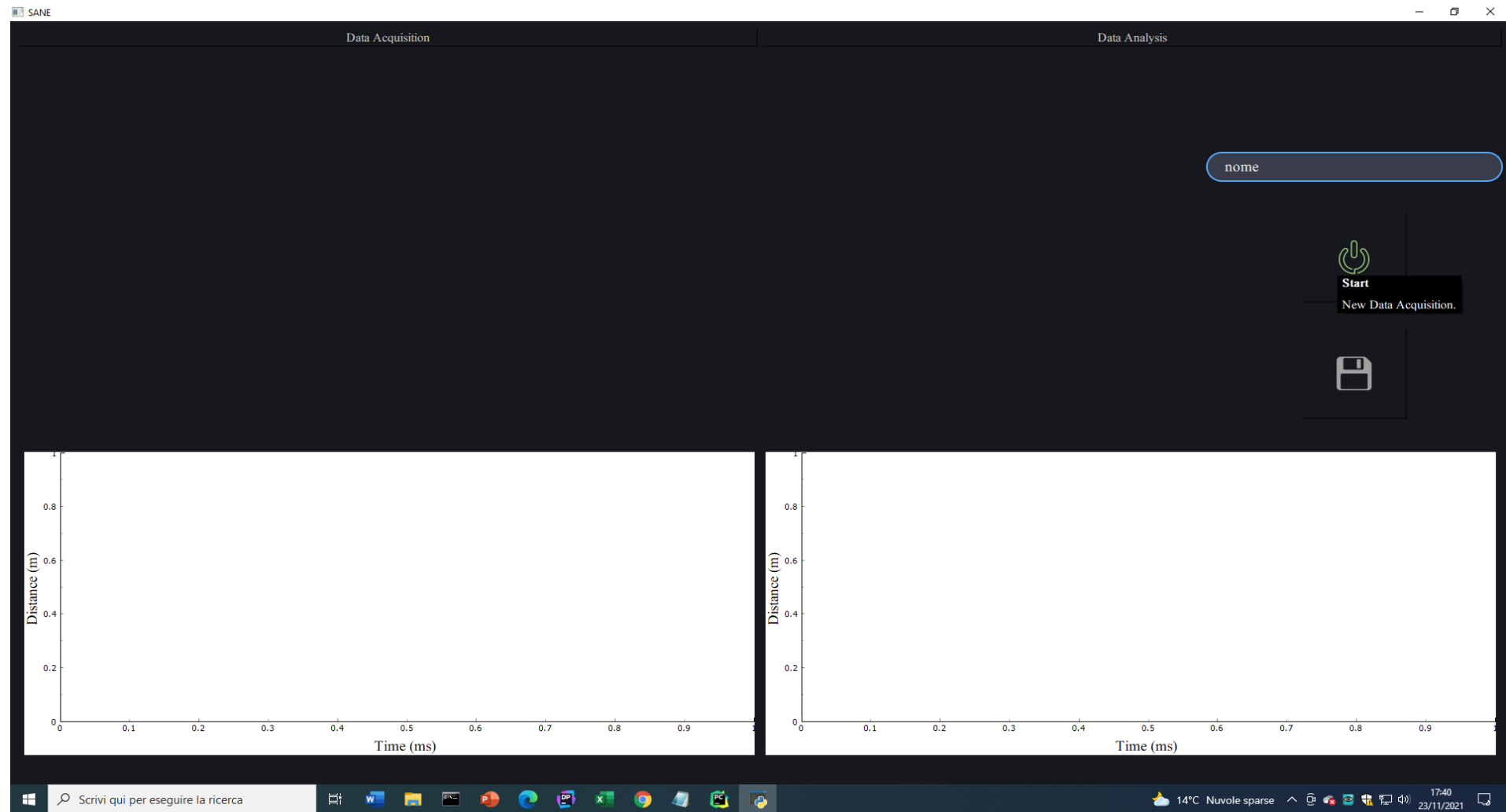


Figure 4. 5 - SANE final version - Phase 2 and tooltip example

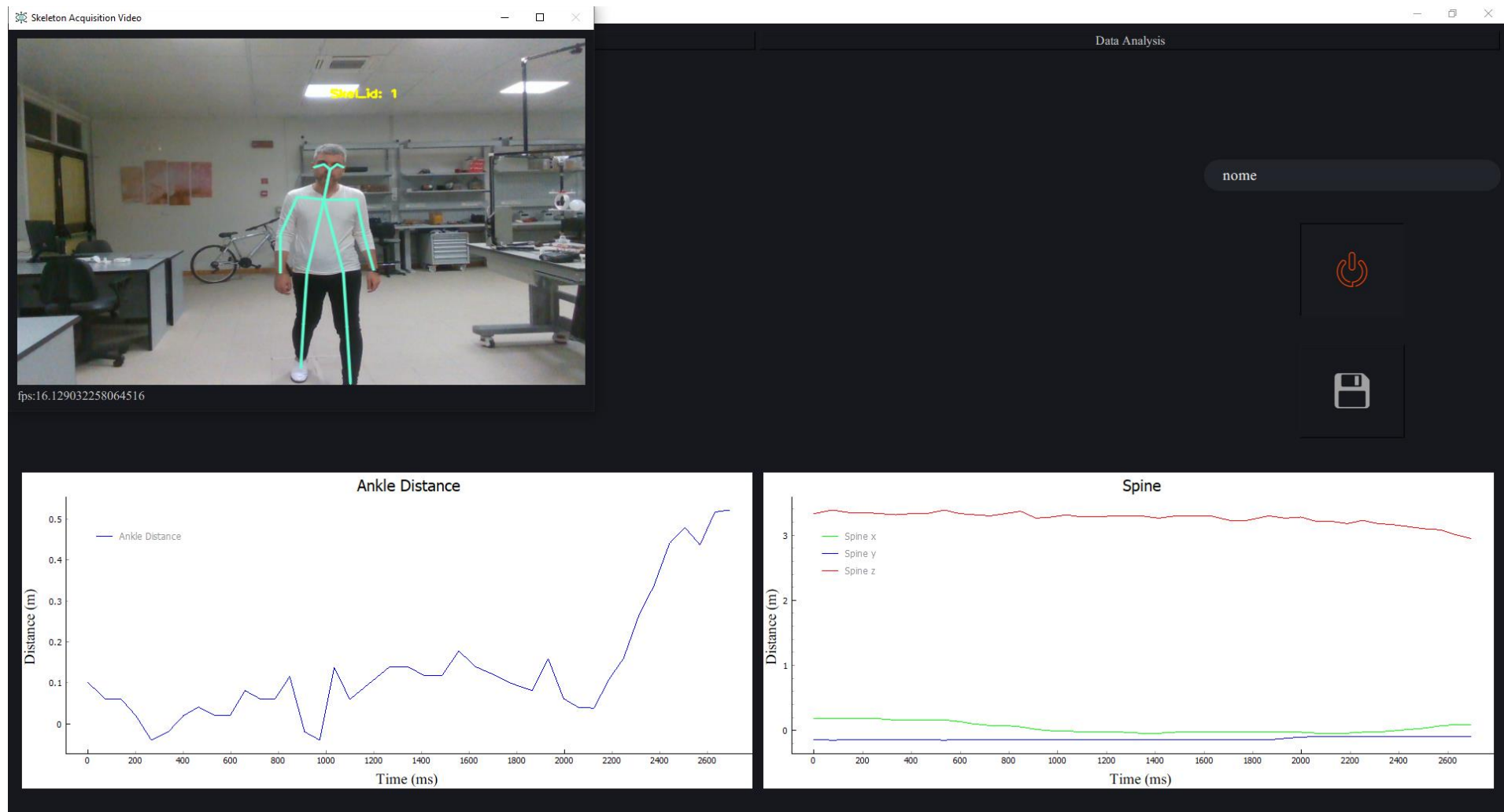


Figure 4. 6 - SANE final version - Phase 3 at the very beginning of a gait cycle

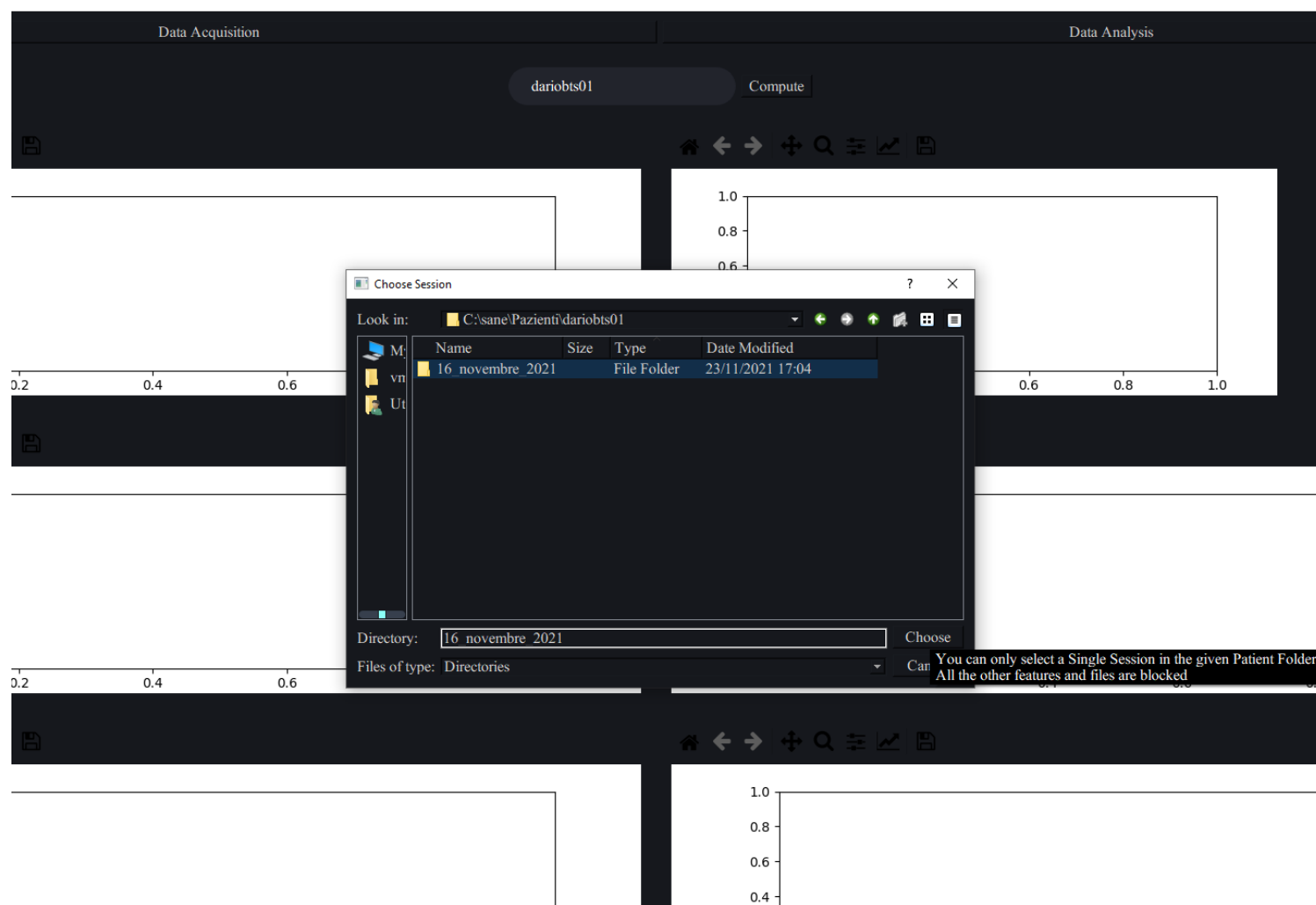


Figure 4. 7 - SANE final version - Phase 6 and tooltip example

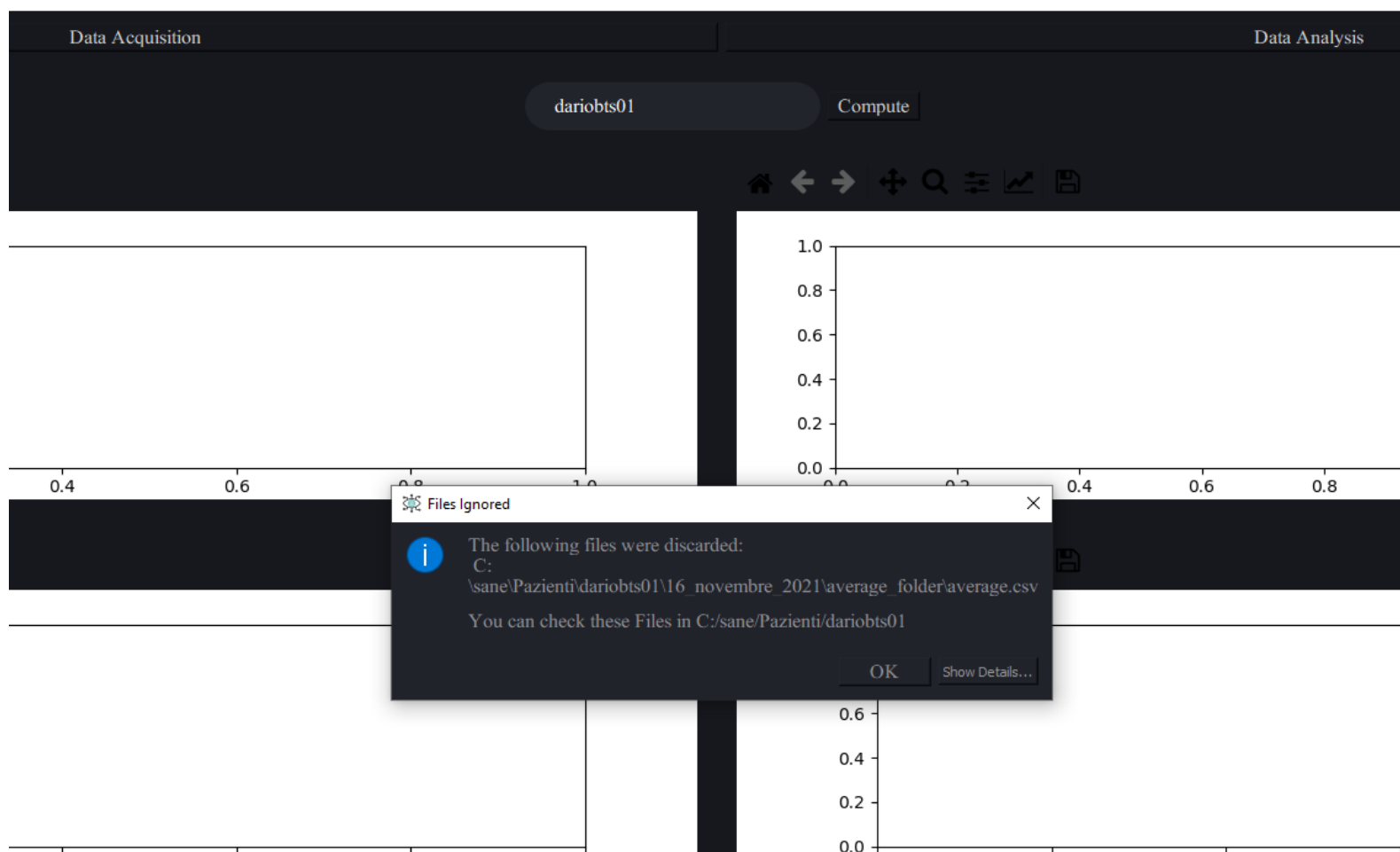


Figure 4. 8 - SANE final version - Phase 6, Message Box example

4.2. Real-Time Data Analysis and Acquisition Modules

This is the most delicate phase of the project since it is extremely important to provide a sampling time that is sufficient for the analysis of each type of gait, facing with the heavy computational effort required by an artificial intelligence and avoiding all interrupts of excessive duration coming either from the interface or from any other concurrent application not making part of the system.

As already mentioned in Chapter 4.1, multicore features of the Cubemos libraries are used in order to reasonably exploit the computational power of the CPU to the maximum of its possibilities and at the same time exploit the QThread module of PyQt5 in order to make the real-time skeleton tracking section independent and asynchronous. In this way the acquisition loop is untied from the graphical interface loop, avoiding application freeze and at the same time improving performance and robustness in acquisition. Everything that has been written and that will be described below takes place in the module designed to the sole management of inputs and outputs between the system and the Intel RealSense d435i camera, `io_hadler.py`.

In order to formulate the code and determine the optimal parameters, several performance tests were conducted on the skeleton tracking module supplied by Cubemos and, in parallel, on the module created for SANE using the functions made available by the cProfile library in order to understand the maximum performance that can be achieved independently from the code written for SANE. The tests were carried out on a desktop computer equipped with an Intel Core i5-4590, 4th Gen, @3.30 GHz CPU and with the USB 3.1 Gen1 cable provided by Intel for its sensor. All the assumptions and calculations that follow from these tests assume that any other hardware structure on which the SANE program is installed will behave similarly to those observed and linearly proportional to the performance that it can provide with respect to the setup available for the test.

Furthermore, the hardware conditions under which the system was tested proved to be very close to the minimum ones that this software can accept, by virtue of the performance reasoning provided in Chapter 4.3. This gives even more robustness to the choices made on the various parameters that will be described below, since the testing conditions correspond precisely to those necessary for everything to run properly in the worst-case scenario.

First, each function and its internal call in all modules of the Cubemos package exploited by `skeleton-tracking-realsense.py`, the higher-level code provided by the skeleton tracking library, were analysed.

Through a run of the given example, with the function `cProfile.runctx()`, a comma-separated values (CSV) file was created for every test containing the name of each analysed function, the line of code and the module in which it is present, the number of times it was called, the total time taken in milliseconds per call and many other statistics for the performance analysis as described in [60]. Next, the CSV was converted into Excel file in .xlsx format for a convenient sorting of the data according to each statistical criterion provided in each column by cProfile. From this last file that it can be inferred that (excluding the function for checking the licence by Cubemos, whose execution time is around 2.7 seconds, called only once at the beginning of the programme) the native `wrapper.py` module, which exploits the core function of the programme for the estimation of keypoints, used iteratively for the analysis of each frame of the video, is the unmodifiable bottleneck of the AI responsible for the skeleton tracking. It

spends an average of 64 ms per call in a 100-call test with 1 frame per call. Therefore, taking into account that the cProfile queue partially slows down performance, the maximum frames per second (FPS) that SANE could ever hope to provide on the computer being tested and with the source code provided by the Cubemos API would be a few Hz greater expressed by Eq. 4.1

$$\frac{1000}{64}ms = \frac{1s}{T_{bottleneck}} = f_{max} = 15,625 FPS \quad (4.2.1)$$

The result of Eq. 4.2.1 will be used to estimate the quality level of the real-time acquisition code created for the SANE system.

The tests using the cProfile library are very good for estimating bottlenecks, especially considering the time spent on each function in relation to the others, but they are less accurate for evaluating times in an absolute way, since the testing itself implies a non-negligible computational effort.

Therefore, a further frequency test will always be done both for SANE and for the Cubemos skeleton-tracking-realsense.py module through the simpler datetime library, with a much lower computational load, not to evaluate the times used by each function in each module, but to analyse the time with which each frame of the video is returned after being submitted to analysis by the AI. This test therefore reflects in absolute value the sum of all the delays of all the code exploited frame by frame for the analysis of the video and is not only dependent on the estimation times of the AI but also on the whole structure of the code around it. From this it emerges that the implementation of the skeleton tracking, proposed as an example by Cubemos, sequential through a while loop and shown on display Using OpenCV inbuilt function, provides on average a data at the frequency of 12Hz, 3 less than the frequency of the pure AI point extraction calculated conservatively through cProfile. Since, as already mentioned, the sampling frequency is a crucial aspect for a good analysis, it was decided not to directly employ the module provided by Cubemos, which has shown to have margins for improvement, but to make changes, wherever possible, to the Cubemos Python package and then to integrate them into SANE in the least possible impactful way on the pure AI analysis times.

The `io_handler.py` is therefore the transposition in form of class, the adaptation to PyQt environment and the optimisation for real-time and in thread of the code proposed by Cubemos for the analysis of an image. Here, all the preliminary settings for the licence check, the resolution configuration, the analysis confidence settings for the tracker, the graphic settings for the acquisition window, the settings for the alignment of the camera stream and the frequencies required for the Depth and RGB channels are moved to the initialisation section of the object created by this class. The last one is called by `main.py` at the opening of the interface and maintained for the duration of the Main Window loop. This very choice shifts all the delays of the functions that do not need to be called at the opening of the program, makes all the calls to the skeleton tracker with immediate response without any lag at the beginning of the analysis, to allow the operator to acquire data at the exact moment he decides to activate the start and to communicate to the patient the beginning of the walking. As instructed by the Intel RealSense documentation for Python environment, the acquisition is configured so that both RGB and D information are available. In detail, the maximum frame frequency request common to both channels is imposed at 60 FPS [58], in order to prevent software bottlenecks if the SANE code would be used on a computer equipped with hardware with high computational performance and capable of resolving skeleton tracking in less than 0.01 seconds. The highest possible resolution has been set. The latter is also still optimal in terms of performance (in other words,

that does not affect at all the maximum frame rate of the skeleton tracker) at 640×480 px, found empirically after testing all combinations of frequency and resolution using the testing functions provided by the cProfile library (Figure 3. 6). Then the frames are aligned and the pipeline is initialised ready to start at the immediate creation of the recording window. The rest of the code for the generation of a video in which skeleton tracking is performed is incorporated in the run() method of the thread. This last one includes the start of the pipeline, the control of the correct alignment of the frames, the queue of new frames waiting for a certain time limit in order to find out if there is a connection problem with the camera, the 2D skeleton tracking functions and the 3D data extraction function by knowing the 2D coordinates. At each frame is sent, as thread safe pyqtSignal, to the modules called by the io_handler.py:

- a timestamp of both the time elapsed between two consecutive frames and the time elapsed since the start of the acquisition, performed by means of a custom class derived from PyQt's built-in QTimer
- the list of keypoints of the 3D skeleton in that frame
- the processed image

to display (via QLabel and Pyqtgraph) and save real-time data and calculate a few new real-time data with negligible computational cost (via the csv_handler.py and computation_handler.py modules).

To guarantee good levels of efficiency, the real-time management of the plots is implemented as described in Chapter 4.1, the update of the image occurs as soon as a frame is available and consists only in the modification of the QPixmap of the QLabel that simulates the video, meanwhile the .csv file that stores the real-time data has already been generated by csv_handler.py, opened and left in append at the beginning of the video stream. The file will be closed only when the video stops and deleted in case of any unexpected interruption.

During the frame-by-frame addition of new data, the csv_handler.py is predisposed to generate a NaN data in case a Keypoint has not been provided by the IA at that instant; moreover, through the support functions provided by the computation_handler.py module, it generates six new signals:

- the signal associated to the “Pelvis” keypoint:
 - a) is calculated as the midpoint between the “Right Hip” and “Left Hip” signals.
 - b) is fundamental for the calculation of different angles during gait analysis and a commonly provided point in the literature of motion tracking programs. However, it is not generated by Cubemos, so it is calculated at this stage.
 - c) is in turn formed by three signals: the projection of the “Pelvis” on the X axis, the projection of the “Pelvis” on the Y axis and the projection of the “Pelvis” on the Z axis.
- the “Ankle Distance” trend
 - a) is calculated as the distance between the Left Ankle and the Right Ankle signals projected onto the Z axis. It is obtained by subtracting the first with the second and is the key signal for gait recognition. In fact, every time a gait cycle is performed, regardless of how unsteady or

asymmetric the stride is, the Ankle Distance signal will have completed a period and will have a sine-like shape with variable amplitudes.

See Chapter 4.3 for a description of how this data will be used.

- the Total Displacement signal
it corresponds to the Range (R) of Intel RealSense, it is calculated from the 3 dimensions of Spine as

$$\sqrt{(SpineX^2 + SpineY^2 + SpineZ^2)} \quad (4.2)$$
 considering, as common in the literature, the “Spine” Keypoint as the reference keypoint for the movement of the whole skeleton.
- the FPS
obtained by the simple reciprocal of the timestamp of the period between two frames, using standard numerical controls for a real time division.

For a reliable analysis all these given parameter generate a datum if and only if all the events from which they originate are not NaN. If at least one of these is NaN, the calculation at that instant will not be performed and the result will also become NaN.

Through repeated tests with both the cProfile library and the datetime library it has been proven that the FPS, with and without the calculations included in the `csv_handler.py` and the lines of code of the module for plot time and video display, remain almost completely unaffected since each of these sections has a total execution time slightly varying depending on the number of keypoints acquired at a given time, but always almost two orders of magnitude less than that employed by the `wrapper.py` of the IA.

It was therefore decided to leave these modules running sequentially with respect to each thread cycle and not to implement a multithreading solution. Even if, indeed, the second option, in the case of a hardware architecture with high computational power, would have been possible in terms of:

- limit video and plot updates with an asynchronous sample of the data acquired at 30 FPS
- save synchronously and sequentially only the numerical data at the highest possible frequency
- release frames immediately after the analysis by the AI so that new ones could be called from the pipeline

this choice would have been too unsafe for an improvement of limited relevance.

In the best-case scenario, this idea, on the basis of the execution reports obtained with cProfile, would have improved the representation time of each frame slightly over than 1%. However, in first place it would have introduced constraints to the project by making many parameters no longer customisable, such as the time span of the plot that can be represented in real-time, because, with the growth of the data to be represented at each new frame, both for the rise of the span and of the sampling frequency, there would have been a risk of making the output thread slower than the input thread, resulting in asynchrony and inconsistency between plots and images, and data accumulation, resulting in a memory consumption fault. Secondly, it would not greatly provide an improvement even if Cubemos would have made its AI far more efficient and faster, since the d435i’s camera would still deliver images at a maximum rate of

60 FPS, which, for instance, is still recommended and not unreasonable for video and plot representation according to the Nyquist criterion applied to the sampling rate of the human eye.

At the end of the acquisition the last real-time check takes place, which simulates the first part of the post-processing calculations, via the `check_signal_minimal_requirements()` function in the `computation_handler.py` module, over all the saved data in order to notify the operator whether the gait can be used for the calculation of average values, how many steps have been recognised and how many signals have a valid data set in the period of these steps. If the total number of steps is zero, the acquisition cannot be saved among the folders for the calculation of the average and the operator will be invited to repeat the analysis of that gait, letting him know whether:

- The number of steps is zero because the signal shape has never been that of a gait cycle, highlighting that a gait analysis cannot be conducted by its own definition if the patient is not able to perform all the gait phases
- The number of steps is zero because the patient stopped himself during each cycle, making the acquisition non-continuous and unsuitable for the criteria of analysis by its very definition
- There is too much noise in the video and too many NaNs from the AI to consider the signal reliable
- The video was conducted on an outdated architecture or on a PC where too many programs were running at the same time in SANE, to the extent that the sampling time was reduced below the minimum 16 FPS threshold (Chapter 4.3). If the number of steps is not zero but in each of them some keypoints have generated signals that are not good enough because of the noise, then the operator is warned that the system will still be able to give reliable averages as long as in at least one of all the acquisitions of the session there will be acceptable data for that signal. Furthermore, the operator is also warned that the acquisition is affected by noise.

SANE showed at this final step that it could analyse the 3D skeleton at a frequency of between 16 and 18 FPS with an average of 17.2 FPS on a 10-walk test. Six more FPS were gained compared to the original Cubemos example, using the CPU only and within an environment with the hardware characteristics mentioned above. Furthermore, a higher frequency was achieved with respect to the maximum one conservatively estimated via cProfile. These data are a good indication to assume that close to ideal and optimal real-time performances are delivered in this context.

4.3. Post-Processing Data Analysis Modules

This chapter is dedicated to all the data calculation processes performed off-line, the mathematical criteria that made possible the automation and the definition of the minimum design requirements for the analysis to be robust. This description will adopt a top-down approach.

The final purpose of this section is to provide:

- scalar data such as speed, step duration, step length, cadence, cycle duration, mediated over all the steps of all the acquisitions of a single session.
- The kinematic data concerning the development over time of some angles associated to the step, also mediated and normalised over all the steps of all the acquisitions of a single session. In particular, all the angles present in the description in Chapter 2.1 and shown in Figure 2. 4 are given, with the exception of the hip and knee rotations, the pelvic obliquity and the two angles associated with the feet, due to the limitations imposed by the points provided by Cubemos, which are either not sufficient for the mathematical definition of an angle or for the recognition of a body section (as in case of the feet).

In order to produce this data, it is essential to store the averages of each acquisition associated with each CSV file in the session folder. Then every mean value is saved in the private “self” parameters of an object generated from the class inside the `computation_handler.py` module. Also saved is the total number of valid steps for each signal in the entire session. So that it is clear at the end of the calculation how many samples and steps the measured values were averaged over and their reliability. Thus, a vector is obtained for each parameter of each walk, from which the total average value in the session and its standard deviation can be deduced. However, in order to define the averages of signals that have the same conceptual value and the same behaviour, but that may have been generated at different times, it is necessary to normalise the time vector associated with the signal so that all behaviours are plotted against a common range. It is therefore chosen to normalise from 0 to 100 each signal of each step of each CSV and resample them to a common and fixed frequency. Such resampling value is evaluated before any calculation and is based on the frequencies of all the acquisitions of the session, it is then passed to the calculation section during the generation of the object belonging to the `computation_handler.py` module.

It is, therefore, necessary to iteratively analyse in a loop for each CSV file and have an average value of it for each signal. Hence, of each signal it is necessary to know in how many steps it was well acquired and in which time span, then, store these data and iterate over this list for each CSV for each signal. This leads to the need to determine how a “good signal” section can be defined, how a step can be recognised and how to deal with the times associated with this information. For example, in order to know the list of times when a given angle started and ended its period in an entire acquisition, it is essential to know the same data for those x, y and z signals associated with the points generating the angle, then find out which time spans in this list are common to all these points and finally define the list of common time spans as the vector of information sought for these angles. Briefly, with each CSV a list of good steps for each angle will be saved in a data frame, which is itself derived from the list of good steps for each point recognised by Cubemos. It is therefore necessary to define the concept of a “good step” in terms of code. The ideal situation is to have a matrix representing all the signals of an acquisition in the form of a list of ordered Time Series. To this matrix must correspond a second one that has the same number of rows and columns and whose elements hold a single binary value that expresses whether the data in the acquisition matrix, in the same position, deserves to be considered or not. The first step to create this matrix is simple: each NaN entry in the data

matrix must be matched by a False entry in the mask matrix related to this data. A further criterion is to find the outliers in the data matrix and set the corresponding data in the mask matrix to False as well. Also, this step is straightforward and is the reason why it was decided to use a second matrix and occupy extra memory with a second temporary structure. To remove the obvious disturbances and outliers, the acquired signals can be filtered at the beginning by means of an IQR filter that automatically creates a mask vector by itself filtering all values that are not included between the 25th and 75th percentile. It is then sufficient to add to this data, which we already have, the information on the position of the NaNs as described above to complete the matrix. After that, in each Time Series vector, namely in each signal that corresponds to the projection on X, Y or Z of a Keypoint, it is necessary to recognise the portions that are contemporary to the event of a recognised step by means of the Ankle Distance, for each step, and on the basis of the distribution of the True and False values in the section of the associated mask matrix, assess whether that range of values is a good step for the current signal. Precisely, in each signal section contemporary to the cycle of a step, the maximum train of consecutive False is found, its elements are counted and it is measured whether this number is less than or equal to 30% of the total number of points needed to reconstruct the highest frequency component of the signal, given the average sampling frequency in real-time.

New needs are enforced by this criterion:

- Define the maximum frequency of the Time Series that can be considered a component of the signal
- Evaluate signal data with these criteria only after it has been well filtered (Figure 4. 10, Figure 4. 11)
- Identify step events and create a list of each start and end point of the cycle

The first two points are resolved in the same section of code that is responsible for data processing, the same section that includes the IQR filter already mentioned. This is where the data frame of the Time Series values of the real-time acquisition is passed through three filters: the IQR which acts as already described, a median filter of width 3 and a Butterworth backward and forward low pass filter with an adaptive cut-off frequency. Both the width of the Median Filter and the frequency and type of the low pass filter, as well as the limit, as a design specification, imposed during real-time for the sampling frequencies, are derived from the analysis of the frequencies of an average gait cycle and a gait in the worst-case scenario.

An ideal system meets the Nyquist conditions on frequency even in the case of the fastest possible movement in front of the acquisition system and is robust especially in the case of walking with a standard performance. According to the study by Luis M. Silva & Nick Stergiou [61], the average frequency of a standard gait cycle of a healthy individual is around 1.07 Hz, and associated signals possess dominant components in comparable low frequencies. So, it is in general completely unacceptable to have an analysis system that is not significantly faster than 2 Hz. Furthermore, this is why the filtering requires a Butterworth type which has no distortion of any kind in modulus in the low frequency section, i.e. in band. It is also desirable that all frequencies of a filtered signal are not disturbed by the filter in magnitude. If, therefore, a Butterworth of order $n = 5$ is used and applied forward and backward, reaching already an appreciable filtering order ($2n = 10$), it is necessary to impose that the gain $G(\omega)$ of a signal at $\omega = 1.07 \text{ Hz}$ is at the very least in these conditions almost unvaried $G(\omega) \rightarrow 1 = 0,999$ and from this data deduce the cut-off frequency ω_c . From the latter we then deduce the minimum

sampling frequency for the whole system, which must be twice the cut-off frequency for adequate sampling by a digital Butterworth filter.

The following equation, typical of the LP filter mentioned above, is then applied:

$$G(\omega)^2 = \frac{G_0^2}{1 + \frac{j\omega}{j\omega_c}^{2n}} \quad (4.3)$$

From which we obtain, by substituting, an $\omega_c = 3,38 \text{ Hz}$ and a new minimum limit for the real-time FPS of the project that rises to at least 6.77 Hz .

The worst-case scenario, however, has frequencies greater than 1.07 Hz . For this study, therefore, we consider the frequency with which the stride cycle of the fastest man in the world occurs during his peak performance in instantaneous speed: $\omega = 4.29 \text{ Hz}$, Bolt [62].

The minimum sampling frequency for the system therefore rises, applying the Nyquist criterion, to 8.58 Hz . Furthermore, to apply the second level of outlier filtering by a median filter of width 3, a signal with a frequency greater than $fps_{min} \approx 3 * \omega \approx 12.87 \text{ Hz}$ is at least desirable. Approximating to the nearest integer, a similar number for minimum FPS is obtained by applying Eq. 4.3 to this case, imposing a $\omega = \omega_{max_Bolt} = 4.29 \text{ Hz}$ and $G(\omega)^2 = 0.99$. Finally, to be conservative with respect to the minimum acceptable frequency, we choose a number arbitrarily slightly higher than the calculated minimum limits, which amounts to $fps_{real_time} = 15$.

To summarize, these very same reasonings in the code for off-line computation have been applied. The Median Filter and the IQR filter are followed by a polynomial interpolator of order 3 of the eliminated outliers (Figure 4. 9), after which Eq. 4.3 is used to define the ω_c of the adaptive LP filter where (Figure 4. 12):

- as ω , this time, the maximum signal frequency $\omega_{worst_case_freq}$ mentioned above is imposed, obtained as the maximum frequency that has the related magnitude in dB of at least 30% of the modulus of the absolute maximum of the Fast Fourier Transform (FFT) of the signal and searching between those included between 0 Hz and the ω_{max_Bolt}
- as $G(\omega)^2$ a value proportional to the weight of the magnitude related to that frequency with respect to the maximum modulus of the signal FFT

This filtering is applied both on the original signals and on the distance-normalised ones, and the solution is chosen between the two that proposes the Time Series set less corrupted by the filters, but free of the frequency components that are not expected in a Gait Cycle associated signal. The reason for this choice derives from the fact that, in the first case, during a long walk, the adaptive filter can recognise as the maximum frequency of the FFT the component of the signal that corresponds to the influence of the approach of the point in a system with a moving frame, while in the second case the problem is avoided but in the case of frequent NaN, the normalisation and the consequent interpolation could still introduce a new low-frequency component and lower the cut-off frequency. In case the walk is both long and with frequent disturbances, it will be discarded.

The filtering is followed by the recognition of the step events, which completes the list of ingredients necessary for the evaluation of the averages and the automation of the analysis.

The function is simple: knowing that the Ankle Distance trend must have concluded a period with a sinusoidal-like shape, to recognise a cycle the signal is divided into sections each time it crosses the 0 axis and a succession of absolute maximum-minimum-maximum or minimum-

maximum-minimum is searched for in these sections, eliminating all those sets that are not always contemporaneous with the patient's approaching, i.e. all those that do not occur while the patient's speed remains continuous, negative and non-zero throughout the cycle (Figure 4. 13, Figure 4. 14).

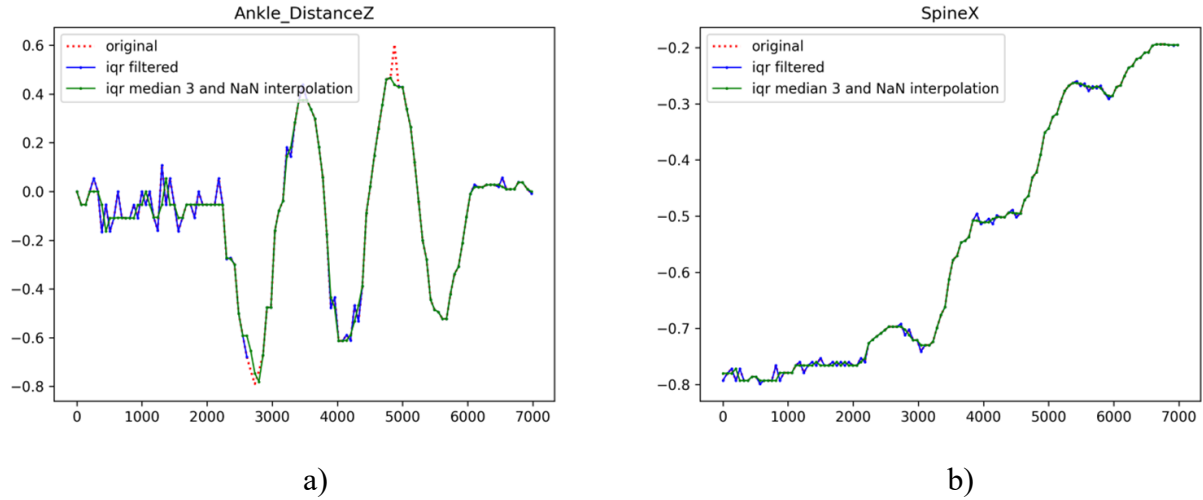


Figure 4. 9 - SANE's first level of filtering for outliers - a) Ankle Distance trend; b) an example of a keypoint signal (the projection on X of the signal related to the Spine joint)

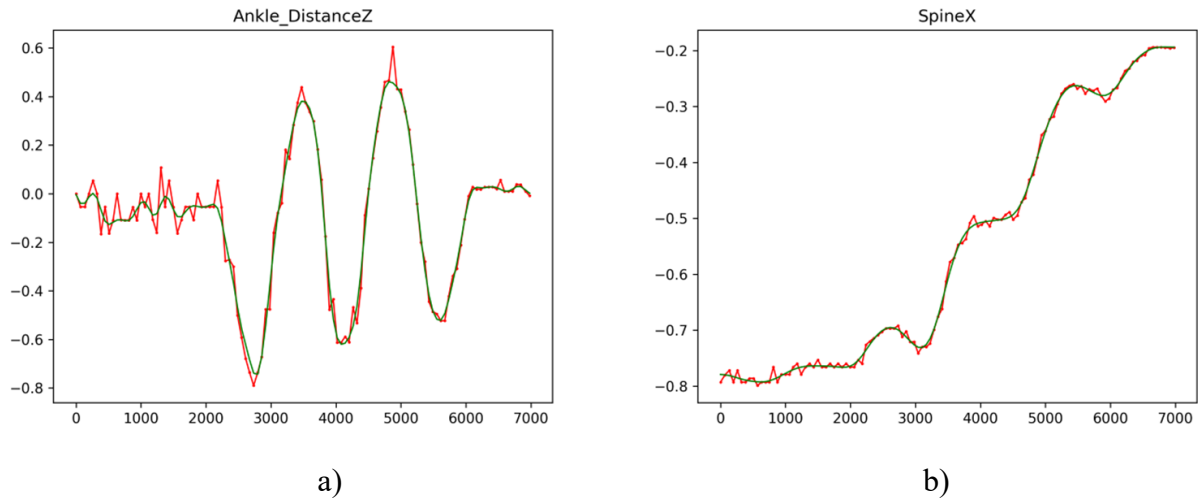


Figure 4. 10 - SANE's completely filtered signal (green line) vs raw data interpolation (red line) - a) Ankle Distance trend; b) an example of a keypoint signal (the projection on X of the signal related to the Spine joint)

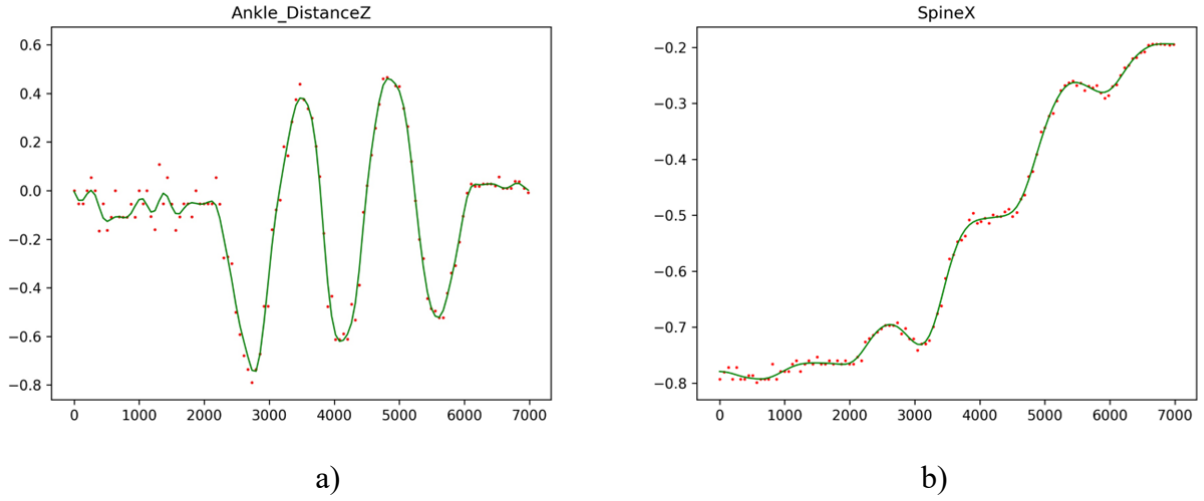


Figure 4. 11 - SANE's completely filtered signal (green line) vs raw data point cloud (red line) - a) Ankle Distance trend; b) an example of a keypoint signal (the projection on X of the signal related to the Spine joint)

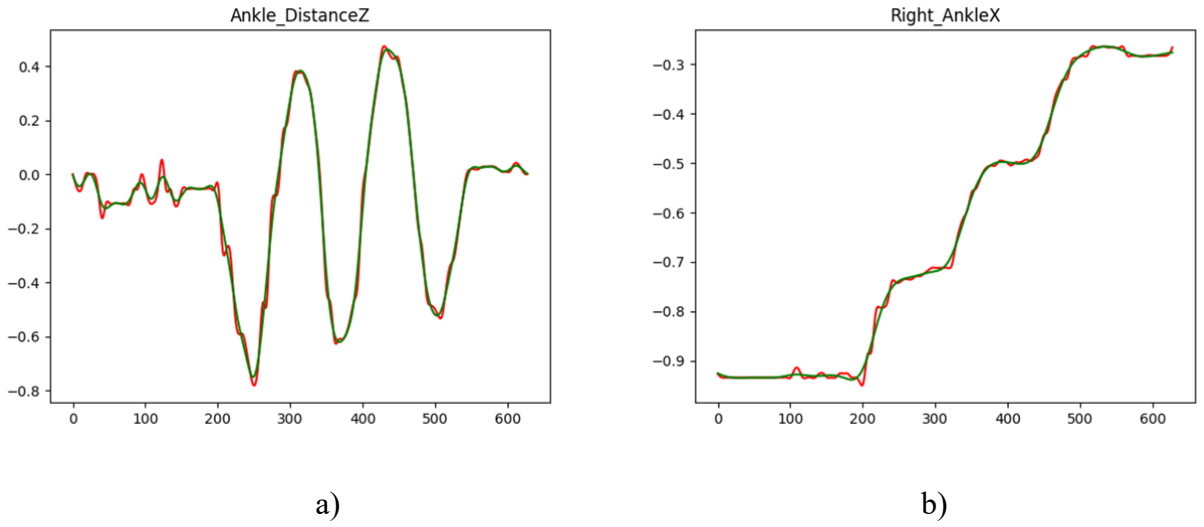


Figure 4. 12 - SANE's completely filtered signal with IQR, Median and LP adaptive Butterworth (green line) vs signals filtered by IQR and Median (red line) - a) Ankle Distance trend; b) an example of a keypoint signal (the projection on X of the signal related to the Right Ankle joint)

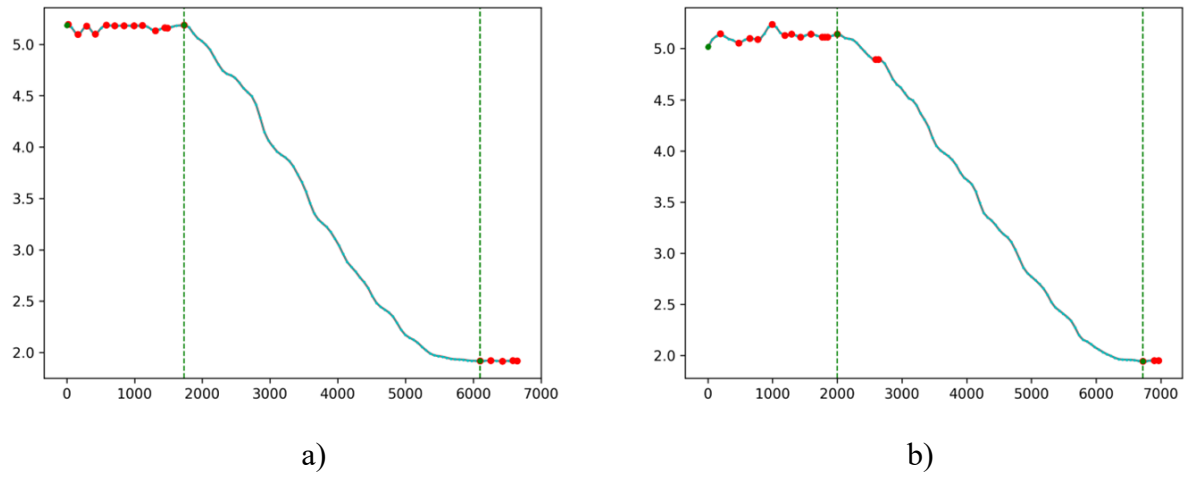


Figure 4.13 - SANE's detection of movement's start and stop (green vertical lines) through the projection on Z of the signal related to the Spine joint and its relative maxima and minima (red dots) - a) a low-noise acquisition while walking; b) a different, slightly noisier acquisition while walking with a maximum and a minimum that are not correctly taken into account during the walk recognition

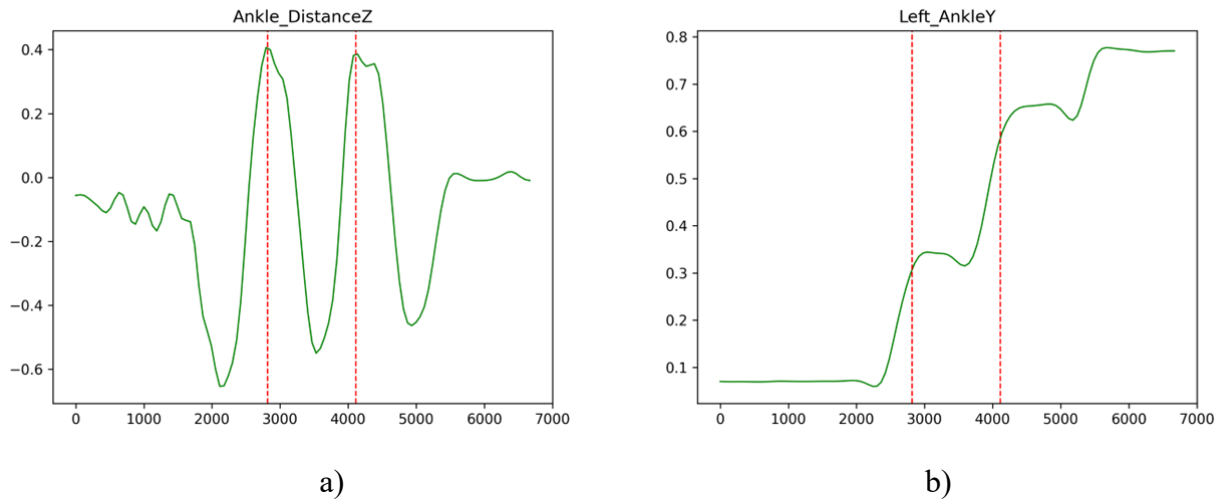


Figure 4.14 - SANE's gait detection (red vertical lines) through the projection on Z of the trend related to the Ankle Distance - a) Ankle Distance trend; b) an example of a keypoint signal cut within the time span associated with the gait (the projection on X of the signal related to the Right Ankle joint)

5. Experimental Tests and results

5.1. Experimental layout

In order to validate the results obtained from SANE, multiple tests were conducted on two separate occasions at the Gait Analysis laboratory of the Clinical Research Centre Neuromed in Pozzilli, IS.

The site is equipped with all the instruments required by the latest BTS GAITLAB protocol, except for the number of dynamometric plates, which amounts to two. The latter, however, were only used to simulate a complete analysis process but are not relevant for the evaluation and comparison of kinematic and scalar data between BTS and SANE. Dynamic data, therefore, as not provided by SANE, will not be reported in this chapter dedicated to comparison tests. Therefore, four sessions of ten acquisitions by two different operators on the same healthy patient in different modalities were performed for a total amount of 40 acquisitions by SANE and another 40 simultaneous acquisitions by BTS.

More specifically, the procedures for (Table 6) have been followed:

- inter-rater test
 - with two different operators who carried out, on the same patient on the same day, ex novo, the whole procedure for the positioning of the markers foreseen by the BTS for the acquisition of two consecutive sessions, one each, of 10 walks, using BTS and SANE simultaneously. The purpose of these tests is not only to provide results from the two systems, but, above all, to highlight through them the error between the measurements due to the operator. In other words, it is an estimate of the dependence of the systems on the operator and their reliability and availability in this regard.
- test-retest
 - executed by the same operator who performed, on the same patient, on two separate days, two days apart [63], ex novo, all the procedure for the positioning of the markers foreseen by the BTS for the acquisition of two discontinuous and distant sessions of 10 walks using of BTS and SANE simultaneously. The purpose of these tests is to show the variation between measurements taken at different times, but with the same operator and the same patient. It is in other words an estimation of the dependency of the systems in relation to time, their reliability and availability in this regard.
- intra-rater test
 - executed by the same operator who performed, on the same patient on the same day, ex novo, all the procedure for the placement of the markers foreseen by the BTS, for the acquisition of two consecutive sessions of 10 walks, using BTS and SANE simultaneously. The purpose of these tests is to show the variation between repeated measurements, with the same operator and the same patient.

For an optimal acquisition the Gait Analysis was performed in the centre of the capture area of the BTS laboratory, the Intel RealSense d435i sensor was positioned along the patient path trajectory delineated on the ground, three metres long and centred on the dynamometer plates.

The RealSense camera was placed on a tripod 1.63 metres from the end of the patient path, 1.30 metres above the floor and at an angle of $+13^\circ$ along its X-axis and 0° for the remaining axes, facing the patient and aligned with its intended trajectory (Figure 5. 1).

Non-reflective tape was used on the floor for marking the path to avoid any form of light disturbance. The chamber is isolated from sunlight in order to avoid infrared disturbances and every object in the acquisition zone has been removed (Figure 5. 2, Figure 5. 3, Figure 5. 4).

The Davis protocol standard was followed for the marker arrangement.

This setup was kept constant and unchanged during the execution of all tests.

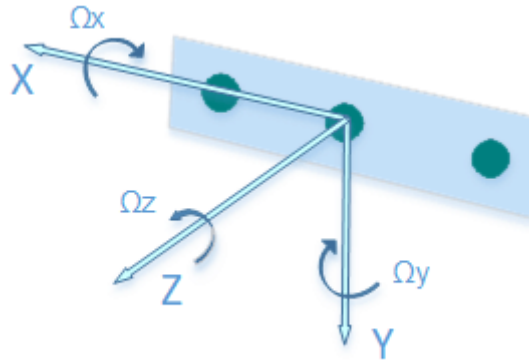


Figure 5. 1 - Intel RealSense d435i and SANE's axis



Figure 5. 2 - gait analysis laboratory before the experimental layout was set up.



Figure 5. 3 - Experimental layout and demarcation of the path. Following the creation of the start and stop lines, the black reflective tape was removed while the opaque white tape remained.

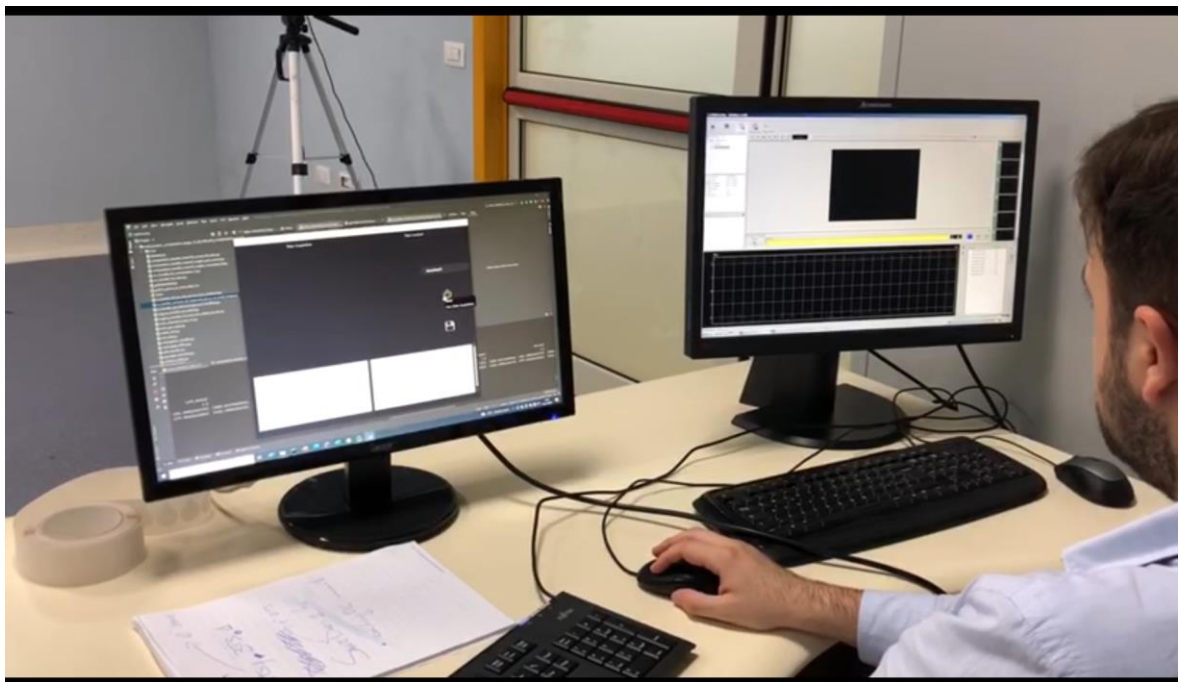


Figure 5. 4 - Experimental layout - on the left: SANE's Interface; on the right: BTS GAITLAB Smart Clinic Interface

5.2. Experimental tests

Table 6 - descriptive table of sessions

	First Day	Two Days Later
Eval 1	Session 1	
Eval 2	Session 2	Session 3
		Session 4

As can be seen in Table 6, by virtue of what has already been said in Chapter 5.1, Sessions number 1 and 2 were used for the inter-rater test, Session 2 and 3 for the test-retest, and Session 3 and 4 for the intra-rater test.

Both operators followed the BTS protocol for preliminary patient preparation and offline analysis.

During the execution of the tests, BTS vulnerabilities emerged. Phantom markers appeared from time to time and some walks, despite appearing to be well captured through the 3D visual feedback window, were not selectable during the offline phase. Based on the recording of the 3D skeleton constructed by the markers in real-time, data was reacquired with both systems whenever the BTS dataset was visibly disturbed. The manual gait selection process was concluded following the meticulous selection and recognition of 20 right stances, 20 left stances, 10 right detachments, 10 left detachments over three sessions and a total of 180 manual signal selections via the 3D window provided by the BTS Smart Clinic program. Occasional crashes of the offline analysis program were also experienced, but none occurred during the real-time acquisition phase.

The SANE system, on the other hand, required the reacquisition of the walks only twice, one of them simultaneously with the BTS. Also in this case, in order to preserve the comparability of the tests, the acquisition was repeated with both systems.

Once all the real-time measurements were completed, the offline averaging for both systems was generated. In this second step, the walks that have been discarded by one system have not been discarded in the other as well, since the comparison of the two methods has to include only the real-time acquisition procedures.

Therefore, after selecting the steps, during the BTS consistency analysis phase for Session 1 of operator 1 it was necessary to discard the acquisitions number 01, 06 and 07; for Session 2 of operator 2 the acquisitions number 02 and 03; for Session 3 of operator 2 the acquisitions 01, 06, 07, 08, 09; for Session 4 of operator 2 the acquisitions 01, 03, 04, 05, 06, 09, 10.

It is important to notice that SANE system did not require the elimination of any of them.

The averages thus obtained are as follows:

Table 7 - Results for Gait Cycle Duration, highlighted the higher REM% values

		SANE		BTS system	
		Mean \pm SD (s)	REM %	Mean \pm SD (s)	REM %
Inter-rater relative error measurement	Session1	1.33 \pm 0.10	8,27	1.35 \pm 0.11	7,41
	Session 2	1.44 \pm 0.07		1.45 \pm 0.04	
Test-retest relative error measurement	Session 2	1.44 \pm 0.07	4,17	1.45 \pm 0.04	4,83
	Session 3	1.38 \pm 0.06		1.38 \pm 0.04	
Intra-rater relative error measurement	Session 3	1.38 \pm 0.06	1,45	1.38 \pm 0.04	3,62
	Session4	1.40 \pm 0.06		1.43 \pm 0.03	

Table 8 - Results for Results for Step Duration, highlighted the higher REM% values

		SANE		BTS system	
		Mean \pm SD (s)	REM %	Mean \pm SD (s)	REM %
Inter-rater relative error measurement	Session1	0.66 \pm 0.05	9,09	0.70 \pm 0.12	22,86
	Session 2	0.72 \pm 0.04		0.86 \pm 0.02	
Test-retest relative error measurement	Session 2	0.72 \pm 0.04	4,17	0.86 \pm 0.02	5,81
	Session 3	0.69 \pm 0.03		0.81 \pm 0.02	
Intra-rater relative error measurement	Session 3	0.69 \pm 0.03	1,45	0.81 \pm 0.02	4,94
	Session4	0.70 \pm 0.03		0.85 \pm 0.02	

Table 9 - Results for Cadence (named Rate in SANE), highlighted the higher REM% values

		SANE		BTS system	
		Mean \pm SD (step/min)	REM %	Mean \pm SD (step/min)	REM %
Inter-rater relative error measurement	Session1	91.48 \pm 8.94	8,59	90.09 \pm 5.24	8,09
	Session 2	83.62 \pm 4.30		82.80 \pm 2.29	
Test-retest relative error measurement	Session 2	83.62 \pm 4.30	4,40	82.80 \pm 2.29	5,51
	Session 3	87.30 \pm 3.57		87.36 \pm 2.34	
Intra-rater relative error measurement	Session 3	87.30 \pm 3.57	1,10	87.36 \pm 2.34	3,85
	Session4	86.34 \pm 3.98		84.00 \pm 1.77	

Table 10 - Results for Gait Cycle Length, highlighted the higher REM% values

		SANE		BTS system	
		Mean \pm SD (m)	REM %	Mean \pm SD (m)	REM %
Inter-rater relative error measurement	Session1	1.40 \pm 0.17	3,57	1.33 \pm 0.16	1,50
	Session 2	1.45 \pm 0.11		1.35 \pm 0.04	
Test-retest relative error measurement	Session 2	1.45 \pm 0.11	0,69	1.35 \pm 0.04	5,93
	Session 3	1.46 \pm 0.07		1.43 \pm 0.03	
Intra-rater relative error measurement	Session 3	1.46 \pm 0.07	2,74	1.43 \pm 0.03	2,80
	Session4	1.42 \pm 0.08		1.39 \pm 0.02	

Table 11 - Results for Mean Velocity, highlighted the higher REM% values

		SANE		BTS system	
		Mean \pm SD (m/s)	REM %	Mean \pm SD (m/s)	REM %
Inter-rater relative error measurement	Session1	1.05 \pm 0.08	3,81	1.00 \pm 0.10	10,00
	Session 2	1.01 \pm 0.07		0.90 \pm 0	
Test-retest relative error measurement	Session 2	1.01 \pm 0.07	4,95	0.90 \pm 0	11,11
	Session 3	1.06 \pm 0.07		1.00 \pm 0	
Intra-rater relative error measurement	Session 3	1.06 \pm 0.07	3,77	1.00 \pm 0	0,00
	Session4	1.02 \pm 0.06		1.00 \pm 0	

Where SD stands for Standard Deviation and REM% for Relative Mean Percentage Error, defined as in Eq. 5.2.1:

$$REM\% = \frac{\bar{x}_{SANE} - \bar{x}_{BTS}}{\bar{x}_{BTS}} \times 100 \quad (5.2.1)$$

5.3. Results

From what can be inferred from Chapter 5.2 the data are quite promising.

In all test-retests SANE has a lower relative percentage error than BTS, lower than 5%, with a maximum value of 4.95% when calculating the average speed against the BTS maximum of 11.11% with an improvement of more than double. This is the first clue that might suggest that SANE enjoys greater repeatability.

Regarding intra-rater tests SANE returns very positive results, always less than 5% REM% and always lower than those of BTS except in the case of the average speed table. On the other hand, the latter measure of the REM% for the BTS is not at all plausible and derives from two factors: the tendency by the BTS to truncate too many digits of the standard deviation, declaring, very often, an unrealistic standard deviation of 0 and the smaller number of acquisitions present in session 3 and 4 for the BTS, discarded for the reasons in Chapter 5.2. At the same time, the same dataset was fully averaged by SANE without any deviation. This is the second clue that could tip the scales in favour of SANE, not only from the viewpoint of repeatability, but also from the aspect of the mathematical rigour of the measurements.

In the inter-rater tests SANE returned two times out of five a better value in terms of REM% than BTS up to a gap of 7%, three times out of five a slightly higher value than BTS making the measurements comparable between the two systems, with a maximum gap of 0.5%, 0.86% and 2.07%. SANE, however, meanwhile, has a maximum REM% of 9.09% while BTS reaches 22.86%. This third term of comparison leaves margins for interpretation.

For what concerns the mean and standard deviation measures of SANE, they appear comparable to those of BTS. While it is, however, difficult to understand which of the two systems returned the closest measurement to reality in terms of absolute value, given the nature of a human step, it is much easier to assess the value of repeatability and reliability of both systems, emphasising that the latter evaluation is more important than the numerical accuracy of the measurement. After all, an inaccurate measurement from a repeatable system can be corrected by calibration, while a fortuitously accurate measurement from a non-repeatable system will never have a guarantee of reliability, nor can it be improved in any way.

By virtue of what has been observed, in several cases SANE has been shown to enjoy greater repeatability and less susceptibility to human factors, giving reason to conduct further future experiments on the system to substantiate this thesis.

6. Conclusion

In conclusion, as shown in the results of the study, SANE is an appropriate system for Gait Analysis. According to the test findings, what was lost in accuracy due to the employment of Artificial Intelligence and a frontal camera with a lower sample rate than stereophotogrammetry systems is regained due to the elimination of human error, automation, and high repeatability.

Furthermore, because the patient does not have to go through long marker preparation and wearing processes, the method has shown to be significantly less stressful for the patient. During the experiments conducted at the Clinical Research Centre Neuromed, a decreased incidence of acquisition failure was observed, due to the smaller number of factors that may affect the measurement while walking.

Positives also include a significant improvement in terms of time and costs, two orders of magnitude cheaper than those of the BTS.

The system's portability is another key benefit, allowing acquisitions to take place even in non-clinical contexts. Furthermore, the system's high level of automation and completely guided interface enable it to be utilized by an untrained operator, further lowering costs and system limitations.

The system's robustness is also attributable to its real-time feedback and auto-debugging capabilities, which allow it to detect the presence of a problem and its nature at the moment of the acquisition.

The usage of a frontal camera can have its limitations as it is possible to have moments of non-direct detection of a point with the consequent reconstruction of the latter by Artificial Intelligence.

Therefore, the use of SANE would be in the field of preliminary Gait Analysis systems to get immediate feedback on the characteristics of a patient and decide on the basis of these whether to perform more in-depth examinations.

Furthermore, SANE appears to be an extremely useful system for analyzing the gait of weaker subjects who are unable to physically support the preparatory processes for marker analysis, opening up new opportunities for a portion of the population who previously had no access to this type of examinations.

The use of Cubemos as Artificial Intelligence poses, however, some limitations to the system. Firstly, as mentioned in Chapter 4.3, there is a subset of BTS angles that cannot be analysed using SANE due to the absence of sufficient points provided by Cubemos. Furthermore, in terms of performance, the AI has known problems in the use of the GPU, to the point where it is impossible to do so, making the code produced for SANE potentially more promising on one hand, but limited by external modules on the other. Cubemos has not produced any updates for its software lately, and its relationship with Intel has soured. In addition, Intel has decided to stop focusing on the sensor sector such as the RealSense camera, endangering the future of the project.

For these reasons, in the final phases of development, SANE was made highly scalable, adaptable, and modular, allowing it to be utilized with different kinds of AI and acquisition systems with just minor modifications.

SANE, moreover, being an optical system, cannot provide dynamic information, so the lab team's future plans include the integration of dynamometric systems such as smart insoles or a portable sensorised mat.

Future objectives for the system include testing potential enhancements, implementing AI to recognize patterns other than skeletal tracking, adapting SANE to analyze other regions of the body, recognizing geometries in the pathway, or recognizing the patient's emotional response during therapy. The options for AI training, deployment, and enhancement are nearly endless.

Research takes a step forward.

References

- [1] Somalvico, M. (1987). *Intelligenza artificiale*. Scienza & vita nuova.
- [2] Nilsson, N. J. (1971). *Problem-solving methods in artificial intelligence*, McGraw-Hill, New York, USA.
- [3] Nilsson, N. J. (1998). *Artificial Intelligence: A New Synthesis*. Morgan Kaufmann, San Mateo, CA, USA.
- [4] Tom Mitchell, McGraw Hill(1997). *Machine Learning*
- [5] Lo-Ciganic, W. H., Donohue, J. M., Thorpe, J. M., Perera, S., Thorpe, C. T., Marcum, Z. A., & Gellad, W. F. (2015). Using machine learning to examine medication adherence thresholds and risk of hospitalization. *Medical care*, 53(8), 720.
- [6] Alanazi, H. O., Abdullah, A. H., Qureshi, K. N., & Ismail, A. S. (2018). Accurate and dynamic predictive model for better prediction in medicine and healthcare. *Irish Journal of Medical Science (1971-)*, 187(2), 501-513.
- [7] Musacchio, N., Guaita, G., Oz-zello, A., Pellegrini, M. A., Ponzani, P., Zilich, R., & De Micheli, A. (2018). *Intelligenza Artificiale e Big Data in ambito medico: prospettive, opportunità, criticità*. The Journal of AMD, 21, 3.
- [8] Malva, A., & Zurlo, V. *La medicina nell'era dell'Intelligenza Artificiale: applicazioni in Medicina Generale*. Dibattito Scientifico Professionale, 28.
- [9] Annarumma, M., Withey, S. J., Bakewell, R. J., Pesce, E., Goh, V., & Montana, G. (2019). Automated triaging of adult chest radiographs with deep artificial neural networks. *Radiology*, 291(1), 196-202.
- [10] Strodthoff, N., & Strodthoff, C. (2019). Detecting and interpreting myocardial infarction using fully convolutional neural networks. *Physiological measurement*, 40(1), 015001.
- [11] Rajpurkar, P., Hannun, A. Y., Haghpanahi, M., Bourn, C., & Ng, A. Y. (2017). Cardiologist-level arrhythmia detection with convolutional neural networks. *arXiv preprint arXiv:1707.01836*.
- [12] Madani, A., Arnaout, R., Mofrad, M., & Arnaout, R. (2018). Fast and accurate view classification of echocardiograms using deep learning. *NPJ digital medicine*, 1(1), 1-8.
- [13] Zhang, J., Gajjala, S., Agrawal, P., Tison, G. H., Hallock, L. A., Beussink-Nelson, L., ... & Deo, R. C. (2018). Fully automated echocardiogram interpretation in clinical practice: feasibility and diagnostic accuracy. *Circulation*, 138(16), 1623-1635.
- [14] Esteva, A., Kuprel, B., Novoa, R. A., Ko, J., Swetter, S. M., Blau, H. M., & Thrun, S. (2017). Dermatologist-level classification of skin cancer with deep neural networks. *nature*, 542(7639), 115-118.
- [15] Han, S. S., Kim, M. S., Lim, W., Park, G. H., Park, I., & Chang, S. E. (2018). Classification of the clinical images for benign and malignant cutaneous tumors using a deep learning algorithm. *Journal of Investigative Dermatology*, 138(7), 1529-1538.
- [16] Poria, S., Majumder, N., Mihalcea, R., & Hovy, E. (2019). Emotion recognition in conversation: Research challenges, datasets, and recent advances. *IEEE Access*, 7, 100943-100953.

- [17] Eichstaedt, J. C., Smith, R. J., Merchant, R. M., Ungar, L. H., Crutchley, P., Preotiuc-Pietro, D., ... & Schwartz, H. A. (2018). Facebook language predicts depression in medical records. *Proceedings of the National Academy of Sciences*, 115(44), 11203-1120
- [18] Reece, A. G., & Danforth, C. M. (2017). Instagram photos reveal predictive markers of depression. *EPJ Data Science*, 6, 1-12.
- [19] Fitzpatrick, K. K., Darcy, A., & Vierhile, M. (2017). Delivering cognitive behavior therapy to young adults with symptoms of depression and anxiety using a fully automated conversational agent (Woebot): a randomized controlled trial. *JMIR mental health*, 4(2), e7785.
- [20] Kennedy, C. (2018). Pear approval signals FDA readiness for digital treatments. *Nature biotechnology*, 36(6).
- [21] Strelkova, O. (2017). Three types of artificial intelligence.
- [22] Real-time human pose estimation in the browser with tensorflow.js. The TensorFlow Blog. (n.d.). Retrieved October 19, 2021, from <https://blog.tensorflow.org/2018/05/real-time-human-pose-estimation-in.html>.
- [23] Demarchi, d., Rabbito, R., & Bonato, P. Using Deep Learning-Based Pose Estimation Algorithms for Markerless Gait Analysis in Rehabilitation Medicine.
- [24] NuiTrack: NuiTrack.skeleton class reference. (n.d.). Retrieved October 19, 2021, from https://download.3divi.com/NuiTrack/doc/classnuiTrack_1_1Skeleton.html.
- [25] Skeleton tracking - SDK for Body Tracking Applications. Intel® RealSense™ Depth and Tracking Cameras. Retrieved October 19, 2021, from <https://www.intelrealsense.com/skeleton-tracking/>.
- [26] Zhang, D., Mishra, S., Brynjolfsson, E., Etchemendy, J., Ganguli, D., Grosz, B., ... & Perrault, R. (2021). The ai index 2021 annual report. arXiv preprint arXiv:2103.06312.
- [27] Cao, Z., Hidalgo, G., Simon, T., Wei, S. E., & Sheikh, Y. (2019). OpenPose: realtime multi-person 2D pose estimation using Part Affinity Fields. *IEEE transactions on pattern analysis and machine intelligence*, 43(1), 172-186.
- [28] Silva, V., Soares, F., Leão, C. P., Esteves, J. S., & Vercelli, G. (2021). Skeleton driven action recognition using an image-based spatial-temporal representation and convolution neural network. *Sensors*, 21(13), 4342.
- [29] Heaton, J. (2015). AIFH, volume 3: deep learning and neural networks. *Journal of Chemical Information and Modeling*, 3.
- [30] Nordin, M., & Frankel, V. H. (Eds.). (2001). *Basic biomechanics of the musculoskeletal system*. Lippincott Williams & Wilkins.
- [31] Caldas, R., Mundt, M., Potthast, W., de Lima Neto, F. B., & Markert, B. (2017). A systematic review of gait analysis methods based on inertial sensors and adaptive algorithms. *Gait & posture*, 57, 204-210.
- [32] Hsu, C. Y., Tsai, Y. S., Yau, C. S., Shie, H. H., & Wu, C. M. (2016). Test-retest reliability of an automated infrared-assisted trunk accelerometer-based gait analysis system. *Sensors*, 16(8), 1156.
- [33] Muro-De-La-Herran, A., Garcia-Zapirain, B., & Mendez-Zorrilla, A. (2014). Gait analysis methods: An overview of wearable and non-wearable systems, highlighting clinical applications. *Sensors*, 14(2), 3362-3394

- [34] Balta, D. (2019). Two dimensional markerless gait analysis protocol for estimating the sagittal lower limb joint kinematics with a single RGB-D camera for clinical applications (Doctoral dissertation, Politecnico di Torino).
- [35] Pirlo, G., & Luigi, M. Analisi automatica del gait in malattie neuro-degenerative.
- [36] D'Amico, M., Kinel, E., D'Amico, G., & Roncoletta, P. (2021). A Self-Contained 3D Biomechanical Analysis Lab for Complete Automatic Spine and Full Skeleton Assessment of Posture, Gait and Run. *Sensors*, 21(11), 3930.
- [37] Rosa, A. S., Vargas, L. S., Frizera, A., & Bastos, T. Real-Time Walker-Assisted Gait Analysis System Using Wearable Inertial Measurement Units.
- [38] Sánchez, A., & Ricardo, M. (2014). Desenvolvimento de sensor MARG para análise de movimento. Desenvolvimento de Sensor MARG Para Análise de Movimento.
- [39] Baker, R. (2006). Gait analysis methods in rehabilitation. *Journal of neuroengineering and rehabilitation*, 3(1), 1-10.
- [40] L. (2018, September 1). The eight phases of human gait cycle - Streifeneder. The eight phases of human gait cycle PRO.vision. Vdocuments.Mx. <https://vdocuments.mx/the-eight-phases-of-human-gait-cycle-streifeneder-the-eight-phases-of-human.html>
- [41] BTS GAITLAB | Sistemi integrati. (2020, May 4). BTS Bioengineering. <https://www.btsbioengineering.com/it/prodotti/bts-gaitlab-gait-analysis/>
- [42] Edwards, N., Stokes, A., Dickin, C., & Wang, H., (2019) Clinical Gait Analysis for Assessing Bilateral Lower Extremity Function: A Case Study. *J Ann Bioeng* 2019(1): 01-10.
- [43] Example of motion capture system. (n.d.). [Illustration]. Example of Motion Capture System. http://www.phasespace.com/images/products/impulse_splash.jpg
- [44] BTS WEBINAR SERIES GAITLAB on Vimeo. (n.d.). BTS WEBINAR. Retrieved November 5, 2021, from <https://vimeo.com/showcase/btsgaitlab>
- [45] Calibration | Ensuring Precise Tracking For Your Optical System. (2019, October 15). Vicon. <https://www.vicon.com/hardware/devices/calibration/>
- [46] Zhang, J. T., Novak, A. C., Brouwer, B., & Li, Q. (2013). Concurrent validation of Xsens MVN measurement of lower limb joint angular kinematics. *Physiological measurement*, 34(8), N63.
- [47] M3D Force Plate (Wired) | Products | Tec Gihan Co., Ltd. (n.d.). 株式会社テック技販 . Retrieved November 24, 2021, from <https://www.tecgihan.co.jp/en/products/force-plate/small-for-shoes/m3d-force-plate-wired/>
- [48] Bamberg, S. J. M., Benbasat, A. Y., Scarborough, D. M., Krebs, D. E., & Paradiso, J. A. (2008). Gait analysis using a shoe-integrated wireless sensor system. *IEEE transactions on information technology in biomedicine*, 12(4), 413-423.
- [49] Cutter, G. R., Baier, M. L., Rudick, R. A., Cookfair, D. L., Fischer, J. S., Petkau, J., ... & Willoughby, E. (1999). Development of a multiple sclerosis functional composite as a clinical trial outcome measure. *Brain*, 122(5), 871-882.
- [50] Hobart, J. C., Riazi, A., Lamping, D. L., Fitzpatrick, R., & Thompson, A. J. (2003). Measuring the impact of MS on walking ability: the 12-Item MS Walking Scale (MSWS-12). *Neurology*, 60(1), 31-36.
- [51] Holland, A., O'Connor, R. J., Thompson, A. J., Playford, E. D., & Hobart, J. C. (2006). Talking the talk on walking the walk. *Journal of neurology*, 253(12), 1594-1602.

- [52] Tinetti, M. E. (1986). Performance-oriented assessment of mobility problems in elderly patients. *Journal of the American Geriatrics Society*, 34(2), 119-126.
- [53] Gomatam, A. N. M., & Sasi, S. (2004, March). Multimodal Gait Recognition Based on Stereo Vision and 3D Template Matching. In *Cisst* (pp. 405-410).
- [54] Liu, H., Cao, Y., & Wang, Z. (2010, May). Automatic gait recognition from a distance. In *2010 Chinese Control and Decision Conference* (pp. 2777-2782). IEEE.
- [55] Gabel, M., Gilad-Bachrach, R., Renshaw, E., & Schuster, A. (2012, August). Full body gait analysis with Kinect. In *2012 Annual International Conference of the IEEE Engineering in Medicine and Biology Society* (pp. 1964-1967). IEEE.
- [56] Clark, R. A., Pua, Y. H., Bryant, A. L., & Hunt, M. A. (2013). Validity of the Microsoft Kinect for providing lateral trunk lean feedback during gait retraining. *Gait & posture*, 38(4), 1064-1066.
- [57] Xue, Z., Ming, D., Song, W., Wan, B., & Jin, S. (2010). Infrared gait recognition based on wavelet transform and support vector machine. *Pattern recognition*, 43(8), 2904-2910.
- [58] Intel RealSense D400 Series Product Family Datasheet, New Technologies Group, Intel Corporation, 2019, Document Number: 337029-005
- [59] Intel RealSense Store. (n.d.). Intel® RealSense™ Depth Camera D435i. Retrieved November 24, 2021, from <https://store.intelrealsense.com/buy-intel-realsense-depth-camera-d435i.html>
- [60] The Python Profilers — Python 3.10.0 documentation. (n.d.). The Python Profilers — Python 3.10.0 Documentation. Retrieved November 27, 2021, from <https://docs.python.org/3/library/profile.html#module-cProfile>
- [61] Silva, L. M., & Stergiou, N. (2020). The basics of gait analysis. *Biomechanics and Gait Analysis*, 164, 231.
- [62] Krzysztow, M., & Mero, A. (2013). A kinematics analysis of three best 100 m performances ever. *Journal of human kinetics*, 36, 149.
- [63] Marx, R. G., Menezes, A., Horovitz, L., Jones, E. C., & Warren, R. F. (2003). A comparison of two time intervals for test-retest reliability of health status instruments. *Journal of clinical epidemiology*, 56(8), 730-735.